The Role of Syntaxin-1A on Excitation-Contraction Coupling in the Adult Male and Female Mouse Heart

Amanvir Virdi

A THESIS SUBMITTED TO
THE FACULTY OF GRADUATE STUDIES
IN PARTIAL FULFILLMENT OF THE REQUIREMENTS
FOR THE DEGREE OF
MASTER OF SCIENCE

GRADUATE PROGRAM IN BIOLOGY
YORK UNIVERSITY
TORONTO, ONTARIO

April 2022

© Amanvir Virdi, 2022

Abstract

The SNARE protein, syntaxin-1A (STX1A) is expressed in the adult rodent heart, yet its role is not fully established. This thesis explored STX1A's role in cardiac excitation-contraction (EC) coupling in male and female mouse hearts. Heart-specific homozygous and heterozygous STX1A knockouts were achieved via a tamoxifen-inducible Cre-Lox system. Echocardiography revealed significant systolic dysfunction post-STX1A knockout (week 0), with recovery beginning at week 1 and an absence of sex differences in cardiac function. Transient thickening of the posterior wall (week 1) and delayed contractions (week 0-3) were seen. No genetic compensation of STX2, 3, or 4 was seen, however, EC coupling genes, $Ca_V1.2$, RyR2, and SERCA2a, declined at week 0 and recovered at week 3, aligning with the phenotype recovery. Control Cre+ mice remained unchanged, suggesting the transient systolic dysfunction stems from compromised transcription of Ca^{2+} handling genes. Therefore, STX1A may facilitate normal EC coupling gene expression in adult mouse hearts.

Acknowledgments

Graduate school has been an experience like no other. I would like to take this time to acknowledge all the people who have helped me along the way and have contributed to the work presented in this thesis. My supervisor, Dr. Robert G Tsushima, who guided and encouraged me throughout this process. My advisor, Dr. Peter H Backx, who provided valuable suggestions and advice. Xiaodong Gao who taught me the foundational skills of a good researcher and provided continuous support over the years. I would also like to thank the Paluzzi Lab and Hood Lab for the use of their qPCR machine. Although my research, like many others, was interrupted by the COVID-19 pandemic, my community of fellow graduate students was a great support during these unfamiliar times, particularly Gurnoor Brar and Salwa Afifi. And finally, thank you to my family who have supported me in my decisions and encouraged me to follow my heart. Thank you.

Table of Contents

Abstract ii
Acknowledgments iii
Table of Contents iv
List of Tables vi
List of Figures vii
Chapter 1: Introduction 1
1.1. Anatomy of the heart 1
1.2. Cardiac excitation-contraction coupling 2
1.2.1. Calcium-induced-calcium release proteins 6
1.3. Sex differences in cardiac excitation-contraction coupling 7
1.4. Endocrine function of the heart 10
1.5. SNARE mediated exocytosis 12
1.5.1. SNAREs in the heart 15
1.6. Previous work done in the Tsushima Lab 19
1.7. Objectives and Hypotheses 22
Chapter 2: Materials and Methods 23
2.1. Mouse model 23
2.2. Mouse genotyping 23
2.3. Tamoxifen treatment 25
2.4. Echocardiography 25
2.5. Tissue isolation 27
2.6. Protein isolation 28
2.7. Bradford-Lowry protein assay 28
2.8. Western blot 29
2.9. Densitometry analysis 31
2.10. RNA isolation and cDNA conversation 31
2.11. qPCR primer design and primer efficiency 32
2.12. Quantitative real-time PCR 33

2.13. Statistical Analysis 35
Chapter 3: Results 36
3.1. Confirmation of transgenic genotypes 36
3.2. Confirmation of inducible Cre-Lox system 38
3.3. Left ventricle dimension and volume changes of STX1A deficient mice 41
3.4. Left ventricular function of STX1A deficient mice 47
3.5. Left ventricular remodeling in STX1A deficient mice 55
3.6. Delayed R-wave to onset of contraction 57
3.7. Changes in syntaxin gene expression 59
3.8. Changes in calcium-handling gene expression 65
3.9. Average C_t values for Housekeeping Genes 72
Chapter 4: Discussion 73
4.1. Summary of Results 73
4.2. Haploinsufficiency of STX1A to retain normal cardiac function in adult mouse hearts 75
4.3. Decline of syntaxin genes in STX1A deficient mice 78
4.4. EC coupling gene expression in STX1A deficient mice 81
4.5. Sex differences in STX1A deficient mice 88
4.6. Conclusion and Future Directions 90
References 93
Appendix A 101

List of Tables

Table 1: List of antibodies used for western blotting. 31
Table 2: List of forward and reverse primers used for qPCR. 34
Table 3A: Stroke volume and cardiac output for male groups. 50
Table 3B: Stroke volume and cardiac output for female groups. 50
Table 4A: Ejection fraction and fractional shortening of male groups. 54
Table 4B: Ejection fraction and fractional shortening of female groups. 54

List of Figures

Figure 1: Cardiac excitation-contraction coupling. 5
Figure 2: Calcium transient (A) and sarcomere shortening (B) of a mouse left ventricular cardiomyocyte.. 7
Figure 3: Summary of sex differences in murine hearts. 10
Figure 4: SNARE mediated exocytosis. 14
Figure 5: Simplified schematic of possible syntaxin 1A and $Ca_V1.2$ interaction sites. 18
Figure 6: Schematic of the tamoxifen-inducible Cre-Lox system for heart-specific STX1A KO. 20
Figure 7: Ejection fraction (A) and fractional shortening (B) of STX1A knockout (KO) mice compared to Cre-expression mice (Cre+). 21
Figure 8: Positioning of left ventricle relative to transducer probe (A) in order to capture the widest part of the chamber and representative M-mode measurements (B) from Vevo 2100 high frequency, high-resolution digital imaging system. 27
Figure 9: Representative genotyping results for MCM and flanking LoxP (flox) syntaxin-1A transgenes. 37
Figure 10: MerCreMer protein expression. 38
Figure 11: STX1A protein expression in the left ventricular free wall post-TAM. 40
Figure 12: Effect of STX1A deficiency on left ventricular systolic dimension (A, B) and volume (C, D) in male and female mice. 44
Figure 13: Effect of STX1A deficiency on left ventricular diastolic dimension (A, B) and volume (C, D) in male and female mice. 46
Figure 14: Effect of STX1A deficiency on heart rate. (A, B), stroke volume (C, D), and cardiac output (E, F) in male and female mice. 49
Figure 15: Effect of STX1A deficiency on left ventricular ejection fraction (A, B) and fractional shortening (C, D) in male and female mice. 53
Figure 16: Left ventricular posterior wall thickness (mm) in STX1A deficient male (A) and female (A) mice. 56
Figure 17: Time (msec) delay between ECG R-wave and the onset of left ventricular contraction in STX1A deficient male (A) and female (B) mice. 58
Figure 18: STX1A gene expression in the left ventricular free wall of male (A) and female (B) groups. 61
Figure 19: STX2, 3, and 4 gene expression in left ventricular free wall of male (A, C, D) and female (B, D, F) groups. 64
Figure 20: Calcium handling gene expression in left ventricular free wall of male (A, C, E, G) and female (B, D, F, H) groups. 70
Figure 21: Average threshold cycle (Ct) values of housekeeping genes, GAPDH and β-actin, in left ventricular free wall of male and female groups.. 72
Figure 22: Cardiac excitation-contraction (EC) coupling and the proposed changes to this pathway after STX1A loss. 87

Chapter 1: Introduction

1.1. Anatomy of the heart

The cardiovascular system transports blood by way of a pump—the heart. The mammalian heart is the site where the pulmonary and systemic circuits reconvene (Humphrey & McCulloch, 2003; Thiriet, 2008). The right side of the heart receives deoxygenated blood which is then sent to the lungs for oxygenation via the pulmonary circuit (Thiriet, 2008). The left side receives oxygenated blood from the lungs and supplies it to the rest of the body via the systemic circuit (Thiriet, 2008). The heart has four chambers which are divided into two atria and two ventricles; this allows for the separation of the two circuits with the right atrium and ventricle circulating deoxygenated blood and the left atrium and ventricle circulating oxygenated blood (Humphrey & McCulloch, 2003). The general anatomy of the heart is as such.

Located in the mediastinum, the great vessels and atria form the base of the heart while the ventricles form the apex (Thiriet, 2008). The right atrium opens into to the right ventricle via the tricuspid valve and the left atrium opens into the left ventricle via the mitral valve (Humphrey & McCulloch, 2003; Thiriet, 2008). These atrioventricular valves are one-way to prevent backflow of blood, and are anchored by collagenous fibers known as chordae tendineae that are further connected to papillary muscles within the ventricles (Wessels & Sedmera, 2003). The ventricles are kept separate by an interventricular septum. The left ventricle opens into the aorta via the aortic valve and the right ventricle opens into the pulmonary arteries via the pulmonary valve (Humphrey & McCulloch, 2003). Upon contraction, the mitral and tricuspid valves close and the outflow valves are opened due to a pressure differential between the ventricles and the outflow tracts (Humphrey & McCulloch, 2003; Thiriet, 2008). The wall of the heart is made of three distinct layers: endocardium, myocardium, and epicardium (Humphrey & McCulloch, 2003).

The innermost endocardium is a thin layer comprised of endothelial cells, collagen, and elastin. The middle myocardium is the thickest, and primarily composed of contractile cardiomyocytes, which form the functional layer of the heart. The outermost epicardium is another thin layer of collagen and elastic fibers. The heart is further contained by a pericardium, a fluid filled sac that physically limits heart distension (Thiriet, 2008). In this thesis, the left side of the heart, specifically the left ventricle will be the main focus.

1.2. Cardiac excitation-contraction coupling

Pathways which use calcium (Ca^{2+}) as a second messenger are highly sophisticated and tightly regulated both spatially and temporally. In cardiomyocytes, the concentration of intracellular Ca^{2+} ($[Ca^{2+}]_i$) facilitates the conversion of an electrical signal to a physical response in the form of cardiac contractions (Bers, 2002).

Cardiac muscle is unique in its myogenic characteristics. Meaning that, although heart rate is influenced by the autonomic nervous system, the myocardium holds the ability to generate its own electrical stimulus to trigger a contraction. In a healthy heart, these electrical signals originate in pacemaker cells found in the sinoatrial node (Nerbonne & Kass, 2005). These electrical signals are then converted to a physical response at the level of the myocytes in a process called excitation-contraction (EC) coupling.

Pacemaker cells will auto-depolarized due to a depolarizing funny current (I_f) supplied by hyperpolarization-activated cyclic nucleotide-gated cation (HCN) channels (Bers, 2002). Once the I_f brings the pacemaker membrane potential above its depolarization threshold, voltage-gated sodium (Na^+) channels will open contributing to the rapid upstroke of phase 0 in a cardiac action potential (AP). This electrical signal will then arrive at the myocyte sarcolemma and open L-type calcium channels (LTCCs), which respond to the change in membrane potential allowing an

influx of extracellular Ca^{2+} (Bers, 2002; Eisner et al., 2017). This influx of positive charge will counteract any repolarizing effects and keep the myocytes in a depolarized state, entering phase 2 of the cardiac AP. However, the influx of extracellular Ca^{2+} at the surface of myocytes is not sufficient to trigger contraction. The AP will instead propagate along invaginations of the sarcolemma known as transverse tubules (t-tubules) (Figure 1-1) to open LTCCs along its surface and deliver Ca^{2+} to the dyadic space (Eisner et al., 2017). The dyadic space is the region between the t-tubules and the sarcoplasmic reticulum (SR) which situates the LTCCs in close proximity to clusters of ryanodine receptor 2 (RyR2) on the SR (Eisner et al., 2017) (Figure 1-2). The distance between RyR2 clusters and LTCCs is approximately 15 nm with each cluster having 14-100 RyR2s (Eisner et al., 2017; Soeller & Baddeley, 2013). This spatial distribution is essential in EC coupling because the initial Ca^{2+} influx via LTCCs opens RyR2 clusters to produce a much larger efflux of Ca^{2+} from the SR. This process of calcium release is known as calcium-induced-calcium release (CICR) (Figure 1-3).

Following this rapid rise in $[Ca^{2+}]_i$, the contractile machinery is then activated. Ca^{2+}, acting as a second messenger, triggers the shortening of sarcomeres and thus produces the physical response of contraction. The bulk of sarcomeres comes from the myosin thick filaments and actin thin filaments which are sequestered by the troponin regulatory complex (Parmacek & Solaro, 2004). In low $[Ca^{2+}]_i$ states, the three cardiac troponin subunits (cTnC, cTnI, and cTnT) block the myosin-actin binding sites by anchoring tropomyosin to the actin thin filament (Parmacek & Solaro, 2004). Tropomyosin is an alpha-helical coiled-coil protein bound by cTnT and spans seven actin subunits (Yamada et al., 2020). In high $[Ca^{2+}]_i$ states, free Ca^{2+} binds cTnC inducing a conformational change that lifts the inhibitory region of cTnI from the actin thin filaments. This conformational change also shifts tropomyosin, exposing the myosin binding

sites on the actin subunits (Gordon et al., 2001). Thereafter, the actin thin filament is bound by the myosin thick filament and ATP dependent cross-bridge cycling pulls the ends of the sarcomere, shortening the unit and by extension producing cardiac contraction (Gordon et al., 2001) (Figure 1-4). However, for the heart to distribute blood in the body, it must also fill, and so cardiac muscle must relax (Figure 1-5). Relaxation of cardiac muscle follows the closure of RyR2 and the removal of Ca^{2+} via a sarco/endoplasmic reticulum Ca^{2+}-ATPase 2a (SERCA2a), which actively pumps the free Ca^{2+} back into the SR, and a sodium-calcium exchanger 1 (NCX1), which moves Ca^{2+} out of the myocyte in exchange of Na^{+} moving into the cell (Figure 1-6). The reduction in Ca^{2+} influx coupled with repolarizing potassium currents brings the cardiac AP into phase 3 and back to the resting membrane potential in phase 4.

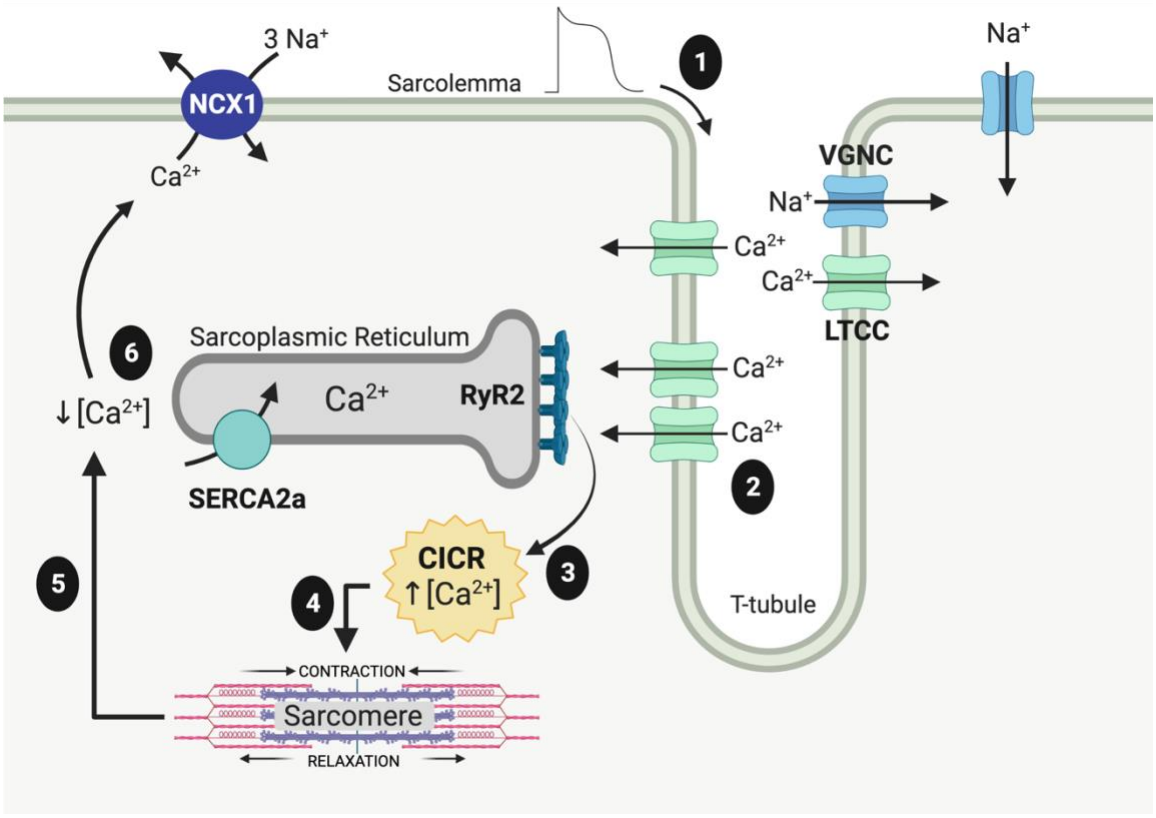


Figure 1: Cardiac excitation-contraction coupling. An electric signal (1) will propagate along the sarcolemma and down t-tubules to activate voltage-gated sodium channels (VGNC) and (2) L-type calcium channels (LTCC). Extracellular calcium will enter the dyadic space and (3) open ryanodine receptors (RyR2) on the sarcoplasmic reticulum (SR) to release calcium from a much larger store in a process called calcium-induced-calcium release (CICR). This creates a rapid increase in intracellular calcium concentrations [Ca^{2+}] which (4) activate sarcomeric actin and myosin cross-bridge cycling and thus contraction. Relaxation (5) is achieved by returning cytosolic [Ca^{2+}] to diastolic levels by actively transporting Ca^{2+} back to the SR via sarco/endoplasmic reticulum Ca^{2+}-ATPase 2a (SERCA2a) and shuttling Ca^{2+} back to the extracellular space via a sodium-calcium exchanger 1 (NCX1) (6). Figure was generated using BioRender.com.

1.2.1. Calcium-induced-calcium release proteins

After having introduced EC coupling, one can recognize the importance of CICR and the involved proteins. As previously mentioned, RyR2 clusters and LTCCs are separated by approximately 15 nm, meaning RyR2s respond to localized increases in $[Ca^{2+}]_i$ to enact a much larger response (Eisner et al., 2017; Soeller & Baddeley, 2013). Each RyR2 is made of 4 subunits and 4 FK506 binding proteins (FKBP12.6) (Brillantes et al., 1994). These binding proteins serve to stabilize the interaction between subunits and coordinate activity. The RyR2 clusters to function together, opening as a unit during contraction and remaining closed as a unit during relaxation (Marx et al., 2001). The opening of RyR2s produce Ca^{2+} sparks which through coupled gating open neighbouring channels and produce Ca^{2+} waves as even more RyR2 clusters open (Zhang et al., 2015). These Ca^{2+} waves can propagate along the myocyte or occur simultaneously to produce a global increase in $[Ca^{2+}]$ known as a Ca^{2+} transient (Figure 2A) (Laver & Honen, 2008). This rapid rise in cytosolic Ca^{2+} activates contractile machinery leading to sarcomere shortening and thus contraction (Figure 2B). When SR luminal Ca^{2+} begins to deplete, RyR2s will inactivate and given their coupled gating, entire clusters will inactivate and remain as such. This stops SR Ca^{2+} efflux and allows for removal of cytosolic Ca^{2+} to begin (Marx et al., 2001). The removal of cytosolic Ca^{2+} is seen as the downstroke of a Ca^{2+} transient waveform and leads to sarcomere lengthening or relaxation.

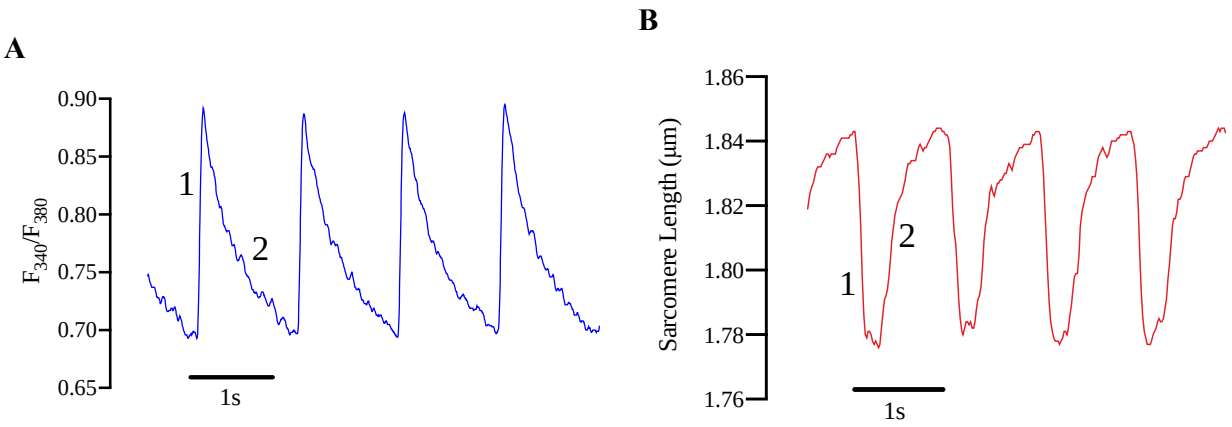


Figure 2: Calcium transient (A) and sarcomere shortening (B) of a mouse left ventricular cardiomyocyte. The rapid upstroke (A1) shows the rapid rise of cytosolic Ca^{2+} via CICR within a single mouse cardiomyocyte, which leads to the shortening of sarcomeres (B1) by activating contractile machinery in the presence of high $[Ca^{2+}]_i$. The removal of cytosolic Ca^{2+} (A2) then allows for relaxation or lengthening of sarcomeres (B2). The cycling of cytosolic Ca^{2+} transients were measured by tracking fluorescence ratios (F340/F380) of Fura-2AM and sarcomere length was measured via pixel tracking in a fixed region spanning seven repeating sarcomeres. The IonOptix myocyte calcium and contractility systems were used to collect data.

1.3. Sex differences in cardiac excitation-contraction coupling

Historically, studies have neglected to take into consideration sex differences of cardiac function. Unless directly being evaluated, many studies have overlooked the structural and functional differences between male and female hearts. Working heart comparisons in rats have shown that females have significantly lower ejection fraction and fractional shortening when compared to age-matched males (Schaible & Scheuer, 1984). Cardiac output and maximum left ventricle systolic pressure were also found to be significantly lower in female rat hearts (Schaible & Scheuer, 1984). These differences persist when evaluating the molecular components of EC coupling in isolated rat left ventricle (LV) myocytes. Female rat LV myocytes display significantly smaller and longer Ca^{2+} transients as seen by slowed time-to-peak and 50%-relaxation when compared to LV myocytes of age-matched males (Curl et al., 2001; Leblanc et

al., 1998). Female rat myocytes also display slower transient decay rates and thus have slowed reuptake of Ca^{2+} (Curl et al., 2001; Wasserstrom et al., 2008). Farrell and colleagues did voltage clamp experiments in which contraction, Ca^{2+} transients, and LTCC Ca^{2+} currents were simultaneously recorded from female rat ventricular myocytes (Farrell et al., 2010). In this series of experiments, different components of EC coupling were evaluated. Female rat LV myocytes had significantly lower peak contractions and slower rate of shortening, similar to the intact/working heart experiments (Farrell et al., 2010; Schaible & Scheuer, 1984). The peak magnitudes of Ca^{2+} transients and contractions were both significantly lower in females, however, the LTCC Ca^{2+} currents were similar between males and females (Farrell et al., 2010). Notably, female LV myocytes had significantly longer time-to-peak transient measures and lower rate of rise of Ca^{2+} transients when compared to males (Farrell et al., 2010). The reduced contraction coupled with low magnitude Ca^{2+} transients led the researchers to evaluate calcium gain. Calcium gain was measured as Ca^{2+} flux per unit of LTCC Ca^{2+} current and was found to be significantly lower in female myocytes (Farrell et al., 2010). Caffeine-induced Ca^{2+} transients revealed that there was no difference in SR Ca^{2+} stores between male and female rats (Farrell et al., 2010). The difference in calcium gain was deemed not to be due to changes in Ca^{2+} current through LTCCs or SR Ca^{2+} stores, which were similar in male and female rats. Studies focused on the expression profiles of EC coupling genes have identified sex differences in gene and protein expression. Chu et al. (2005) reported higher protein levels of $Ca_V1.2$ (the α subunit of LTCC), RyR2, and NCX1 in female rats compared to males. RNA message of RyR2 and NCX1 was significantly higher in females, while $Ca_V1.2$ mRNA was more abundant in males (Chu et al., 2005). SERCA2a expression was similar in male and female rats, both at protein and message stages (Chu et al., 2005).

In CD1 mice, however, no difference in ejection fraction or fractional shortening was seen in Doppler-echocardiography studies (Stypmann et al., 2006). The contrasting results in CD1 mice could be contributed to the use of ketamine-xylazine-narcosis as an anaesthetic which led to lower than normal heart rates. Since narcotics impact the autonomic tone and thus alter heart rate, any sex differences in CD1 mice of this particular study could have been masked by the anesthetic (Stypmann et al., 2006). Sex differences as seen in rat models were observed in isolated LV myocytes of mice as well. C57BL/6 mice showed significantly smaller Ca^{2+} transients in female ventricular myocytes when compared to age-matched males (Parks et al., 2014). LTCC Ca^{2+} currents and decay were similar between female and male mice. Calcium gain, reported as the ratio of SR Ca^{2+} release to peak LTCC Ca^{2+} current, was significantly lower in female mice (Parks et al., 2014). In another study, contraction times were found to be significantly longer in female myocytes compared to male myocytes (Grandy & Howlett, 2006). The time-to-peak and half-relaxation time for female myocytes was significantly greater, indicating prolonged Ca^{2+} transient durations as seen in rat myocytes (Farrell et al., 2010; Grandy & Howlett, 2006). Ca^{2+} spark events in female myocytes are significantly smaller in amplitude with faster decay rates, indicating that female myocytes have smaller and rapidly decaying SR Ca^{2+} release units (Parks et al., 2014). Consequently, despite having similar SR Ca^{2+} stores, the percentage of Ca^{2+} released from the SR is lower in female myocytes compared to males (Parks et al., 2014).

As seen from the studies mentioned, sex differences in cardiac EC coupling in murine hearts directly impact intrinsic contractility. Therefore, studies which use murine models to evaluate cardiac response should take into consideration differences based on sex.

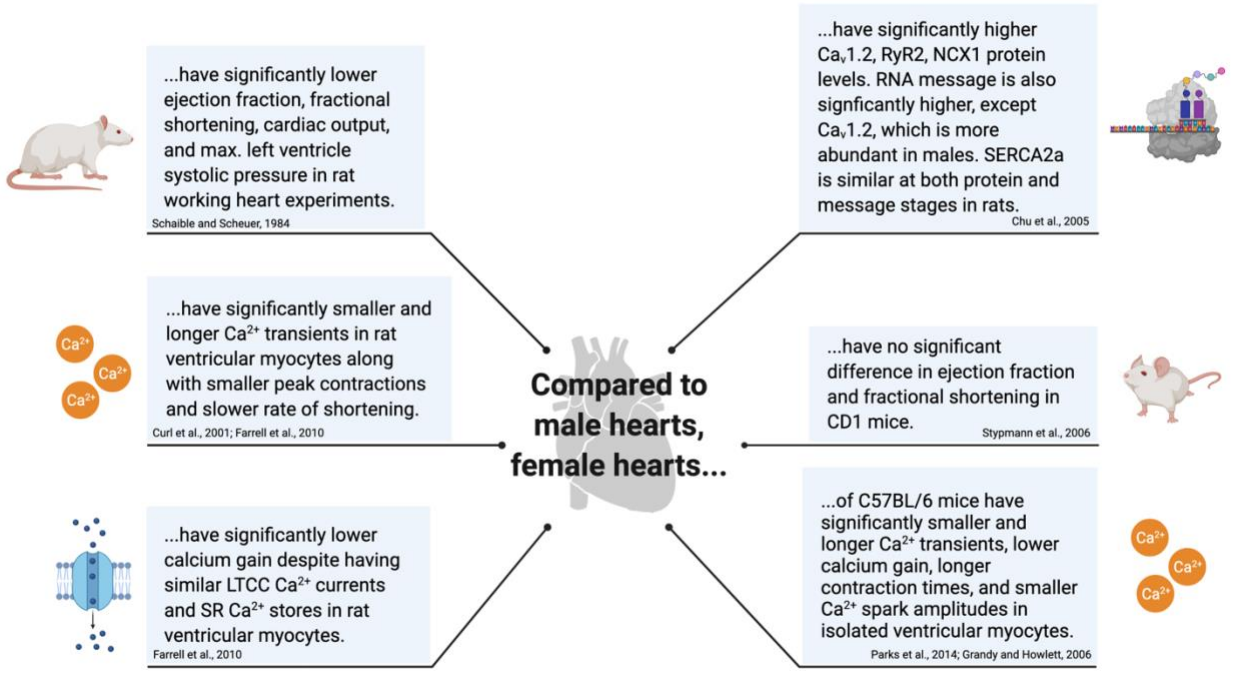


Figure 3: Summary of sex differences in murine hearts. Figure was generated using BioRender.com.

1.4. Endocrine function of the heart

Like all organs and organ systems the heart has the ability to communicate via hormone signals to enact body-wide changes in blood volume and thus blood pressure (McGrath et al., 2005; Rubattu et al., 2004). The endocrine function of cardiac tissue was first identified by de Bold and colleagues in 1978. The researcher's 1978 paper presented data which indicated highly developed Golgi complexes, greater rough endoplasmic reticulum, and membrane bound storage granules in rat atrial cardiomyocytes (de Bold et al., 1978). These findings suggested a site of active protein synthesis and modification in cells previously thought to only partake in contraction. When compared to adult rat ventricular cardiomyocytes these features were not seen. The team speculated that the granules seen in atrial histological slides were those reminiscent of granules present in cells which are actively synthesizing, storing, and releasing

peptide hormones. The researchers investigated these features further and, in a follow up paper, concluded that there was indeed a "factor" in atrial muscle that was causing body wide changes as a hormone would (de Bold et al., 1981). The author utilized anesthetised non-diuretic rats and injected those rats with the supernatant of atrial and ventricular myocardial homogenates (de Bold et al., 1981). The atrial muscle injections yielded a 30-fold increase in sodium and chloride excretion, a 10-fold increase in urine volume, and a 2-fold increase in potassium excretion (de Bold et al., 1981). When the same experiment was done with ventricular muscle homogenates no change was seen allowing the group to conclude that an "extremely powerful inhibitor" from the atrial extracts was blocking sodium chloride reabsorption at the nephron (de Bold et al., 1981). This factor or inhibitor was later sequences and named atrial natriuretic factor (ANF), now known as the peptide hormone atrial natriuretic peptide (ANP) (Seidah et al., 1984).

Further studies into the release of ANP from cardiomyocytes revealed a developmental disparity in ANP synthesis. Bloch and colleagues in 1986 observed that both atrial and ventricular cardiomyocytes could synthesize and secrete ANP at the neonatal stage. Of the two cell types, atrial cardiomyocytes possessed the ability to synthesize and store ANP in secretory granules while ventricular cells could not store ANP following its synthesis. The team concluded that neonatal cardiomyocytes constitutively secrete ANP, however, atrial cardiomyocytes also had the added ability to store ANP and have regulated, stimulus dependent secretion as well (Bloch et al., 1986). Adult ventricular cardiomyocytes were seen to lack the ability to synthesize ANP but instead became responsible for the synthesis and release of brain natriuretic peptide/factor (BNP/F) (McGrath et al., 2005). Both ANP and BNP, although originating from different regions of the heart, share similar biological effects upon their release such as altering blood volume and/or blood pressure (Nishikimi et al., 2006). One such system that ANP

regulates is the renin-angiotensin-aldosterone system (Wilkins et al., 1997). Since ANP is released in response to atrial stretch, indicating an increase in blood volume and thus blood pressure, its effects counteract those of the renin-angiotensin-aldosterone system to decrease blood volume and blood pressure (Stephenson & Broughton Pipkin, 1990).

1.5. SNARE mediated exocytosis

As mentioned, atrial cardiomyocytes possess the ability to store and release ANP upon a mechanical stimulus in the form of atrial stretch. The secretory granules must, therefore, have the correct membrane proteins to ensure the optimal and timely release of their contents. To achieve this, specialized proteins are required on the vesicle containing the cargo of interest and the target membrane to which the vesicle will fuse. These specialized proteins are known as soluble N-ethylmaleimide-sensitive factor (NSF) attachment protein receptor proteins or "SNARE proteins" (Ungermann & Langosch, 2005). SNAREs share similar structural features such as a central coiled-coil SNARE domain which is flanked by a C-terminal alpha helical transmembrane anchor and a variable N-terminal domain (Ungermann & Langosch, 2005). SNARE proteins can be classified as either R- or Q-SNAREs, named by the conserved arginine (R) or glutamine (Q) residue in their SNARE domain. However, prior to this, the nomenclature classified these proteins as either t-SNAREs or v-SNAREs corresponding to whether they were localized to the incoming vesicle membrane or the target membrane (Gerst, 1999). During regulated exocytosis, v-SNAREs will pair with t-SNAREs to "dock" the vesicle and form a *trans*-SNARE complex or "SNAREpin" (Söllner, 2003; Weber et al., 1998). The SNAREpin itself is a four-helix complex with one helix donated by R-SNAREs and three coming from Q-SNAREs (Ungermann & Langosch, 2005). The SNAREpin will remain in the *trans*

conformation until a signal triggers a conformational change of this structure. The transition from a *trans* to *cis*-SNARE complex will pull the two membrane bilayers together and promote the fusion of the lipid bilayer leaflets (Söllner, 2003). This mode of SNARE-mediated exocytosis has been studied in detail in the setting of axon terminals, specifically the release of neurotransmitters as seen in Figure 4. SNARE complexes made of syntaxin, synaptosomal associated protein of 25 kDa (SNAP-25), and vesicle associated membrane protein (VAMP) also known as synaptobrevin have been identified to mediate regulated exocytosis of neurotransmitters (Chen & Scheller, 2001). For example, vesicles containing neurotransmitters will arrive at the axon terminal where the v-SNARE, synaptobrevin, will complex with cognate t-SNAREs, syntaxin-1A (STX1A) and SNAP-25, to form a *trans*-SNARE complex (Chen & Scheller, 2001; Weber et al., 1998). A voltage gated calcium channel will allow calcium ($Ca^{2+)}$ to enter the cell and bind synaptotagmin, which acts as a Ca^{2+} sensor to induce the conformational change needed to fuse the two membranes and form a pore through which the vesicle cargo can be released (Weber et al., 1998). The close proximity of exocytotic machinery with voltage sensitive Ca^{2+} channels form "excitosome complexes" which place the trigger for membrane fusion near the docked vesicle. This configuration makes exocytosis and the release of vesicle cargo an efficient and rapid process (Cohen et al., 2007; Wiser et al., 1999).

Early work in secretory pathways was done in yeast, with mutations to syntaxin-like genes resulting in impaired membrane fusion as seen by build-up of post-golgi vesicles destined for exocytosis (Aalto et al., 1993). Given that STX1A is participating in neurotransmitter release, this sparked interest in studying the protein *in vivo* by utilizing STX1A knockout models. Early body wide STX1A knockout studies using *Drosophila* and *Caenorhabditis elegans* reported severely compromised neurotransmitter release leading to embryonic lethality (Saifee et al.,

1998; Schulze et al., 1995). When a body-wide STX1A knockout was done in C57BL/6J mice, the mice were surprisingly viable with normal growth and normal neurotransmitter release in the brain (Fujiwara, 2006). Instead, defects in insulin secretion were observed in STX1A knockout mice with fewer insulin secretory granules present in the "docked" configuration in pancreatic beta (β)-cells (Ohara-Imaizumi et al., 2007). Similar to the heart, β-cells have L-type Ca^{2+} channels that can trigger Ca^{2+} release events by opening RyRs on the endoplasmic reticulum; the difference being that the Ca^{2+} oscillations in β-cells trigger waves of insulin secretion and not contraction (Klec et al., 2019). STX1A knockout restricted to β-cells therefore resulted in impaired insulin secretion and no change to the Ca^{2+} current supplied by voltage-gated Ca^{2+} channels (Liang et al., 2017). Given the similarities of Ca^{2+} release events between β-cells and cardiomyocytes as well as the endocrine function of the heart, the role of STX1A in cardiomyocytes poses another unexplored feature of the protein.

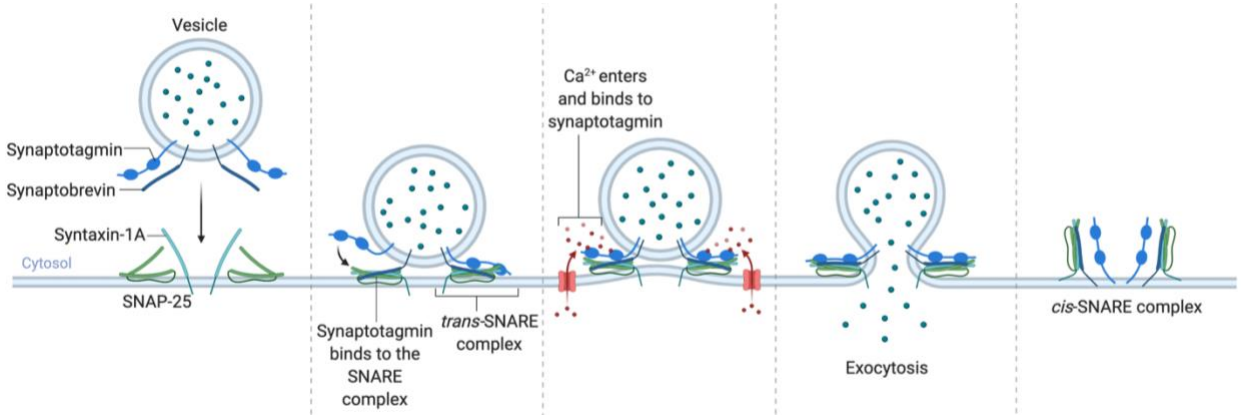


Figure 4: SNARE mediated exocytosis. Simplified schematic of an incoming vesicle carrying v-SNAREs, synaptobrevin and synaptotagmin, complexing with t-SNAREs, syntaxin 1A and SNAP25. The *trans*-SNARE complex undergoes a calcium-dependent conformational change to a *cis*-SNARE complex during which, the two leaflets of the vesicle and target membrane fuse, allowing the vesicle cargo to be released. Figure was generated using BioRender.com.

1.5.1. SNAREs in the heart

Having identified the heart as an endocrine organ and knowing that SNAREs participate in exocytosis, the presence of SNAREs in the heart is expected. Peters et al. (2006) identified that pro-ANP was present in whole heart and atrial myocytes of neonatal and adult rats along with multiple SNAREs, which had differing expression profiles dependent on developmental stages. In atrial myocytes of neonatal and adult rats, syntaxin-4 and SNAP-23 were detected, which are known to participate in GLUT-4 transporter translocation (Peters et al., 2006; Bowman et al., 2019). STX1A and SNAP-25 were also detected, but exclusively in adult atrial myocytes but not neonatal atrial myocytes (Peters et al., 2006). This was a novel finding, because until then, STX1A and SNAP-25 were associated with synaptic transmitter release and not yet identified in the heart. This suggested that the Ca^{2+}-dependent exocytosis of ANP might be controlled by STX1A in adult atrial myocytes. Further, SNARE proteins, VAMP-1, VAMP-2, and synaptotagmin-1, were found to co-fractionate with ANP granules, suggesting direct interaction of SNAREs and ANP (Peters et al., 2006). This provided further evidence supporting the claim that secretory pathways in the heart were governed by SNARE proteins as seen in other endocrine organs. In neonatal atrial myocytes, syntaxin-4, VAMP-1 and VAMP-2 were identified to form complexes (Peters et al., 2006). Within these complexes, VAMP-1 and VAMP-3 directly interacted with ANP granules (Ferlito et al., 2010; Peters et al., 2006). These SNARE proteins were also identified to be present in adult rat ventricles (Ferlito et al., 2010). Using small interfering-ribonucleic acid (siRNA), the functional interactions of SNAREs with ANP release was identified. Knockdown of VAMP1, VAMP2, or syntaxin-4 lead to significantly reduced ANP release (Ferlito et al., 2010). From this it was concluded that ANP release was regulated by SNARE complexes consisting of syntaxin-4 in neonatal rat atrial myocytes.

However, as previously mentioned, SNARE proteins have differing developmental expression profiles (Peters et al., 2006). In adult atrial myocytes, STX1A and SNAP-25 are expressed and associated with Ca^{2+}-dependent exocytosis. This, therefore, raises the question of what role STX1A plays in adult models due to its delayed developmental activation.

SNARES are not solely involved in exocytosis. SNAREs, especially syntaxins, have the ability to alter voltage-gated channel activity. In *Xenopus* oocytes, STX1A was seen to attenuate L-type Ca^{2+} currents through the alpha-1C subunit (α1C/Ca_v1.2) (Wiser et al., 1996). When STX1A was expressed with SNAP-25, the reduction in inward current was modest. SNAP-25 alone did not reduce inward currents but instead altered gating properties of L-type Ca^{2+} channels (Wiser et al., 1996). Further investigation revealed that STX1A physically interacts with voltage-gated Ca^{2+} channels (Wiser et al., 1999, 2002). The cytosolic domains of STX1A and SNAP-25 were identified to specifically bind to the cytoplasmic region separating transmembrane domains II and III of the α1C subunit, known as the synaptic protein interaction (synprint) site (Wiser et al., 1999). The cytosolic domain of STX1A was found to regulate Ca^{2+} channel activity because chemically cleaving this region with botulinum toxin C-1 removed the inhibition STX1A had on Ca^{2+} current amplitudes (Arien et al., 2003; Trus et al., 2001). Notably, in addition to binding the synprint site, cytosolic domain of STX1A also bound synaptotagmin, SNAP-25, synaptobrevin, α-SNAP, and NSF—the major components that facilitate SNARE mediated membrane fusion (Trus et al., 2001). The cytosolic domain of STX1A was also shown to impart channel selectivity, with the cytosolic region of STX1A preferentially binding L-type Ca^{2+} channels with some interaction with R-type channels (Ca_v2.3), while the cytosolic domain of syntaxin-3 preferentially bound R-type Ca^{2+} channels with some L-type interactions (Xie et al., 2016).

In addition to the cytosolic domain of STX1A, the transmembrane region also interacts with L-type calcium channels to modify their kinetic properties (Arien et al., 2003). This was determined by switching the transmembrane domain of STX1A with that of syntaxin-2. By doing so, the inhibition on Ca^{2+} current by STX1A was lost (Arien et al., 2003). However, the reverse, in which the transmembrane domain of STX1A was inserted into syntaxin-2, also did not show inhibition of Ca^{2+} currents (Trus et al., 2001). Therefore, the transmembrane domain of STX1A, although capable of inhibiting Ca^{2+} currents cannot do so independently from its cytosolic domain. Upon closer examination, the transmembrane domain was found to contain two cysteine residues, Cys-271 and Cys-272, which have since been identified to be essential in the regulatory characteristics of STX1A (Arien et al., 2003; Cohen et al., 2007). Point mutations of these cysteine residues to valine residues removed the inhibitory effects of STX1A and prevented STX1A monomers from homodimerizing (Arien et al., 2003)(Arien et al., 2003). However, the dimerized form was not the active form of the protein because Ca^{2+} current inhibition rapidly increased when the STX1A monomer to dimer ratio favoured monomers (Cohen et al., 2007). Hence, it has been proposed that the transmembrane domain of STX1A, is not only a site for homodimerization, but rather functions as a bridge in which each STX1A cysteine residue interacts with a Ca^{2+} channel to form clusters of three STX1A monomers and three Ca^{2+} channels (Liang et al., 2017). This interaction facilitates the formation of excitosome complexes and couples the trigger for exocytosis to the exocytotic machinery. Therefore, both cytosolic and transmembrane regions of STX1A interact with L-type Ca^{2+} channels with varying roles and effects (Figure 5).

Returning to the heart and keeping in mind that L-type Ca^{2+} channels are at the center of EC coupling, the known interactions of STX1A with voltage-gated Ca^{2+} channels pose an

interesting question of what effect STX1A has on cardiac EC coupling. Since cardiac contraction relies on the initial influx of Ca^{2+} via LTCCs to trigger SR Ca^{2+} release and thus contraction, the relationship between SNARES, specifically STX1A, and EC coupling remains yet to be established in the heart.

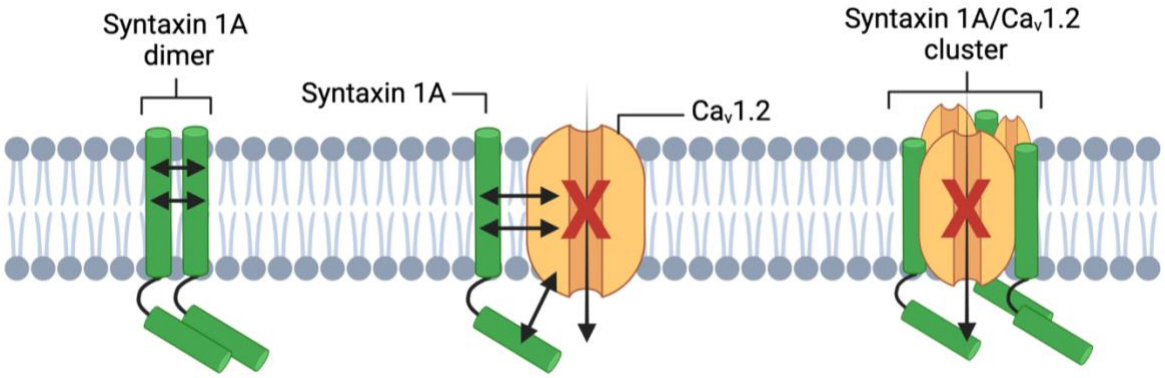


Figure 5: Simplified schematic of possible syntaxin 1A and Cav1.2 interaction sites. Syntaxin 1A is thought to interact with the pore forming subunit (Cav1.2) of voltage-gated calcium channels at cytosolic and transmembrane sites. The cytosolic domain of syntaxin 1A interacts with the synprint site of Cav1.2 and the transmembrane domain interacts with Cav1.2 via cysteine residues 271 and 272 of syntaxin 1A. The transmembrane domain is also thought to mediate the formation of syntaxin 1A and Cav1.2 clusters or allow for syntaxin-1A homodimers to form. Figure was generated using BioRender.com.

1.6. Previous work done in the Tsushima Lab

Due to STX1A's direct inhibitory effects on voltage gated Ca^{2+} currents, it was predicted that STX1A knockout in the heart would lift the negative regulation and result in positive inotropic and chronotropic effects on cardiac function. To explore this and achieve heart specific knockout of STX1A, a tamoxifen (TAM) inducible Cre-Lox system was employed. To limit knockout of STX1A to the heart, the mutated estrogen receptor linked Cre recombinase (MerCreMer) gene was put under the control of an alpha-myosin heavy chain promotor (Sohal et al., 2001). By doing so, the MerCreMer protein would be selectively expressed in the heart. To achieve STX1A knockout, the STX1A gene contained LoxP sites flanking exon 2 and 3 (Virdi, 2019). Therefore, upon TAM injections, the MerCreMer complex would be activated, translocate to the nucleus, and cleave the STX1A gene at the LoxP sites (Figure 6). Mice were then monitored for 6-weeks post-tamoxifen with experimental timepoints being 0-week, corresponding to 1 day after the 4^{th} injection, 1-week, 3-week, 4-week, and 6-week post-TAM.

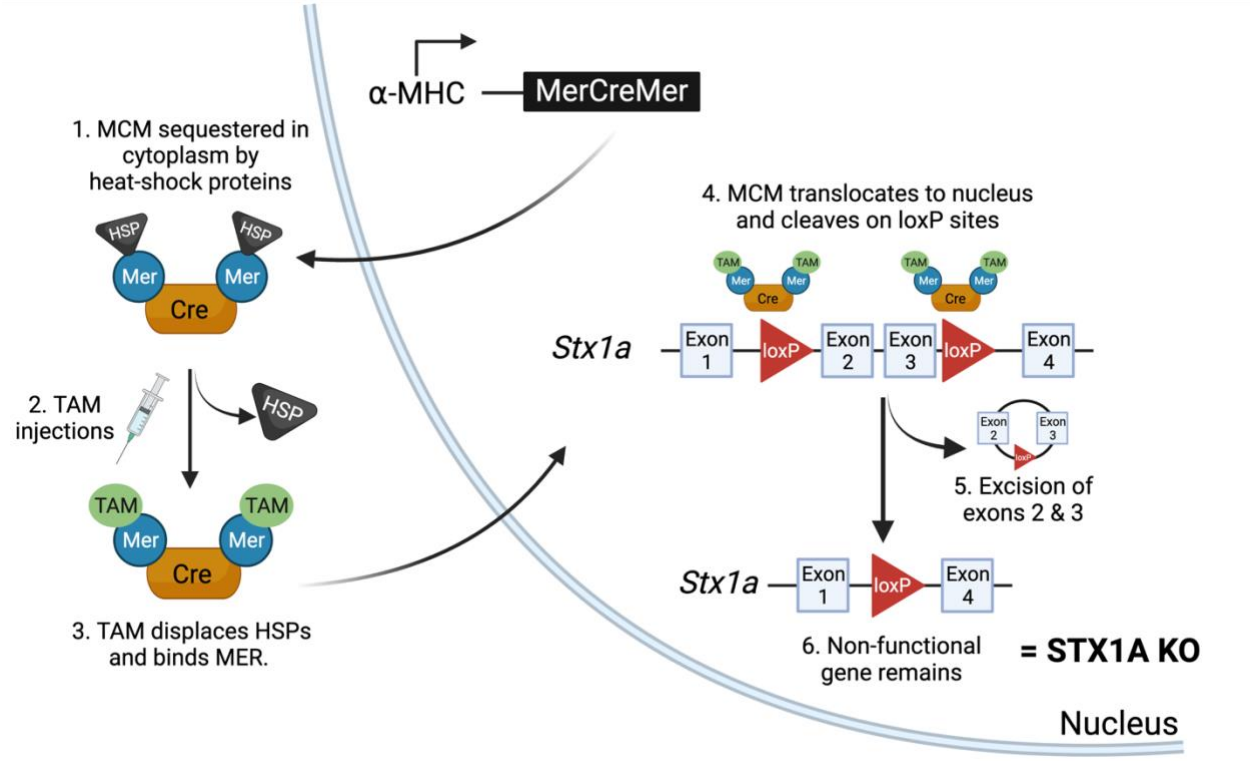


Figure 6: Schematic of the tamoxifen-inducible Cre-Lox system for heart-specific STX1A KO. The MerCreMer construct is put under the control of an α myosin heavy chain promotor (αMHC) allowing the MerCreMer protein (MCM) to be selectively expressed in the heart. MCM is (1) sequestered in the cytoplasm by heat-shock proteins (HSP) and upon (2) tamoxifen (TAM) injections, the (3) HSPs are displaced and TAM binds the mutated estrogen receptors (MERs). MCM (4) translocates to the nucleus where it cleaves loxP sites flanking exon 2 and 3 of the *Stx1a* gene. Excision (5) of exon 2 and 3 renders the *Stx1a* gene non-functional thereby achieving STX1A KO. Figure was generated using BioRender.com.

Contrary to this initial prediction, studied from the Tsushima lab revealed STX1A knockout resulted in severe loss of cardiac function assessed via echocardiographs (Virdi, 2019). Systolic dimension and volume were significantly increased upon STX1A knockout. Diastolic dimension and volume also increased significantly, thought, not as severely as the systolic function of STX1A knockout hearts. This in turn led to reduced ejection fraction and fractional shortening upon STX1A knockout (Figure 7). Of note, is that these changes were transient. The compromised systolic function of left ventricles showed recovery 1-week after STX1A knockout

via the tamoxifen-inducible Cre-Lox system. Recovery occurred from 1-week to 3-week post-tamoxifen treatments and by 4-week, STX1A knockout mice had recovered and were indistinguishable from control mice which received tamoxifen and expressed the Cre recombinase. Comparing ECG waveforms to contraction measured in echocardiographs showed delayed between the R-wave and the onset of contraction at 0-week and 1-week post-tamoxifen. This delay suggests transient electrical and contractile desynchrony and hints at possible uncoupling of excitation and contraction in the heart. By 3-week this delay was seen to recover and be indistinguishable from Cre-expressing mice (Bersell et al., 2013; Hougen et al., 2010; Koitabashi et al., 2009; Pugach et al., 2015).

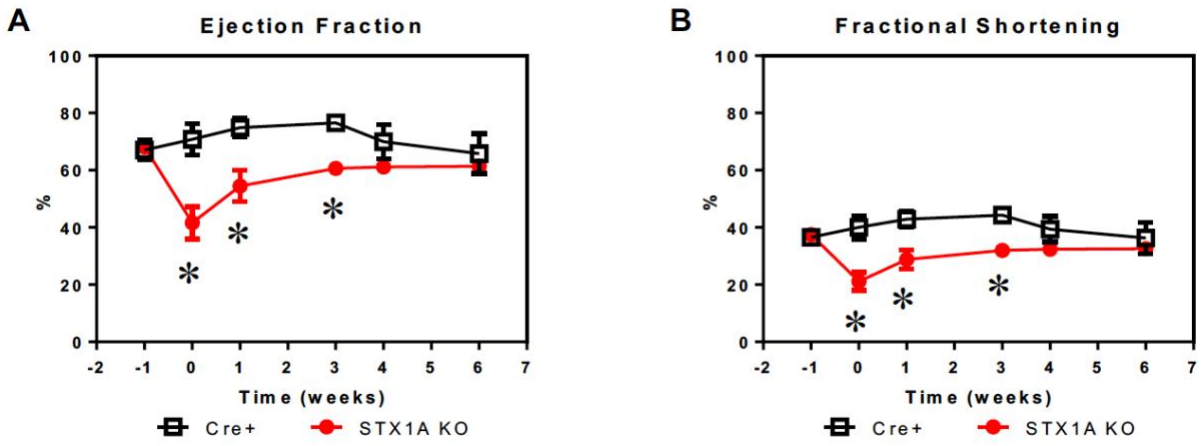


Figure 7: Ejection fraction (A) and fractional shortening (B) of STX1A knockout (KO) mice compared to Cre-expression mice (Cre+). STX1A KO mice (red circles) show significantly reduced ejection fraction and fractional shortening compared to Cre+ mice (black suqares) at 0-week to 3-week post-KO. Recovery occurs in weeks 1 to 3 until STX1A KO mice are similar to Cre+ mice at week 4. Figure has been taken from M.Sc. thesis submitted to York University by Manvir Virdi (2019).

1.7. Objectives and Hypotheses

The objective of this thesis is to further investigate the role STX1A plays in the adult mouse heart in relation to cardiac EC coupling. It is hypothesized that the absence of STX1A manifests as reduced contractility due to impaired CICR and recovery of contraction may occur due to compensatory SNARE interactions.

Given that STX1A knockout has been shown to result in reduced contractility, this begs the question of whether one copy of the wild-type STX1A gene is sufficient to retain the wildtype phenotype. Therefore, in addition to full STX1A knockout, heterozygous mice, which express ~50% STX1A will also be evaluated. To control for confounding cardiotoxic effects reported due to Cre recombinase activity and tamoxifen injections, mice expressing the MerCreMer protein complex that also receive tamoxifen injections will be set as controls (Cre+). Cre recombinase and tamoxifen have been shown to induce acute cardiomyopathy, fibrosis, DNA fragmentation, and be associated with high mortality rates in a dose-dependent manner, therefore, Cre+ control mice will serve as appropriate controls to account for such effects (Liang et al., 2017; Sohal et al., 2001).

Since the severe loss of heart function is transient, and spontaneous recovery has been observed to begin as early as 1-week post-STX1A KO, the question of what is causing the return of normal heart function and whether there are compensatory expression changes to other syntaxins will also be of interest. To address this, RT-qPCR on key calcium handling proteins and related syntaxins will be done. As previously mentioned, there are inherent sex differences in EC coupling. Previous work failed to take into consideration cardiac sex differences, hence, in this thesis the effects of STX1A knockout will be assessed in both male and female mice.

Chapter 2: Materials and Methods

Chemicals and reagents were purchased from Sigma-Aldrich Canada (Oakville, ON) unless specified.

2.1. Mouse model

Transgenic C57BL/6 mice, expressing the alpha-myosin heavy chain (α-MHC) promoter driving a Cre recombinase linked to mutated estrogen receptors (MERs), provided by Dr. Jeffery Molkentin (Cincinnati Children's Hospital Medical Centre, Cincinnati, OH) were crossed with syntaxin-1A$^{flox/flox}$ C57BL/6 mice obtained from Dr. Herbert Gaisano (University of Toronto, Toronto, ON) to produce heterozygous transgenic mice. Hence, Cre recombinase expression was restricted to cardiac myocytes and the LoxP sites flanking exon 2 and 3 of the syntaxin-1A gene allowed for tissue-specific knockout of syntaxin-1A (Bennett et al., 1993; Watson & Pessin, 2001). Both male and female mice 3-4 months of age were included and littermate mice possessing only the MER linked Cre recombinase (MCM) served as controls. Mice were provided normal chow diet with water *ad libitum.* All procedures were approved by the York University Animal Care Committee in accordance to the Canadian Council on Animal Care.

2.2. Mouse genotyping

Mice were anesthetized with isoflurane, ear tagged, and a small tail clipping was collected in a 1.5 mL Eppendorf tube. Bleeding was stopped with Kwik Stop™ styptic powder applied to the tail and mice were returned to their cage. Genomic DNA from the collected tail clippings was used to genotype experimental mice. To each 1.5 mL Eppendorf tube containing a tail clipping, 300 μL of 0.05N NaOH was added and samples were heated to 86°C on a dry bath.

After a 1.5 h incubation, samples were vortexed to disperse tissue and 100 µL of 0.5 M Tris-HCl buffer pH 8.0 (4.44% w/v Tris-HCl and 2.65% w/v Tris-base) was added to neutralize the DNA sample. Samples were stored at -20°C.

PCR on the isolated DNA samples was done to confirm the presence of the desired genotype. Each PCR reaction consisted of: 1 µM forward primer, 1 µM reverse primer, 10 µL of 2X PCR Taq Plus Master Mix (Applied Biological Materials), 4 µL Invitrogen ultra-pure DNase- and RNase-free water, and 2 µL of the isolated genomic DNA sample. Known DNA samples of $MCM^{+/-}$ and syntaxin-$1A^{flox/flox}$ mice were run as positive controls as well as ultra-pure water as the negative control. To determine the presence of α-MHC-MCM and LoxP sites flanking exons 2 and 3 of syntaxin-1A, primers specific to those constructs were used (Liang et al., 2016). Forward and reverse primers for the α-MHC-MCM gene were, forward: CGT CCT CCT GCT GGT ATA G, reverse: GTC TGA CTA GGT GTC CTT CT. Forward and reverse primers for syntaxin-1A were, forward: GCT GCA GAA GCA AGA GAA CC, reverse: CAG CCA TAC AAA AAC CAC CA. α-MHC-MCM reactions were run with an initial activation at 95°C for 5 min followed by 39 cycles of 95°C for 30 sec, 50°C for 30 sec, and 72°C for 30 sec. Syntaxin-1A reactions were run with an initial activation at 95°C for 5 min followed by 34 cycles of 95°C for 30 sec, 60°C for 30 sec, and 72°C for 30 sec. Samples were held at 4°C by the thermal cycler.

PCR products were resolved on a 1.5% (w/v) agarose gel prepared in 0.5X Tris-acetate-EDTA (TAE; 20 mM Tris-base, 10 mM acetic acid, and 0.5 mM EDTA). Agarose powder was dissolved in 0.5X TAE buffer by heating the mixture at 20 sec intervals in a microwave and allowing it to cool for 5 min before adding RedSafe 20 000X at 8% (v/v). The liquid agarose was poured into a casting tray and allowed to solidify for 20 min. PCR samples were prepared by adding 4 µL of 6X DNA loading dye (30% v/v glycerol, 0.25% w/v bromophenol blue, 0.25%

w/v xylene cyanol FF) directly to PCR tubes. The solidified gel was transferred to a gel box and filed with 0.5X TAE buffer, enough to just cover the gel. A 100-base-pair (bp) DNA ladder and 10 μL of the prepared PCR samples were loaded into their respective wells and a 100 V potential was applied for 20-25 min. The gel was visualized using the DNR Bio-Imaging Systems MiniBIS Pro.

2.3. Tamoxifen treatment

Tamoxifen citrate (Tocris Bioscience) was added to peanut oil (Sigma-Aldrich Canada) to get a final tamoxifen concentration of 10 mg/mL in a 1.5 mL Eppendorf tube. The mixture was vortexed 3x for 20 sec and sonicated (10% amplitude) 2x for 30 sec on ice. The prepared tamoxifen was administered via intraperitoneal injection (40 mg/kg) to 3-4-month-old mice of the desired genotypes. Four consecutive tamoxifen injections were administered over a 4-day period.

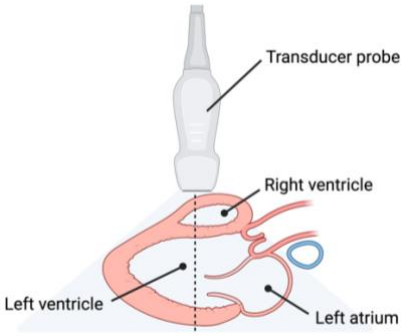
2.4. Echocardiography

Transthoracic 2D, M-mode echocardiography was performed on anaesthetized mice using the VisualSonics Vevo 2011 high resolution ultrasound imaging system (FUJIFILM VisualSonics, Toronto, ON). Mice were placed in a chamber initially supplied with 3% isoflurane in oxygen via an isoflurane vaporizer. Once a breathing rate of 1 Hz was observed, mice were placed supine on a heated electrode pad. A nose cone was positioned over the snout of the mouse which delivered a constant supply of 1.5-2% isoflurane. Electrode gel was applied to front and hind paws and taped securely over electrodes. A rectal probe was inserted, and core body temperature was maintained between 37.2-37.4°C. Using an electric shaver followed by

depilatory cream, fur along the thorax was removed to expose the skin. A generous amount of acoustic gel was placed on the thorax into which an ultrasound probe was lowered. The probe was mounted on a micro-manipulator.

To begin, the mid-sagittal axis of the left ventricle (LV) was identified in long axis B-mode and used to horizontally align the base and apex of the heart. Next, short axis B-mode was used to align the papillary tendineae vertically respective to one another. Long axis B-mode was resumed, and the mid-sagittal axis of the LV was relocated, and proper alignment of the base and apex of the heart was confirmed. Mice were allowed to stabilize. B-mode scans yielded measurements of diastolic dimension, systolic dimension, and posterior wall thickness at the widest part of the LV. M-mode transthoracic views yielded measurements of end-diastolic dimension and volume, end-systolic dimension and volume, stroke volume, ejection fraction, fractional shortening, and cardiac output. Diastolic and systolic dimensions were measured from M-mode images acquired at the widest part of the LV. Remaining parameters such as end-diastolic volume, end-systolic volume, stroke volume, ejection fraction, fractional shortening, and cardiac output were derived automatically by the Vevo 2100 high-frequency, high-resolution digital imaging system (Figure 8). Data was averaged from at least 3 cardiac cycles from a given M-mode loop and an average from 2 M-mode loops was recorded per measurement period. M-mode views were also used to determine the time interval between ECG R-wave to the onset of contraction. Diastolic and systolic dimensions acquired in B-mode views were compared to those found in M-mode loops to ensure an error of only ±0.01 mm. All measurements were taken using the preinstalled VisualSonics cardiology package.

A



B

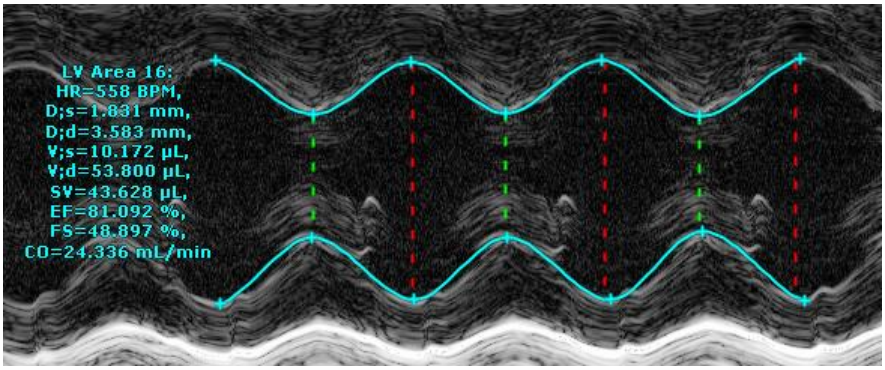


Figure 8: Positioning of left ventricle relative to (A) transducer probe in order to capture the widest part of the chamber and (B) representative M-mode measurements from Vevo 2100 high frequency, high-resolution digital imaging system. M-mode measurements shown include: heart rate (HR), end-systolic dimension (D;s), end-diastolic dimension (D;d), end-systolic volume (V;s), end-diastolic volume (V;d), stroke volume (SV), ejection fraction (EF), fractional shortening (FS), and cardiac output (CO). End-diastolic dimension (red line) and end-systolic dimension (green line) are measured by the user, remaining parameters were derived by the software. The anterior (top) and posterior (bottom) wall movement is shown by the blue line over 3 cardiac cycles. Figure 8A was generated using BioRender.com.

2.5. Tissue isolation

Mice were administered heparin (1000 IU/mL; hepalean, Organon Teknika, Toronto, ON) via IP injections prior to removing the heart. Heparin injections were prepared in 0.9% NaCl saline as a 1:10 ratio and stored at 4°C until use. Collection tubes and 1x Phosphate Buffered Saline (PBS; 145 mM NaCl, 2.7 mM KCl, 8.1 mM Na_2PO_4, pH 7.4) were kept on ice. Following a 5 min waiting period, heparin-injected mice was transferred to a small enclosed chamber and a cotton swab dipped in isoflurane was added. Once the toe-pinch reflex was abolished, mice were

euthanized via cervical dislocation. Mice were positioned supine, taped down, and the chest was sprayed with 75% ethanol. Working quickly, a deep transthoracic incision revealed the diaphragm, which was cut away to gain entry to the chest cavity. Cuts along the ribs allowed the rib cage to be lifted and held back using a hemostat. Using curved forceps, the heart was gripped anterior to the atria and lifted. Once excised, the heart was plunged in ice-cold 1xPBS to wash out any remaining blood. This was repeated once. The washed heart was viewed under a dissecting microscope and the atria, right ventricle, intraventricular septum, and left ventricular free wall were separated and placed in corresponding ice-cold collection tubes. The isolated tissue was stored at -80°C.

2.6. Protein isolation

Working on ice, frozen tissue samples were transferred to a glass homogenizer containing ice-cold freshly prepared NP-40 lysis buffer (10mM NaCl, 10 mM Tris pH 7.4, 3mM $MgCl_2$, 1% Nonidet-40, and 1 Complete Mini EDTA-free protease inhibitor tablet per 10 mL prepared buffer). Samples were manually homogenized, transferred to a 1.5 mL Eppendorf tube, sonicated, and centrifuged for 15 minutes at 13,000 x g at 4°C. The supernatant was collected and stored at -80°C.

2.7. Bradford-Lowry protein assay

Concentration of isolated protein from tissue samples was quantified via a Bradford protein assay. A standard curve of known protein concentrations (1, 0.5, 0.25, 0.125, 0.0625 μg/μL) was generated using bovine serum albumin (BSA). The first set of semi-micro disposable cuvettes contained 20 μL of the prepared BSA standards with an additional "blank" containing 20 μL of

ultrapure water. The second set of cuvettes contained the samples of unknown protein concentration diluted in a 1:10 ratio (2 µL samples + 18 µL ultrapure water). Hereafter, all cuvettes received the following, 100 µL Bio-Rad reagent A+S (1mL Reagent A, Bio-Rad # 5000113, and 20 µL Reagent S, Bio-Rad #5000115, Mississauga, ON) and 800 µL Bio-Rad Reagent B (Bio-Rad #5000114). Cuvettes were mixed, covered, and incubated for 20 minutes in an opaque box. Absorbance at 750 nm was measured using an Eppendorf biophotometer and concentration of isolated protein samples was determined from the BSA protein standard curve.

2.8. Western blot

Protein lysates were diluted to concentrations compatible with western blot loading using 6X SDS reducing buffer (0.28 M Tris-HCl pH 6.8, 30% v/v glycerol, 10% v/v SDS, 0.5 M dithiothreitol, and 0.0012% bromophenol blue) and ultrapure water. Samples were then resolved on a freshly prepared SDS-polyacrylamide gel consisting of a 5% stacking layer (30% acrylamide/Bis solution 35.7:1, 1 M Tris-HCl pH 6.8, 10% SDS, 10% ammonium persulfate, ultrapure water, and TEMED) and a resolving layer with acrylamide percentage selected based on the size of the protein of interest (30% acrylamide/Bis solution 35.7:1, 1.5 M Tris-HCl pH 8.8, 10% SDS, 10% ammonium persulfate, ultrapure water, and TEMED). Prepared gels were clamped in electrophoresis chambers and filled with 1X Running Buffer (24 mM Tris-base, 180 mM glycine, and 3.4 mM SDS). Prepared samples were loaded to achieve the desired total protein amount for a given blot along with 3 µL of BLUelf prestained protein ladder (FroggaBio, PM008, Concord, ON). The electrophoresis chamber was closed, and samples were run at 100 V until samples reached the resolving layer, thereafter samples were run at 150 V until the dye front reached the bottom of the gel.

The electrophoresis chamber was disassembled, and the proteins separated on the SDS-polyacrylamide gel were transferred to a 0.45 μm nitrocellulose membrane. A transfer sandwich was assembled on gel holder cassettes in the following order: sponge, filter paper, gel, soaked nitrocellulose membrane, filter paper, and sponge. All components, except for the gel, were pre-soaked in chilled 1X Transfer Buffer (25 mM Tris base, 192 mM glycine, and 10% methanol). Once assembled, the gel holder cassettes were positioned in the electrode assembly in such a way that the gel faced the negative electrode. The electrode assembly was then submerged in a tank filled with chilled 1X Transfer Buffer and an ice pack. The entire assembly was subsequently placed in an ice-water bath and a constant 100 V was applied for 2h to allow for protein transfer.

Once the transfer was complete, the transfer apparatus was disassembled, and the nitrocellulose membrane was placed in a container and washed at room temperature 3x for 5 min while rocking with 1X Tris-buffered saline containing tween 20 (TBS-T, 2 mM Tris base, 13.7 mM NaCl, and 0.1% v/v tween 20). Next, the membrane was blocked in 5% w/v skim milk blocking solution made in TBS-T for 1 h at room temperature with gentle agitation. The blocking solution was discarded, and the membrane was washed as previously stated. Primary antibodies were prepared at a 1:1000 dilution in 1% BSA (1% w/v BSA in TBS-T and 0.02% v/v of 10% NaN_3) and added to the washed membrane for overnight incubation at 4°C with gentle agitation. Primary antibody solutions were removed and stored at 4°C for future use. The membrane was washed again before adding the secondary antibody solution prepared at a 1:10000 dilution in equal parts 1X PBS and 1% BSA. The membrane was incubated in secondary antibody solution for 1 h at room temperature with gentle agitation. The secondary antibody solution was removed and stored at 4°C for future use. The membrane was washed for 15 mins followed by 3

additional 5 min washes with 1X TBS-T. The membrane was scanned using the LI-COR odyssey infrared imaging system.

Table 1: List of antibodies used for western blotting.

	Host, Class	Supplier, Cat#	Dilution
Primary Antibodies			
Anti-syntaxin 1A	Rabbit, monoclonal	Abcam, #ab170889	1:1000
Anti-estrogen receptor α	Mouse, monoclonal	Invitrogen, #MA1-12692	1:1000
Anti-GAPDH	Mouse, monoclonal	Abcam, #ab8245	1:1000
Anti-β Actin	Mouse, monoclonal	Sigma-Aldrich, #A5441	1:1000
Secondary Antibodies			
Anti-Mouse	Goat, polyclonal	LI-COR, #926-32210	1:10000
Anti-Rabbit	Goat, polyclonal	LI-COR, #926-68071	1:10000

2.9. Densitometry analysis

Western blot images were analyzed using ImageStudioLite. For each western blot, the density of the protein of interest and the respective loading control was determined. The density quotient of the protein of interest and the loading control protein was calculated. The mean±SEM was graphed. All graphs were made using GraphPad Prism 8.

2.10.RNA isolation and cDNA conversation

A designated RNA isolation workbench and all required equipment was thoroughly cleaned with RNase*Zap*^{TM} RNase Decontamination Solution (Invitrogen, AM9780, Burlington, ON). Tissue samples were transferred to a glass homogenizer containing 1 mL of ice-cold

TRIzol Reagent (Invitrogen, 15596026). Samples were manually homogenized on ice before transferring the homogenate to RNase/DNase-free 1.5 mL Eppendorf tubes. Samples were incubated at room temperature for 5 minutes before adding chloroform in a 1:5 ratio of chloroform to homogenate. After a 3-minute incubation at room temperature, samples were centrifuged for 15 minutes at 12000 x g at 4°C. The aqueous phase was retained, to which 0.5 mL isopropanol was added and incubated for an additional 10 minutes. Next, samples were centrifuged for 10 minutes at 12000 x g at 4°C. The supernatant was discarded, and the RNA pellet was washed by resuspending the pellet in 75% ethanol followed by centrifuging the sample for 5 minutes at 7500 x g at 4°C. The ethanol wash was discarded, and the pellet was airdried before resuspending in DNase/RNase-free water. RNA samples were quantified using the NanoDrop Spectrophotometer and samples with a A260/A280 of ~2 were deemed pure.

Complementary DNA (cDNA) was generated the same day of RNA isolation. A total of 2 µg of total RNA was converted to cDNA using the High-Capacity RNA-to-cDNA kit (Applied Biosystems, Cat# 4387406, Waltham, MA). A single 20 µL reaction consisted of 2 µg of RNA, 1x reverse transcriptase (RT) buffer, 10x RT enzyme, and nuclease-free water. Using a thermal cycler, the reaction tubes were incubated at 37°C for 60 minutes followed by a 5 minutes incubation at 95°C to stop the reaction. Samples were held at 4°C by the thermal cycler before transferring tubes to -20°C for long-term storage.

2.11. qPCR primer design and primer efficiency

Primers were designed with Primer3 (https://bioinfo.ut.ee/primer3-0.4.0/) and specificity was determined using NCBI Primer Blast (https://www.ncbi.nlm.nih.gov/tools/primer-blast/). Primers were selected to be 10-22 bps with amplicon size restricted to 100-150 bps. Primer

melting temperatures were restricted to 58°C to 62°C, with a difference of ±2°C between primer pairs. Acceptable primer GC content was 50 to 60%. Primer pairs were then analyzed for possible hairpin structures, self-complementarity, primer-primer interactions, and mismatched annealing. For each gene, four candidate primers were selected and tested.

Efficiency of candidate primers was determined by conducting a serial qPCR with varying cDNA dilutions and primer dilutions. Control template cDNA diluted to 1:40 was used to generate cDNA standards of the following dilution ratios, 1:1, 1:2, 1:4, 1:8, and 1:16. Candidate primer pairs were tested at the following concentrations, 1μM, 0.5 μM, and 0.2 μM. At each primer concentration, qPCR for the cDNA standards was done. qPCR reactions were run using the StepOne Plus PCR System (Applied Biosystems) with SsoAdvanced Universal SYBR Green Supermix (Bio-Rad, Cat# 1725271). Standard cycling (95°C for 10 mins and, 40 cycles of 95°C for 15 sec and 60°C for 60 sec) followed by a melt curve stage (60°C to 95°C, at 0.3°C increments) was selected. Reactions were run in duplicates, along with negative controls lacking cDNA. Average C_t values were plotted against the logarithm cDNA standard. The slope of this relationship was used to calculate the primer efficiency (%).

$$Primer\ efficency\ (\%) = \left(10^{\frac{-1}{slope}} - 1\right) \times 100.$$

Primer efficiency within 90-110% was deemed acceptable. Dissociation melt curves were analyzed to confirm primer specificity. The candidate primer pairs which passed these tests were selected and the optimal primer dilutions were noted.

2.12.Quantitative real-time PCR

The mRNA expression of the genes of interest was quantified using the StepOne Plus PCR System (Applied Biosystems) with SsoAdvanced Universal SYBR Green Supermix (Bio-Rad,

Cat# 1725271). qPCR primers were optimized as previously mentioned and cDNA diluted to 1:40 in UltraPure™ DNase/RNase-free water (Invitrogen, 10977015) was used. Standard reaction protocol was selected from the thermal cycler, 95°C for 10 mins, 40 cycles of 95°C for 15 sec and 60°C for 60 sec, followed by a melt curve stage with stepwise heating from 60°C to 95°C, at 0.3°C increments. Transcript levels were compared to two housekeeping genes, *Gapdh and Actb*. Results were analyzed using the $2^{-\Delta\Delta Ct}$ method. All primers were purchased from Integrated DNA Technologies (Coralville, IA, USA).

Table 2: List of forward and reverse primers used for qPCR.

Gene	Forward Primer	Reverse Primer
Stx1a	CACTCAGTCAGACTACCGAGAA	TGATGATCCCAGAGGCAAAGAT
Stx2	TCTCAAGGACACCACAGAGATT	CGCAGAGCACACCCTAATTAC
Stx3	ACACGGACGAGGTTGAGATT	TCGGTGCAGAGAGAATGATACT
Stx4	GGAGTCCTGTCCCAGCAATTT	GCTCCTCGTCAGACACCATTC
Cacna1c	CATCACAATCAGCAGGCTAACA	TGTGACACAAAGATGCCCATAT
Ryr2	CACACTCACCCAGGCTCTTTAT	CTGCATAGCTCAACCCACTTAT
Slc8a1	AGTTGATGAGAGGGACCAAGAT	AGGACCTGGTAGTTGGCTAATT
Atp2a2	CCCAGAGAGATGCCTGCTTAAA	TCACACCATCACCAGTCATAGC
Actb	TGTGACGTTGACATCCGTAA	GCTAGGAGCCAGAGCAGTAA
Gapdh	ACCCAGAAGACTGTGGATGG	CACATTGGGGGTAGGAACAC

2.13.Statistical Analysis

Graphpad Prism 8 was used to generate all figures and perform all statistical tests. One-way ANOVA ($\alpha<0.05$) followed by multiple comparisons test in which p-values less that 0.05 were deemed significantly different.

Chapter 3: Results

3.1. Confirmation of transgenic genotypes

In order to selectively induce the excision of syntaxin-1A (STX1A) in only the heart, a two-part molecular mechanism was employed—the first being a tamoxifen (TAM) inducible Cre recombinase expressed specifically in the heart and the second being LoxP sites flanking (flox) the STX1A gene. PCR genotyping was used to confirm the presences of the desired transgenes (Figure 9). The STX1A flox sites were seen as a band at 239 bp and wild-type (WT) STX1A was seen as a band at 404 bp. In order to localize expression to the heart, the mutated estrogen receptor linked Cre-recombinase was put under the control of the alpha-myosin heavy chain promoter, forming the αMHC-MerCreMer (MCM) construct. All mice possessed the MCM construct, appearing as a band at 406 bp (Figure 9). STX1A knockout mice were homozygous for STX1A flox sites ($STX1A^{flox/flox}$; $MCM^{+/-}$) and appeared as a single band at 239 bp. Heterozygous STX1A knockout mice showed two bands at 404 bp and 239 bp, corresponding to WT and flox-ed STX1A genes ($STX1A^{flox/+}$; $MCM^{+/-}$), respectively. To account for MCM activity, mice lacking STX1A flox sites but expressing MCM ($STX1A^{+/+}$; $MCM^{+/-}$) were set as the control group and appeared as a single band at 404 bp indicating WT STX1A.

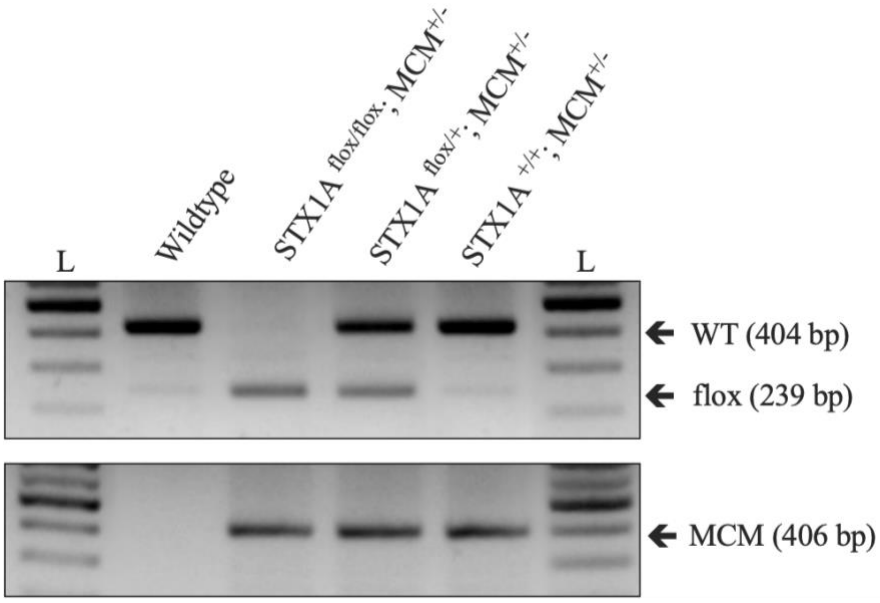


Figure 9: Representative genotyping results for MCM and flanking LoxP (flox) syntaxin-1A transgenes. PCR products were amplified from genomic DNA from tail clippings and resolved on a 1.5% agarose gel. The MCM band appeared at ~406 bp, the wildtype (WT) band for syntaxin-1A appeared at ~404 bp, and the syntaxin-1A flox band appeared at 239 bp. Image was taken using the DNR Bio-Imaging systems MiniBIS Pro.

3.2. Confirmation of inducible Cre-Lox system

To confirm the successful activation of the Cre-Lox system, western blots on left ventricular free wall samples were done. First, the presence of the MerCreMer (MCM) protein complex was confirmed. Initial attempts using multiple Cre antibodies failed to detect the MCM protein complex. As a result, MCM was indirectly identified by probing for mutated estrogen receptors physically linked to the Cre recombinase. MCM was therefore identified in western blots by using an antibody for the alpha subunit of estrogen receptors (α-ER). In addition to the α-ER band at 67 kDa, MCM positive ($MCM^{+/-}$) mice showed a band at 113 kDa, corresponding to the MCM protein complex while MCM negative ($MCM^{-/-}$) mice only possessed the α-ER band (Figure 10). β-actin served as a loading control to ensure consistent loading.

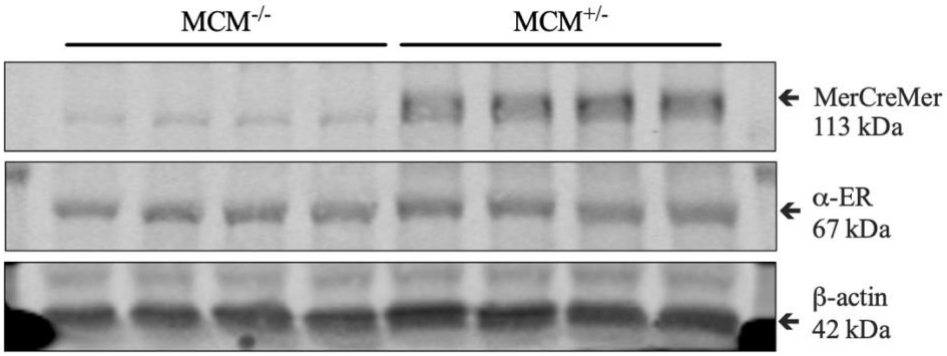


Figure 10: MerCreMer protein expression. Left ventricular free wall samples of $MCM^{-/-}$ (n=4) and $MCM^{+/-}$ (n=4) mice were tested. An estrogen receptor alpha subunit (α-ER) antibody (1:1000) was used to detect the mutated estrogen receptor in the MerCreMer protein complex. Hence, $MCM^{+/-}$ mice showed both the α-ER bands at 67 kDa and the MerCreMer bands at 113 kDa. β-actin was used as a loading control, appearing at 42 kDa. Each well contained 40 μg of protein. Image was acquired using the LI-COR Odyssey infrared imaging system.

Next, western blots on STX1A protein expression were done to determine successful protein knockout post-tamoxifen (TAM) injections. Homozygous STX1A knockout (STX1A KO) mice show successful knockout at 0-week, corresponding to 1 day after the 4th TAM injection, in both male and female mice (Figure 11A). Heterozygous STX1A knockout (STX1A+/-) mice showed successful partial knockout of STX1A at 0-week, post-TAM (Figure 11B). Control mice (Cre+) showed no change in STX1A expression post-TAM (Figure 11C). STX1A protein expression was further quantified by normalizing expression to GAPDH via densitometry analysis (Figure 11D). STX1A protein expression was reduced by 90% in STX1A KO mice (0.03, $p<0.0001$, n=12) when compared to pre-injection levels from non-injected mice (0.32, n=22). STX1A+/- mice (0.15, $p<0.0001$, n=11) showed a significant ~50% drop in STX1A protein expression when compared to pre-injection levels. In control Cre+ mice (0.32, n=6), STX1A protein expression remained comparable to that in pre-injection mice. Western blots used for densitometry are included in Appendix A.

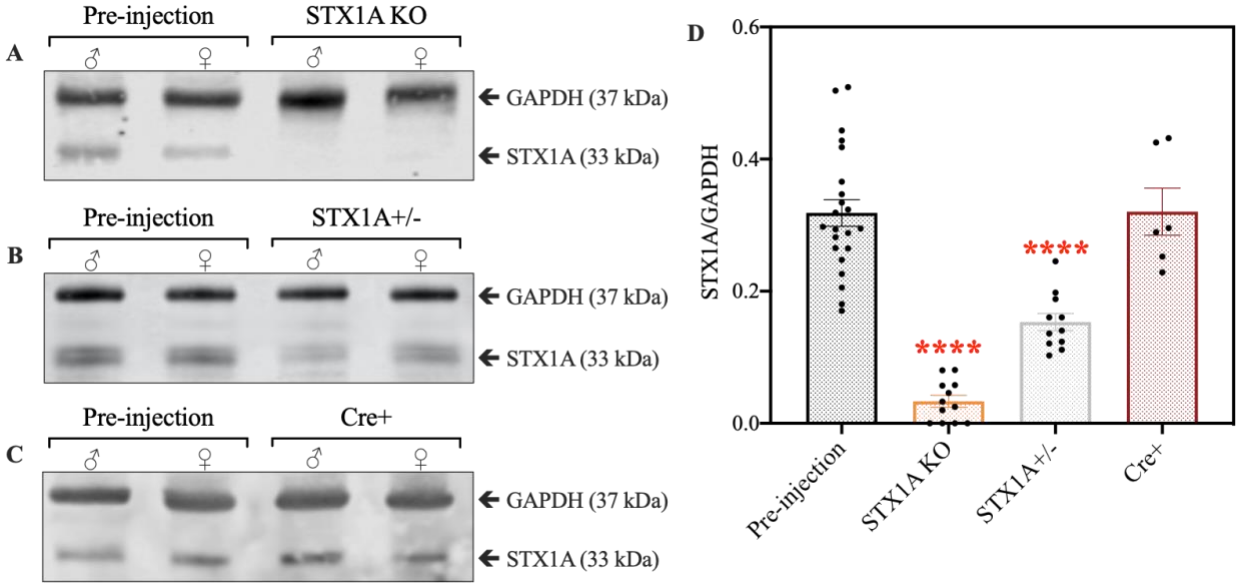


Figure 11: STX1A protein expression in the left ventricular free wall post-TAM. STX1A protein expression was compared between pre-injection and 0-week, post-TAM samples of male and female mice. Representative blots of STX1A KO (A), STX1A+/- (B) and control Cre+ (C) are shown. Each well contained 30 µg of protein. Full and partial STX1A knockout was seen in STX1A KO and STX1A+/- mice, respectively. STX1A protein expression was further quantified via densitometry analysis (D). STX1A band intensity was determined using ImageStudioLite and normalized to GAPDH. Bars represent mean±SEM and individual points are shown as black points. A significant 90% drop in STX1A protein expression was seen in STX1A KO mice (n=12), a significant ~50% drop was seen in STX1A+/- mice (n=11), and no change was seen in control Cre+ mice (n=6) when compared to pre-injection mice (n=22). One-way ANOVA followed by Tukey's multiple comparisons test was employed to determine statistical significance (********$p<0.0001$).

3.3. Left ventricle dimension and volume changes of STX1A deficient mice

Following confirmation of successful knockdown of STX1A protein, morphological and functional changes to the STX1A KO and STX1A+/- mouse hearts were tracked and compared to control MerCreMer-expressing tamoxifen-treated mice (Cre+) using 2D M-mode echocardiographic measurements. Baseline measurements before TAM treatment were denoted as -1-week measures. One day after the 4th TAM injection is denoted as 0-week, with the longitudinal study continuing for 6-weeks. The study was conducted in male and female mice.

First, dimensional and volume changes measured by end-systolic and end-diastolic dimension and volume were determined. Parameters relevant to systole showed that end-systolic dimension (mm) and volume (μL) significantly increase in STX1A KO and STX1A+/- mice at 0-week when compared to control Cre+ mice (Figure 12A-D). This rapid increase was followed by a robust recovery by 1-week post-TAM whereby, STX1A KO mice and STX1A+/- mice were comparable in end-systolic dimension and volume to control Cre+ mice. Interestingly, the rapid rise and subsequent recovery of end-systolic dimension and volume was seen in both STX1A knockout (STX1A KO) and heterozygous STX1A knockout (STX1A+/-) male and female mice.

In male groups, end-systolic dimension of STX1A KO and STX1A+/- mice increased by 1.6-fold and 1.7-fold, respectively, at 0-week post-TAM ($p<0.0001$). Both groups were statistically different than Cre+ mice (Figure 12A). This rapid rise in end-systolic dimension did not persist for long and by 1-week post-TAM, end-systolic dimension returned to values comparable to Cre+ mice. Due to the rise in dimension during systole, a consequential rise in end-systolic volume was also seen. At 0-week, end-systolic volume in STX1A KO and STX1A+/- mice increased by 3.6-fold and 3.9-fold, respectively ($p<0.0001$). As seen in dimensional changes, the rise in end-systolic volume also recovered by 1-week post-TAM

(Figure 12C). STX1A KO and STX1A+/- did not differ in end-systolic dimension and volume changes as seen in Figure 12A and Figure 12C, respectively. Additional statistical comparisons showed no significant differences between STX1A KO and STX1A+/- mice, further suggesting that full and partial STX1A loss yielded the same degree of systolic dysfunction. Given that both groups recovered by 1-week post-TAM, it can be speculated that the mode of recovery occurring from 0-week to 1-week post-TAM is similar. Notably, Cre+ mice which had also received TAM did not show changes in end-systolic dimension and volume, allowing the effects of TAM and MCM activation to be eliminated as possible explanations for this transient change.

When evaluated in female mice, STX1A KO and STX1A+/- groups showed identical qualitative changes to end-systolic dimension and volume (Figure 12B, D). End-systolic dimension in female STX1A KO mice showed a 1.8-fold increase at 0-week ($p<0.0001$) while STX1A+/- mice showed a 1.7-fold increase at 0-week ($p<0.0001$) post-TAM (Figure 12B). This was comparable to the changes observed in male STX1A KO (1.6-fold) and STX1A+/- (1.7-fold) mice. Analogous to male groups, STX1A KO and STX1A+/- female mice both underwent a rapid rise in end-systolic dimension at 0-week post-TAM followed by recovery at 1-week post-TAM during which control Cre+ mice remained relatively unchanged. As expected, the rise in end-systolic dimension also brought on a rise in end-systolic volume. At 0-week post-TAM, end-systolic volume in STX1A KO and STX1A+/-mice significantly increased by 4.6-fold ($p<0.0001$) and 4.0-fold ($p<0.0002$), respectively (Figure 12D), which again were comparable to the alterations observed in corresponding male mice. By 1-week post-TAM, end-systolic volumes of STX1A KO and STX1A+/- female groups were once again comparable to control Cre+ mice. Additional statistical comparisons between STX1A KO and STX1A+/- mice at 0-week indicated no difference between the groups in regards to end-systolic dimension or volume.

From these trends, similar conclusions as those drawn in male groups can be made for female groups; first, full and partial STX1A loss yields similar effects as seen by the shared trends of STX1A KO and STX1A+/- mice and, second, TAM and MCM activation can be eliminated as the source of this change due to Cre+ mice remaining stable during this time. One of the main objectives of evaluating trends in female mice was to elucidate possible sex differences which might inherently exist in mice. However, a clear distinction between male and female mice was not found because end-systolic dimension and volume were deemed not statistically different at baseline measurements (-1 week) in male and female mice (Figure 12).

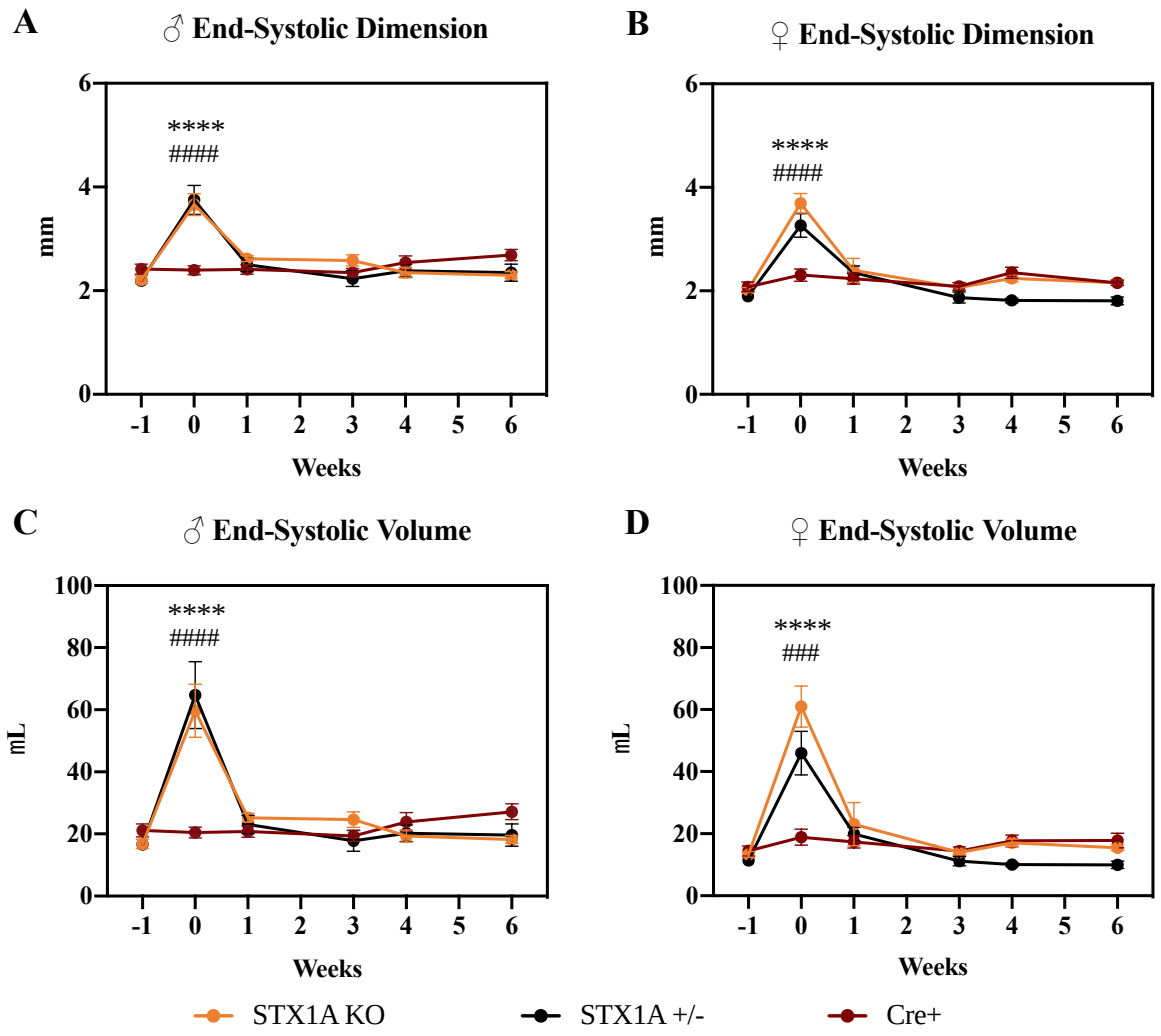


Figure 12: Effect of STX1A deficiency on left ventricular systolic dimension (A, B) and volume (C, D) in male and female mice. STX1A KO (orange; male: n=5-13, female: n=4-17), STX1A+/- (black; male: n=4-19, female: n=5-15), and control Cre+ (red; male: n=7-11, female: n=6-8) are displayed. The study was conducted over an 8-week period, with baseline measurements denoted as -1-week and post-TAM measurements beginning at 0-week, corresponding to 1 day after the 4th injection. Each point represents the mean±SEM. One-way ANOVA followed by Sidak's multiple comparisons test was done to determine significance. Significant comparisons between STX1A KO and Cre+ are shown by asterisks (****p<0.0001) and comparisons between STX1A+/- and Cre+ shown by the pound signs (####p<0.0001, ###p<0.0002).

Unlike end-systolic changes, end-diastolic dimension and volume showed a modest increase in male STX1A KO and STX1A+/- mice after STX1A loss (Figure 13A, C) but an equivalent change in female mice was not seen (Figure 13B, D). At 0-week post-TAM, a 1.2-fold increase in end-diastolic dimension for male STX1A KO ($p=0.0435$) and STX1A +/- ($p=0.0006$) mice from baseline measurements was observed (Figure 13A). The dilated ventricles seen at 0-week post-TAM soon recovered by 1-week and end-diastolic dimension was comparable to Cre+ mice. End-diastolic volume followed a similar trend in which an increase at week 0 followed by recovery at week 1 was seen post-TAM. A 1.5-fold increase from baseline end-diastolic volume measurements was seen in STX1A KO ($p=0.0186$) and STX1A+/- ($p<0.0001$) mice at 0-week post-TAM before returning to values comparable to Cre+ mice by 1-week post-TAM (Figure 13C). Since STX1A KO and STX1A+/- showed the same degree of end-diastolic dimensional and volume changes, which were absent in control Cre+ mice, this further supports the claim that full and partial loss of STX1A yields similar effects.

In stark contrast, the end-diastolic dimension and volume did not statistically differ throughout the 6-week study in female STX1A KO and STX1A+/- mice (Figure 13B, D). Furthermore, statistical comparisons between male and female groups assess any inherent sex differences showed no significant differences in end-diastolic dimension and volume at baseline measurements between male and female mice.

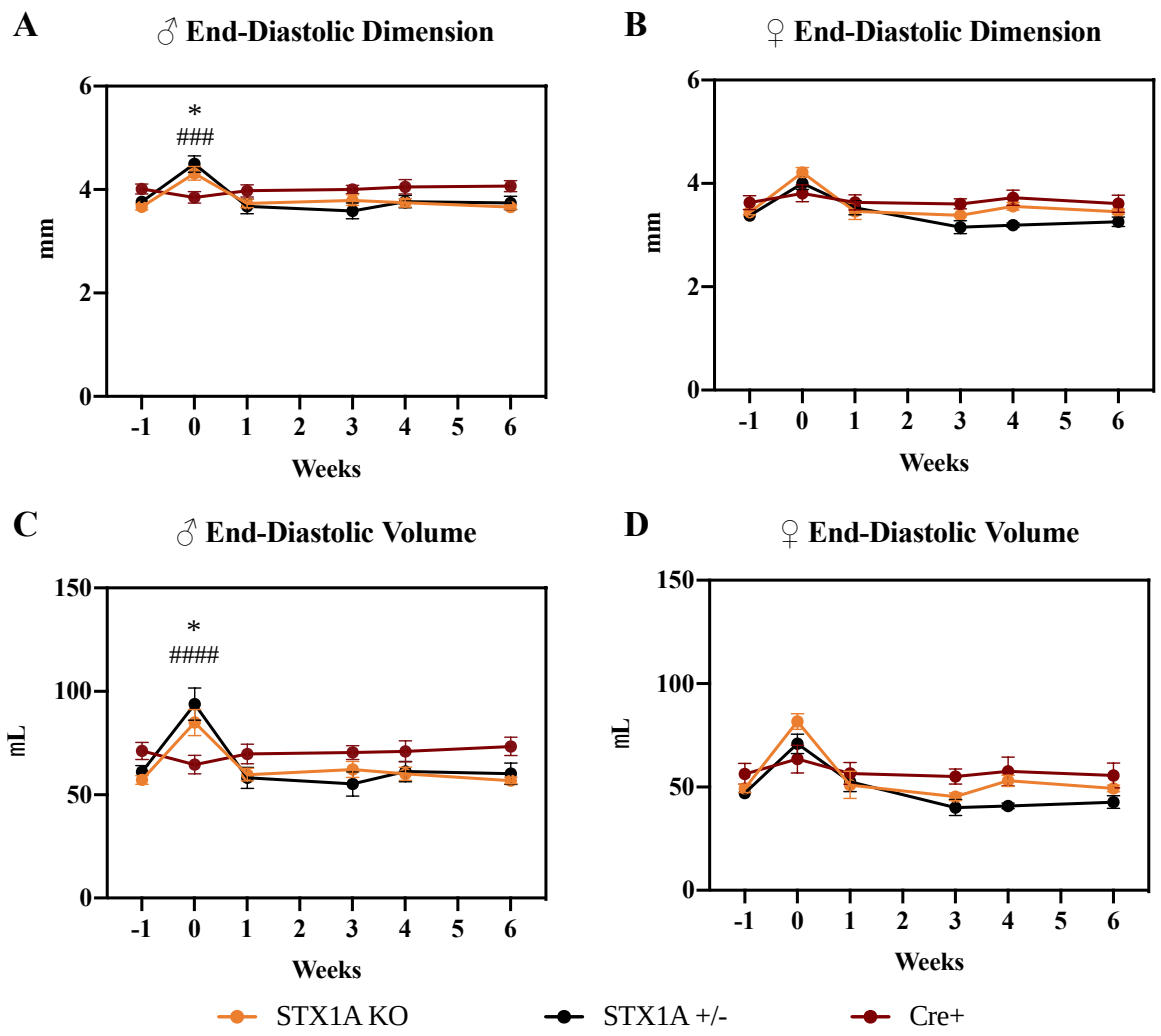


Figure 13: Effect of STX1A deficiency on left ventricular diastolic dimension (A, B) and volume (C, D) in male and female mice. STX1A KO (orange; male: n=5-13, female: n=4-17), STX1A+/- (black; male: n=4-19, female: n=5-15), and control Cre+ (red; male: n=7-11, female: n=6-8) are displayed. The study was conducted over an 8-week period, with baseline measurements denoted as -1-week and post-TAM measurements beginning at 0-week, corresponding to 1 day after the 4th injection. Each point represents the mean±SEM. One-way ANOVA and Sidak's multiple comparisons test were done to determine significance. Significance between STX1A KO and Cre+ is shown by asterisks (*p<0.0332) and significance between STX1A+/- and Cre+ is shown by pound signs (####p<0.0001, ###p<0.0002).

3.4. Left ventricular function of STX1A deficient mice

Left ventricular function of STX1A KO, STX1A+/-, and Cre+ deficient mice was determined via cardiac output (mL/min), ejection fraction (%), and fractional shortening (%).

Cardiac output is a measure of volume of blood ejected per min, computed by reporting the mathematical product of heart rate (beats per min; BPM) and stroke volume (μL). Stroke volume is the difference between end-diastolic volume and end-systolic volume, representing the amount of blood ejected per cardiac cycle. Heart rate in male and female mice across all groups did not statistically differ and remained stable throughout the 6-weeks after TAM injections (Figure 14A, B). Stroke volume, however, significantly decreased at post-TAM and showed varying recovery in the weeks following full and partial STX1A knockout.

Stroke volume in male STX1A KO and STX1A+/- mice decreased by 0.6-fold ($p<0.0001$) and 0.7-fold ($p=0.0016$), respectively, at 0-week post-TAM from baseline measurements (Figure 14C; Table 3A). Following this, stroke volume remained significantly lower than control Cre+ mice from 1-week (STX1A KO, $p=0.0146$; STX1A+/-, $p=0.0150$) to 3-week post-TAM (STX1A KO, $p=0.0335$; STX1A, $p=0.0185$). During this time stroke volume gradually increased and by 4-week, both STX1A KO and STX1A+/- mice were not statistically different than control Cre+ mice (Figure 14C). Since heart rate remained stable, the changes in cardiac output were influenced by stroke volume which in turn reflected the severely altered end-systolic dimension and volume. Male STX1A KO and STX1A+/- mice displayed significantly lower cardiac output, with both groups showing a 0.6-fold decrease ($p<0.0001$) at 0-week from baseline measurements. At 1-week post-TAM, recovery had begun, but cardiac output for STX1A KO ($p=0.0268$) and STX1A+/- ($p=0.0430$) mice was still lower compared to Cre+ mice. Statistical significance was not observed beyond 1-week (Figure 14E; Table 3A).

In female groups, stroke volume decreased at 0-week, where female STX1A KO mice showed a 0.5-fold decrease ($p<0.0001$) at 0-week while female STX1A+/- mice showed a 0.7-fold decrease ($p<0.0001$) from baseline measurements (Figure 14D; Table 3B). Where these two groups differ is in their recovery. Stroke volume for female STX1A+/- mice recovered by 1-week post-TAM, while it took up to 3 weeks for STX1A KO mice to return to values comparable to Cre+ control mice (Figure 14D; Table 3B).

Cardiac output in female mice reflected the trends seen in stroke volume with cardiac output of STX1A KO and STX1A+/- mice displaying a 0.5-fold decrease ($p<0.0001$) and 0.7-fold decrease ($p<0.0001$), respectively. However, cardiac output returned to control values in both STX1A KO and STX1A+/- mice by 1-week post-TAM (Figure 14F; Table 3B). Therefore, similar to male groups, female groups also showed gradual recovery of stroke volume and cardiac output but this trend was less pronounced in females as seen by the rapid recovery of STX1A+/- female mice and the inability to establish statistical significance at 3-week for stroke volume and 1-week for cardiac output in STX1A KO female mice.

Comparisons between STX1A KO and STX1A+/- mice yielded no differences between the groups for heart rate, stroke volume, or cardiac output—indicating that full and partial STX1A loss led to the same decline in stroke volume and cardiac output. This was seen in both male and female groups. However, when comparing male and female groups, stroke volume and cardiac output of STX1A+/- mice was found to be statistically different at baseline measurements (-1-week). Although this difference was not seen in STX1A KO or Cre+ baseline values (-1 week), this comparison suggests that male mice have a greater stroke volume and cardiac output compared to female mice.

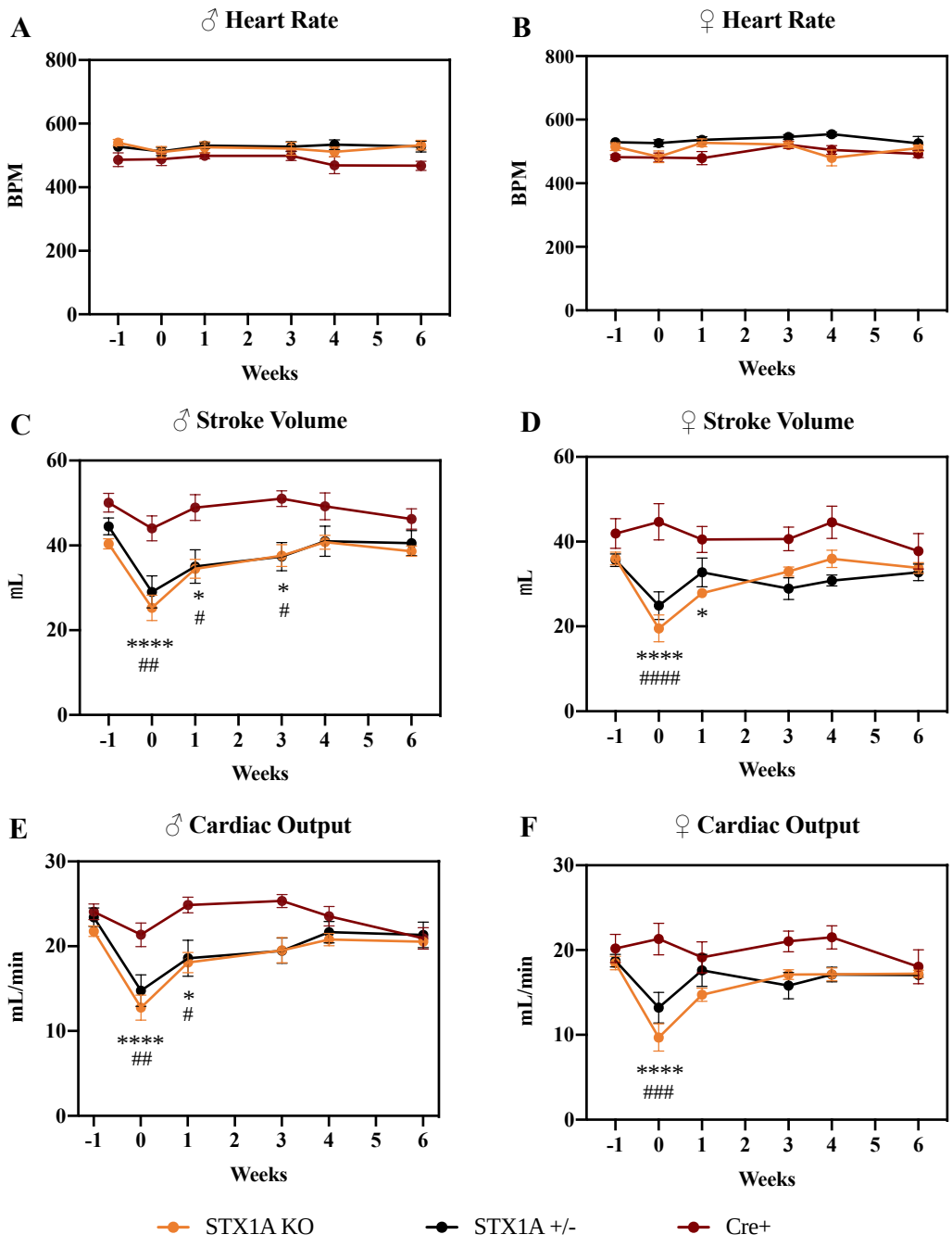


Figure 14: Effect of STX1A deficiency on heart rate. (A, B), stroke volume (C, D), and cardiac output (E, F) in male and female mice. STX1A KO (orange; male: n=5-13, female: n=4-17), STX1A+/- (black; male: n=4-19, female: n=5-15), and control Cre+ (red; male: n=7-11, female: n=6-8) are displayed. Mean±SEM of M-mode measurements obtained from the VisualSonics Vevo 2011 high resolution ultrasound imaging system is shown. One-way ANOVA followed by Sidak's multiple comparisons test was done. Significant comparisons between STX1A KO and Cre+ are shown by asterisks (****p<0.0001 and *p<0.0332) and comparisons between STX1A+/- and Cre+ are shown by pound signs (####p<0.0001, ###p<0.0002, ##p<0.0021).

Table 3A: Stroke volume and cardiac output for male groups. Statistical differences from control Cre+ mice are shown by by asterisks (****p<0.0001 and *p<0.0332) and pound signs ($^{\#\#}$p<0.0021, $^{\#}$p<0.0332).

Stroke Volume (µL)					
	-1 week	0-week	1-week	3-week	4-week
Cre+	50.1±2.2 (n=11)	44.0±3.0 (n=9)	48.9±1.0 (n=8)	51.0±1.9 (n=8)	49.2±1.2 (n=7)
STX1A KO	40.4±1.2 (n=13)	25.3±0.3 (n=11) ****	34.5±2.2 (n=7) *	37.6±2.6 (n=7) *	40.8±1.6 (n=6)
STX1A+/-	44.5±2.0 (n=19)	29.0±3.8 (n=10) $^{\#\#}$	35.0±3.9 (n=8) $^{\#}$	37.4±3.3 (n=8) $^{\#}$	41.0±3.6 (n=5)
Cardiac Output (mL/min)					
	-1-week	0-week	1-week	3-week	4-week
Cre+	24.1±0.9 (n=11)	21.4±1.4 (n=9)	24.9±0.9 (n=8)	25.3±0.8 (n=8)	23.5±1.2 (n=7)
STX1A KO	21.8±0.6 (n=13)	12.8±1.5 (n=11) ****	18.1±1.2 (n=7) *	19.5±1.5 (n=7)	20.8±0.7 (n=6)
STX1A+/-	23.4±1.1 (n=19)	14.8±1.9 (n=10) $^{\#\#}$	18.6±2.1 (n=8) $^{\#}$	19.5±1.5 (n=8)	21.7±1.3 (n=5)

Table 3B: Stroke volume and cardiac output for female groups. Statistical differences from control Cre+ mice are shown by by asterisks (****p<0.0001 and *p<0.0332) and pound signs ($^{\#\#\#\#}$p<0.0001, $^{\#\#\#}$p<0.0002).

Stroke Volume (µL)					
	-1 week	0-week	1-week	3-week	4-week
Cre+	41.9±3.5 (n=8)	44.7±4.3 (n=8)	40.5±3.0 (n=8)	40.6±2.8 (n=8)	44.6±3.8 (n=6)
STX1A KO	36.0±1.5 (n=17)	19.5±3.2 (n=14) ****	27.9±1.1 (n=10) *	33.0±1.1 (n=10)	36.0±2.0 (n=4)
STX1A+/-	35.7±1.5 (n=15)	24.9±3.3 (n=10) $^{\#\#\#\#}$	32.8±3.4 (n=7)	28.9±2.6 (n=7)	30.8±1.3 (n=5)
Cardiac Output (mL/min)					
	-1-week	0-week	1-week	3-week	4-week
Cre+	20.2±1.7 (n=8)	21.3±1.9 (n=8)	19.1±1.8 (n=8)	21.0±1.2 (n=8)	21.5±1.4 (n=6)
STX1A KO	18.5±0.8 (n=17)	9.7±1.6 (n=14) ****	14.7±0.8 (n=10)	17.1±0.6 (n=10)	17.1±0.7 (n=4)
STX1A+/-	18.7±0.7 (n=15)	13.2±1.8 (n=10) $^{\#\#\#}$	17.6±1.9 (n=7)	15.8±1.5 (n=7)	17.1±0.9 (n=5)

Next, ejection fraction and fractional shortening were examined to further gauge possible alterations in cardiac function of STX1A deficient mice. Ejection fraction (EF) is the fractional change in volume ejected resulting from contraction, computed by taking the quotient of stroke volume with end-diastolic volume (EF=SV/EDV). Similarly, fractional shortening (FS) is the fractional change in chamber dimension, computed by taking the quotient of end-diastolic dimension and difference of end-systolic dimension and end-diastolic dimension [FS=EDD/(ESD-EDD)]. Both parameters are reported as percentages (%) and used to infer how well the left ventricle is contracting.

In males, ejection fraction of STX1A KO and STX1A+/- mice displayed a 0.5-fold decrease ($p<0.0001$) at 0-week post-TAM from baseline measurements before recovering at week 1. Cre+ mice remained unchanged post-TAM, further supporting the claim that neither TAM nor MCM activation were responsible for the changes seen in STX1A deficient mice (Figure 15A; Table 4A). Fractional shortening followed a similar trend where a 0.4-fold and 0.5-fold decrease ($p<0.0001$) was observed in STX1A KO and STX1A+/- mice, respectively, at 0-week post-TAM. Fractional shortening also displayed recovery at 1-week post-TAM (Figure 15C; Table 4A).

Comparatively, female mice showed similar trends with ejection fraction and fractional shortening after STX1A knockout. In STX1A KO female mice, ejection fraction and fractional shortening decreased by 0.4-fold and 0.3-fold, respectively, at 0-week post-TAM ($p<0.0001$). In the case of STX1A+/- female mice the relative change was slightly greater with ejection fraction and fractional shortening decreasing by 0.5-fold and 0.4-fold, respectively, at 0-week post-TAM ($p<0.0001$). STX1A KO and STX1A+/- female mice were not statistically different, indicating full and partial knockout of STX1A elicited equivalent degrees of decline in left ventricular

function. After the initial decrease seen in both groups and in both parameters, substantial recovery was seen at 1-week post-TAM. When compared between male and female groups, ejection fraction and fractional shortening were not significantly different, therefore, from the current data clear sex differences in heart function *in vivo* were not observed.

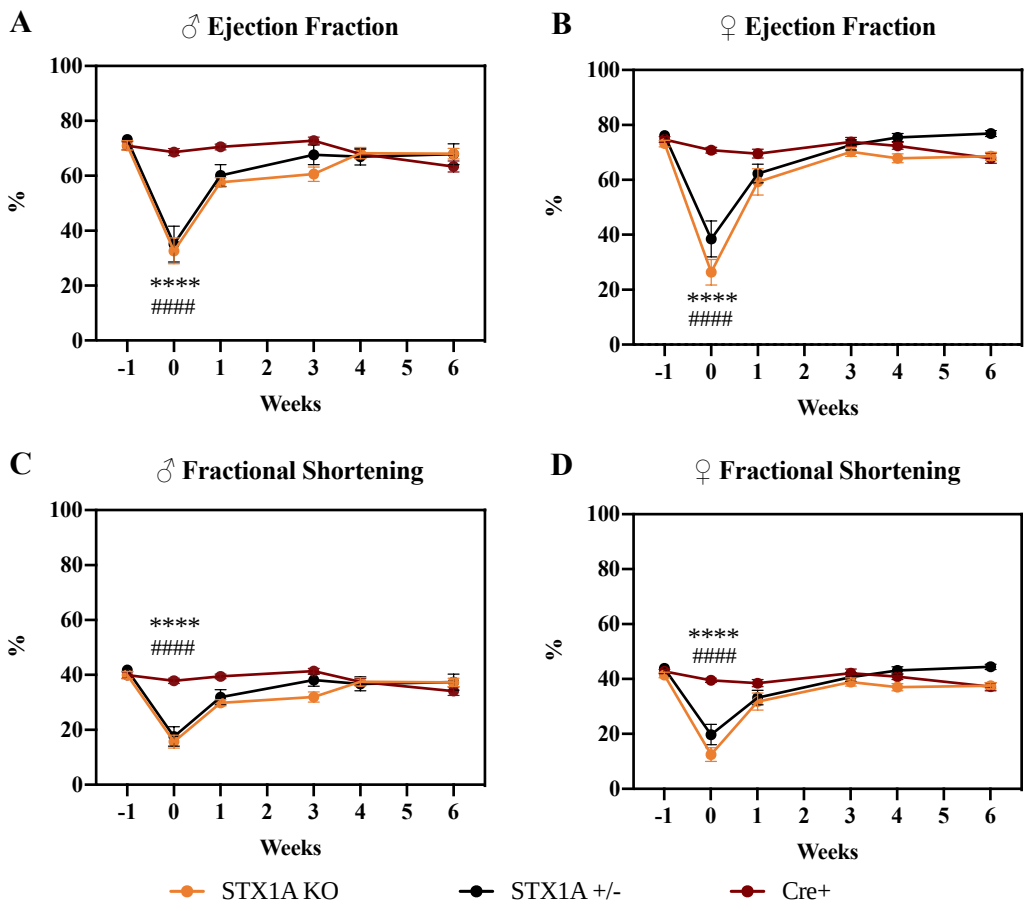


Figure 15: Effect of STX1A deficiency on left ventricular ejection fraction (A, B) and fractional shortening (C, D) in male and female mice. STX1A KO (orange; male: n=5-13, female: n=4-17), STX1A+/- (black; male: n=4-19, female: n=5-15), and control Cre+ (red; male: n=7-11, female: n=6-8) are displayed. Baseline measurements are denoted as -1-week and 1-week corresponds to 1 day after the 4th TAM injection. Each point represents the mean±SEM. One-way ANOVA followed by Sidak's multiple comparisons test was done to determine significance. Significant comparisons between STX1A KO and Cre+ are shown by asterisks (****p<0.0001) and comparisons between STX1A+/- and Cre+ are shown by pound signs (####p<0.0001).

Table 4A: Ejection fraction and fractional shortening of male groups. Statistical differences from control Cre+ mice are shown by by asterisks (****p<0.0001) and pound signs (####p<0.0001).

Ejection Fraction					
	-1 week	0-week	1-week	3-week	4-week
Cre+	70.9±1.5% (n=11)	68.6±1.2% (n=9)	70.5±1.0% (n=8)	72.8±1.3% (n=8)	67.9±2.0% (n=7)
STX1A KO	71.1±1.7% (n=13)	32.7±4.7% (n=11) ****	57.6±1.7% (n=7)	60.6±2.6% (n=7)	68.2±2.0% (n=6)
STX1A+/-	73.2±1.3% (n=19)	35.1±6.5% (n=10) ####	60.1±4.0% (n=8)	67.6±3.6% (n=8)	67.0±3.0% (n=5)
Fractional Shortening					
	-1 week	0-week	1-week	3-week	4-week
Cre+	40.0±1.2% (n=11)	37.8±1.0% (n=9)	39.5±0.8% (n=8)	41.4±1.3% (n=8)	37.5±1.3% (n=7)
STX1A KO	39.9±1.3% (n=13)	15.7±2.4% (n=11) ****	29.8±1.1% (n=7)	32.0±1.8% (n=7)	37.5±1.5% (n=6)
STX1A+/-	41.8±1.1% (n=19)	17.6±3.6% (n=10) ####	31.9±2.8% (n=8)	38.1±2.2% (n=8)	36.7±2.5% (n=5)

Table 4B: Ejection fraction and fractional shortening of female groups. Statistical differences from control Cre+ mice are shown by by asterisks (****p<0.0001) and pound signs (####p<0.0001).

Ejection Fraction					
	-1 week	0-week	1-week	3-week	4-week
Cre+	74.7±1.0% (n=8)	70.8±1.0% (n=8)	69.5±1.6% (n=8)	73.8±1.7% (n=8)	72.4±1.3% (n=7)
STX1A KO	73.2±1.2% (n=17)	26.5±4.7% (n=14) ****	59.3±4.8% (n=10)	70.2±1.6% (n=10)	67.9±1.6% (n=4)
STX1A+/-	76.1±0.9% (n=15)	38.5±6.5% (n=10) ####	62.3±3.4% (n=7)	72.7±1.8% (n=7)	75.4±1.5% (n=5)
Fractional Shortening					
	-1 week	0-week	1-week	3-week	4-week
Cre+	42.8±0.8% (n=8)	39.6±0.7% (n=8)	38.5±1.3% (n=8)	42.1±1.5% (n=8)	40.9±1.1% (n=7)
STX1A KO	41.5±1.0% (n=17)	12.5±2.5% (n=14) ****	31.8±3.1% (n=10)	38.9±1.4% (n=10)	37.0±1.3% (n=4)
STX1A+/-	43.9±0.8% (n=15)	19.7±3.7% (n=10) ####	33.2±2.6% (n=7)	40.7±1.6% (n=7)	43.1±1.3% (n=5)

3.5. Left ventricular remodeling in STX1A deficient mice

To assess whether STX1A deficiency induced morphological changes, posterior wall thickness (mm) of the left ventricle was examined.

Male STX1A+/- mice displayed significant thickening of the posterior wall at 1-week post-TAM before recovering to values comparable to Cre+ mice at 3-week post-TAM. Specifically, posterior wall thickness of STX1A+/- male mice began at 0.87±0.03 mm (n=13), remained stable at 0-week post-TAM but then rose to 1.16±0.09 mm (n=6, $p<0.0001$) at 1-week post-TAM, a 1.3-fold increase from baseline measures (Figure 16A). At 3-week, posterior wall thickness of STX1A+/- mice (0.80±0.03; n=6) had returned to values similar to Cre+ mice (0.75±0.03; n=7). Interestingly, male STX1A KO mice did not show significant change to posterior wall thickness when compared to control Cre+ mice. No permanent changes to posterior wall thickness in male STX1A deficient mice were observed, ruling out structural alterations stemming from STX1A loss.

In contrast to the altered posterior wall thickness in STX1A+/- male mice, both STX1A KO and STX1A+/- female mice displayed significant increase in posterior wall thickness compared to Cre+ mice at 1-week post-TAM. Posterior wall thickness increased from 0.85±0.03 mm (n=11) to 1.14±0.08 mm (n=10, $p<0.0001$) in STX1A KO mice and 0.83±0.02 mm (n=13) to 1.06±0.06 mm (n=6, $p=0.0020$) in STX1A+/- mice at 1-week post-TAM (Figure 16B). This represented a 1.3-fold increase in posterior wall thickness for both groups. By 3-week, posterior wall thickness in STX1A KO and STX1A+/- female mice returned to values comparable to Cre+ and remained as such for the remainder of the study. Similar to males, female mice did not display permanent posterior wall thickness changes induced by full or partial STX1A loss in left ventricles.

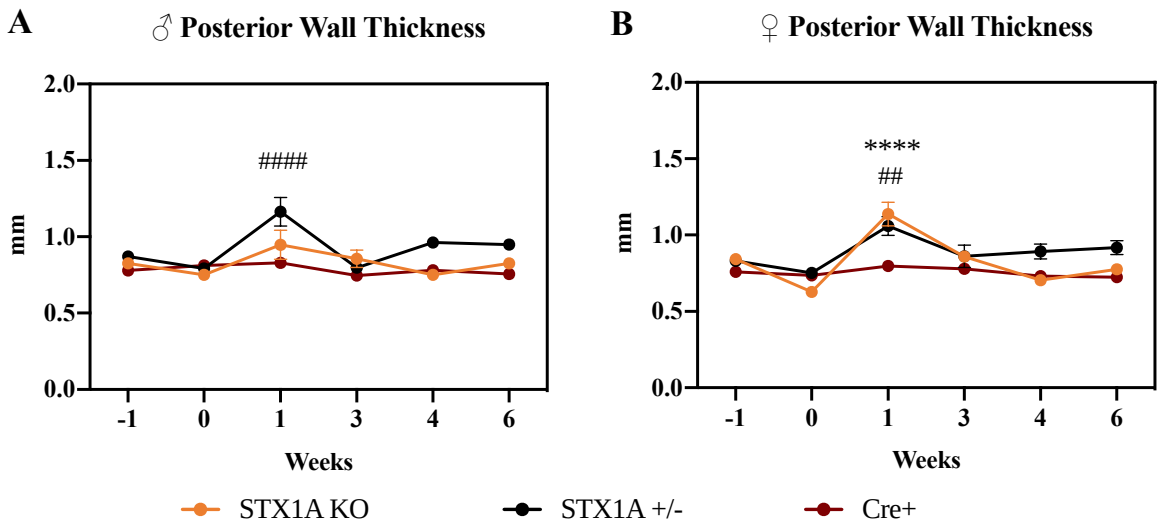


Figure 16: Left ventricular posterior wall thickness (mm) in STX1A deficient male (A) and female (A) mice. STX1A KO (orange; male: n=4-10, female: n=4-11), STX1A+/- (black; male: n=4-7, female: n=5-7), and control Cre+ (red; male: n=6-8, female: n=5-8) are displayed and reported as mean±SEM. One-way ANOVA followed by Sidak's multiple comparisons test was done to determine significance. Significant comparisons between STX1A KO and Cre+ are shown by asterisks (****p<0.0001) and comparisons between STX1A+/- and Cre+ shown by pound signs (####p<0.0001, ##p<0.0021).

3.6. Delayed R-wave to onset of contraction

An intriguing finding in an earlier study in the Tsushima lab revealed a delay in the onset of contraction in STX1A KO mice as measured by echocardiography (Virdi, 2019). To verify this phenomenon, the time between the R-wave of the ECG to the onset of left ventricular contraction was measured.

In male STX1A KO mice, there was a prolongation in the time between the R-waves to the onset of contraction compared to control Cre+ from 0- to 3-week post-TAM. Compared to baseline values, R-wave delay at 0-week ($p<0.0001$) and 1-week ($p=0.0017$) post-TAM was greater by 1.5-fold. By week 3, recovery had begun but R-wave delay was still significantly different ($p=0.0454$) than Cre+ mice (Figure 17A). Full recovery was seen by week 4 in male STX1A KO mice. Male STX1A+/- mice showed a similar pattern in which the duration between R-wave delay and onset of contraction significantly increased at 0-week by 1.4-fold ($p=0.0212$) (Figure 17A) but was no longer significantly different than Cre+ mice at week 1.

In female STX1A KO mice, R-wave delay significantly lengthened at 0-week post-TAM ($p<0.0001$) and remained as such at 1-week ($p=0.0198$) before recovering to values comparable to Cre+ mice at 3-week (Figure 17B). R-wave delay in female STX1A+/- mice followed a similar pattern to that seen in male STX1A+/- mice, in which R-wave delay significantly increased by 1.4-fold at 0-week ($p=0.0017$) and was not significantly different after this point (Figure 17B).

No difference was found between male and female mice, however, male STX1A KO mice showed significant R-wave delay until 3-week while female STX1A KO mice began showing recovery at 1-week and were comparable to control Cre+ female mice by 3-week. STX1A+/-

mice showed similar trends within male and female mice, with significant delay seen at 0-week and recovery at 3-week post-TAM.

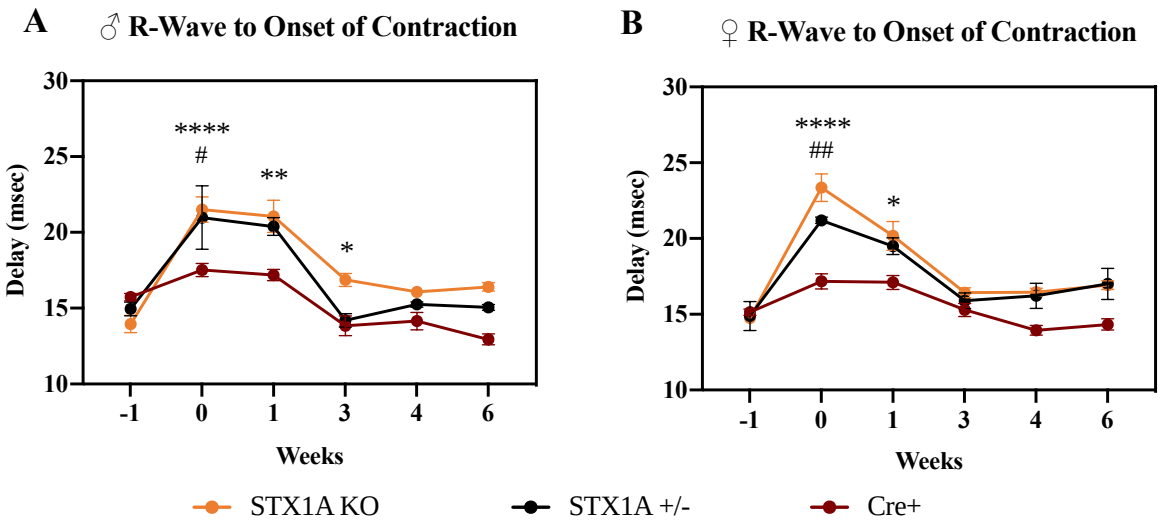


Figure 17: Time (msec) delay between ECG R-wave and the onset of left ventricular contraction in STX1A deficient male (A) and female (B) mice. STX1A KO (orange; male: n=4-10, female: n=4-11), STX1A+/- (black; male: n=4-7, female: n=4-7), and control Cre+ (red; male: n=6-8, female: n=5-8) are displayed and reported as mean±SEM. One-way ANOVA followed by Sidak's multiple comparisons test was done to determine significance. Significant comparisons between STX1A KO and Cre+ are shown by asterisks (****p<0.0001, **p<0.0021, *p<0.0332) and comparisons between STX1A+/- and Cre+ shown by pound signs (##p<0.0021, #p<0.00332).

3.7. Changes in syntaxin gene expression

As seen from the echocardiographs, the loss of cardiac function was determined to be transient, with full recovery seen at 3- to 4-weeks after STX1A loss in both male and female STX1A KO and STX1A+/- groups. To explore the underlying mechanisms associated with this recovery, we evaluated the possible compensatory changes as a result of full or partial loss of STX1A. RT-qPCR on select syntaxins (STXs) was done. Gene expression in mice before TAM injections (Pre-injection) was established as the baseline to which average fold-change of expression one day after the 4th TAM injection (0 Week Post-TAM) and 3 weeks after the 4th TAM injection (3 Week Post-TAM) was compared. STX1A, 2, 3, and 4 gene expression was measured at these time points. STX2, 3, and 4 were selected due to their shared homology with STX1A (Bennett et al., 1993), localization on the plasma membrane of cells (Bowman et al., 2019), and documented expression in the heart (Bennett et al., 1993). STX2 and STX3 are closely related to STX1A with 79% and 77% sequence homology, respectively (Bennett et al., 1993; Bowman et al., 2019; Ferlito et al., 2010). STX4, in addition to sharing 65% sequence homology with STX1A, has been identified to participate in ANP release and insulin-stimulated GLUT-4 translocation in cardiomyocytes (Bowman et al., 2019; Ferlito et al., 2010; Peters et al., 2006). Keeping this mind, STX2, 3, and 4 were selected as likely candidates to evaluate compensatory gene expression changes.

To begin, knockout of STX1A in STX1A KO and STX1A+/- mice was confirmed at 0-week and 3-week post-TAM (Figure 18). From a baseline of 1.0±0.054 (n=9), STX1A transcript levels in male STX1A KO decreased to 0.16±0.043 (n=5, $p<0.0001$) while in male STX1A+/- mice, STX1A fold-expression decreased to 0.35±0.040 (n=5, $p<0.0001$) at 0-week post-TAM (Figure 18A). This represented an 84% drop in STX1A mRNA levels in STX1A KO mice and a

65% drop in STX1A+/- mice. Similarly, from a baseline of 1.1±0.13 (n=10), STX1A fold-expression in female mice dropped to 0.13±0.034 (n=5, $p<0.0001$) for STX1A KO mice and 0.36±0.050 (n=4, $p=0.0005$) for STX1A+/- mice, representing an 87% and 64% drop in STX1A mRNA expression, respectively (Figure 18B). This drop in STX1A expression was maintained at 3-week post-TAM with STX1A KO mice displaying an 86% drop in males (0.14±0.038, n=4, $p<0.0001$) and an 81% drop in females (0.19±0.042, n=4, $p<0.0001$) at 3-week post-TAM (Figure 18). In the case of STX1A+/- mice, STX1A fold-expression at 3-week post-TAM was decreased by 45% in males (0.55±0.034, n=6, $p<0.0001$) and 59% in females (0.41±0.085, n=4, $p=0.0013$). Therefore, in addition to the protein analyses shown in Figure 11, successful STX1A knockout was further confirmed via mRNA expression levels. Male and female Cre+ mice showed no significant change to STX1A mRNA levels at 0-week and 3-week post-TAM (Figure 18). Hence, transcriptional STX1A knockout (STX1A KO) and knockdown (STX1A+/-) was successfully achieved and agreed with protein analyses. In contrast to these results, there were no significant changes to the STX1A transcript levels in Cre+ (MCM-expressing, tamoxifen-treated) male and female mice.

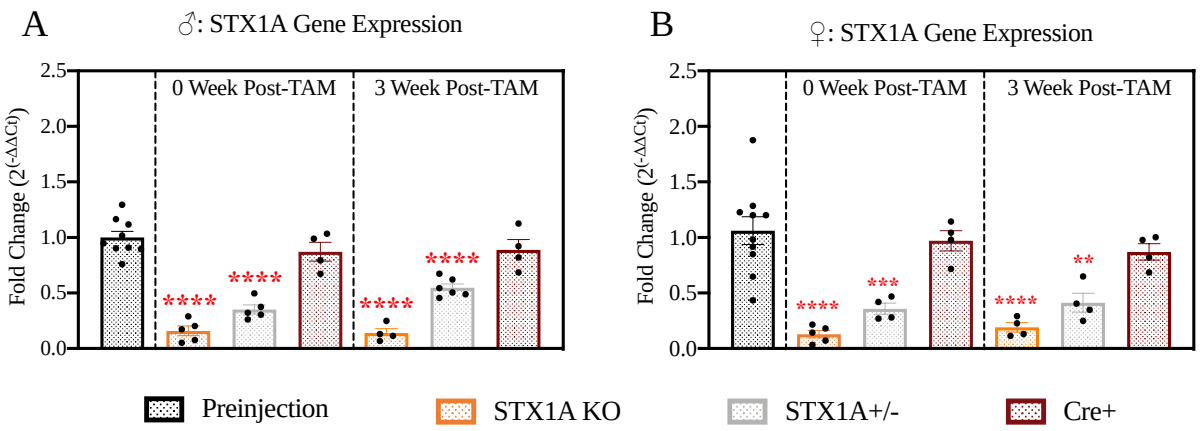


Figure 18: STX1A gene expression in the left ventricular free wall of male (A) and female (B) groups. Gene expression prior to TAM injections (Pre-injection; black bars; male n=9; female n=10), after TAM injections (0 Week Post-TAM), and 3 weeks after TAM injections (3 Week Post-TAM) was measured and reported as fold-change from pre-injection mice. STX1A KO (orange bars; male n=4, female n=5), STX1A+/- (grey bars; male n=4, female n=4), and control Cre+ (red bars; male n=4, female n=4) are displayed. RT-qPCR reactions were run as duplicates with fold-change computed using the $2^{(-\Delta\Delta Ct)}$ method and reported as mean±SEM. Individual values are shown as black dots. One-way ANOVA followed by Sidak's multiple comparisons test was done to determine significance indicated by red asterisks (****p<0.0001, ***p<0.0002, and **p<0.0021).

Next, gene expression of STX2, 3, and 4 was determined to probe for any compensatory changes that may arise from STX1A loss (Figure 19).

Syntaxin-2 (STX2)

Unexpectedly, STX2 fold-expression dropped by 90% (0.093±0.052, n=5, p<0.0001) in male STX1A KO mice and 99% (0.013±0.0046, n=5, p<0.0001) in female STX1A KO mice at 0-week post-TAM. A similar decline in STX2 fold-expression was seen in STX1A+/- mice at 0-week post-TAM as well, with male mice displaying a 90% decrease (0.098±0.078, n=5, p<0.0001) and female mice displaying a 74% decrease (0.25±0.074, n=4, p<0.0001) (Figure 19A, B). An interesting event occurred in male groups at 3-week post-TAM. STX2 mRNA fold-expression in male STX1A+/- mice recovered at 3-week post-TAM (0.78±0.037; n=6). While

partial recovery was observed in male STX1A KO mice at 3-week (0.63±0.22, n=4, p=0.0250) since STX2 gene expression were still significantly lower that pre injection levels (0.99±0.042; n=9) but had increased in comparison to week 1. Therefore, STX2 expression recovered in male STX1A+/- mice but did not recover in male STX1A KO mice at 3-week post-TAM (Figure 19A).

In the case of female mice at 3-week post-TAM, STX2 mRNA fold-expression remained lower in STX1A KO mice (0.42±0.13, n=4, p=0.0036) but recovered in the STX1A+/- mice (0.71±0.13; n=4) compared to pre-injection levels (0.95±0.080; n=10) (Figure 19B).

Syntaxin-3 (STX3)

Similar to the findings with STX2, STX3 expression in male and female STX1A KO and STX1A+/- mice showed significant reduction in fold-expression at 0-week post-TAM (Figure 19C, D). STX3 expression in male STX1A KO and STX1A+/- mice decreased by 80% (0.18±0.090, n=5, p<0.0001) and 90% (0.092±0.090, n=5, p<0.0001), respectively. By 3-week post-TAM, male STX1A+/- mice showed recovery (0.619±0.16, n=6) from 0-week STX3 levels and were comparable to pre-injection levels (0.93±0.10; n=9). STX3 levels in male STX1A KO mice at 3-week post-TAM (0.18±0.043; n=4, p=0.0001) did not deviate from 0-week levels and was lower than pre-injection levels, indicating no recovery (Figure 19C). Hence, STX3 levels were dampened and remained as such in STX1A KO male mice, while STX3 expression recovered in STX1A+/- male mice.

In female groups, STX3 fold-expression decreased at 0-week post-TAM by 98% in STX1A KO mice (0.020±0.01, n=5, p<0.0001) and 72% in STX1A +/- mice (0.29±0.07; n=4, p=0.0017). At 3-week post-TAM, STX3 fold-expression in female STX1A KO mice was not

statistically different than pre-injection states nor 0-week levels but showed an increase (0.52±0.19; n=4) from 0-week levels. This trend suggests a return to pre-injection STX3 levels but does not support the claim that significant recovery has taken place from 0-week to 3-week post-TAM in female STX1A KO mice. In female STX1A+/- mice, STX3 fold-expression remained significantly lower than pre-injection levels at 3-week post-TAM (p=0.0193), indicating no recovery in this group (Figure 19D).

Syntaxin-4 (STX4)

STX4 fold-expression in male groups showed high variability compared to STX1A, STX2, and STX3. No obvious trend in expression could be elucidated from the data (Figure 19E). However, in female STX1A KO mice, a 57% drop in STX4 mRNA fold-expression at 0-week post-TAM was seen (0.44±0.14, n=5, p=0.0166) (Figure 19F). At 3-week post-TAM, STX4 mRNA fold-expression (1.3±0.070; n=4, p=0.0084) increased from 0-week levels thus showing a recovery of STX4 gene expression at week 3 from week 1 levels. Compared to pre-injection levels (1.0±0.47; n=10), a significant difference was not found. STX4 fold-expression in female STX1A+/- mice did not differ from pre-injection levels at 0-week nor 3-week post-TAM. Therefore, only female STX1A KO mice showed a decline in STX4 fold-expression at 0-week before showing a significant fold-increase at 3-week post-TAM (Figure 19F).

An increase in STX2, 3 or 4 gene expression would have suggested compensatory changes that might contribute to the recovery of cardiac function seen in echocardiographs. However, clear candidates in male and female groups were not seen, thus, compensatory changes of these genes can be ruled out as a possible line of inquiry in the phenotype identified in our STX1A-deficient mice.

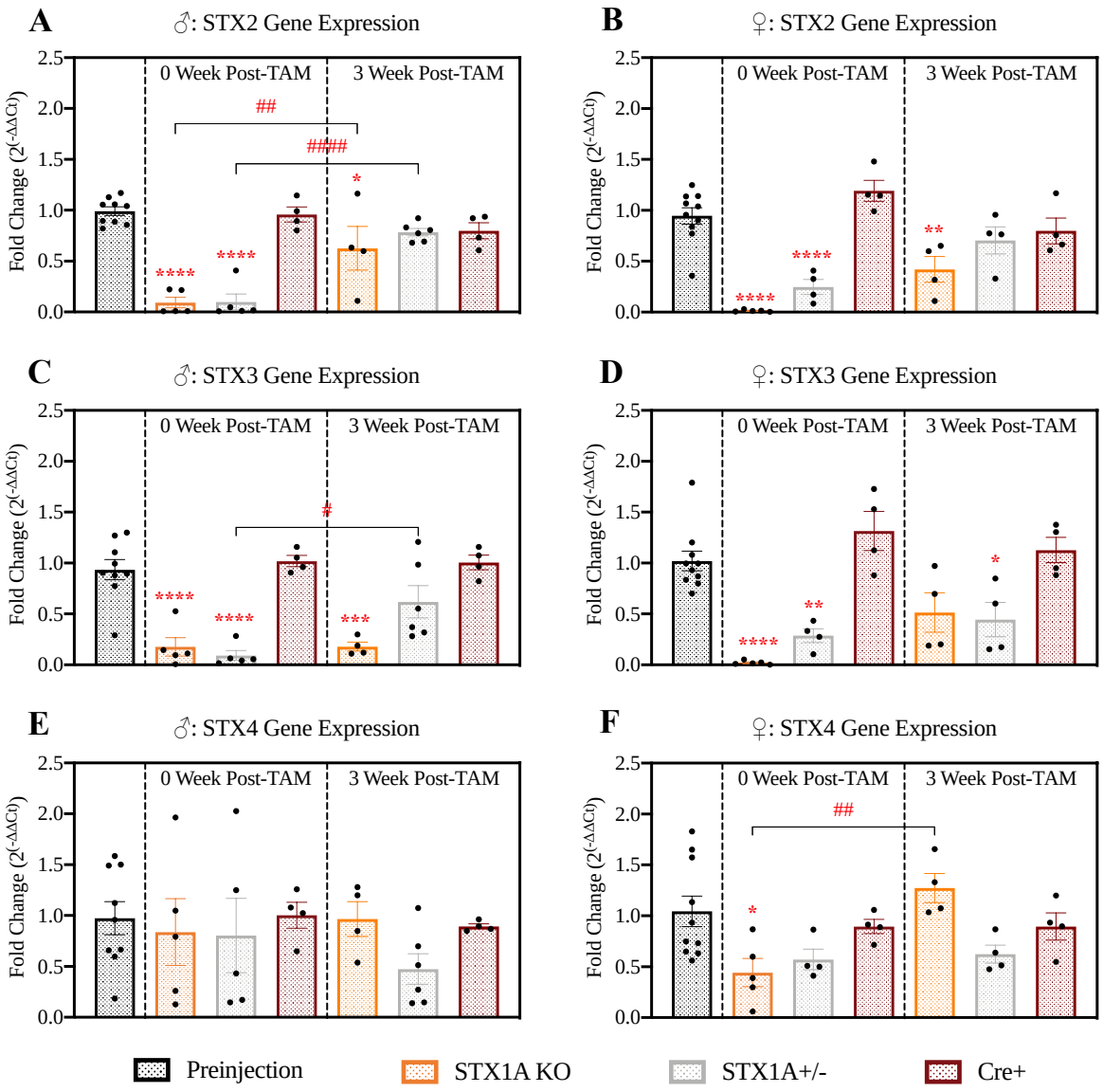


Figure 19: STX2, 3, and 4 gene expression in left ventricular free wall of male (A, C, D) and female (B, D, F) groups. Gene expression before TAM injections (Pre-injection; black bars; male n=9; female n=10), directly after TAM injections (0 Week Post-TAM), and 3 weeks after TAM injections (3 Week Post-TAM) was measures. STX1A KO (orange bars; male n=4, female n=5), STX1A+/- (grey bars; male n=4, female n=4), and control Cre+ groups (red bars; male n=4, female n=4) are displayed. Reactions were run as duplicates with fold-change was computed using the $2^{(-\Delta\Delta Ct)}$ method and reported as mean±SEM. Individual values are shown as black dots. One-way ANOVA followed by Sidak's multiple comparisons test was done to determine significance, with comparisons to pre-injection states shown as red asterisks (****p<0.0001, ***p<0.0002, **p<0.0021, and *p<0.0332) and comparisons between 0 week and 3 week values shown as red pound signs (####p<0.0001, ##p<0.0021, and #p<0.0332).

3.8. Changes in calcium-handling gene expression

The notable phenotypic feature of STX1A deficient mice is the recovery of cardiac function after a period of severe functional loss. The question of what is causing the initial decline and eventual recovery leads one to investigate the key calcium handling genes that regulate cardiac excitation-contraction (EC) coupling. Hence, this section will focus on gene expression changes of the pore-forming subunit of the voltage-gated L-type Ca^{2+} channel (LTCC $Ca_v1.2$), ryanodine receptor 2 (RyR2), sarco/endoplasmic reticulum Ca^{2+} ATPase 2 (SERCA2a), and Na^+/Ca^{2+} exchanger 1 (NCX1) as a result of STX1A loss (Figure 20).

Voltage-Gated Calcium α-Subunit $Ca_v1.2$

The voltage-gated L-type Ca^{2+} channel is responsible for Ca^{2+} entry into the cardiomyocyte to initiate Ca^{2+}-induced Ca^{2+} release. Gene expression of the main pore forming alpha subunit of LTCCs, $Ca_v1.2$, decreased at 0-week post-TAM. Male STX1A KO and STX1A+/- mice each displayed an 87% drop in $Ca_v1.2$ fold-expression at 0-week post-TAM (STX1A KO: 0.16±0.094, n=5 and STX1A+/-: 0.15±0.11, n=5, p=0.001). This drop was transient because by 3-week post-TAM, $Ca_v1.2$ fold-expression increased in STX1A KO (1.52±0.22; n=6) and STX1A+/- mice (0.82±0.10; n=4). At 3-week post-TAM, $Ca_v1.2$ expression increased from 0-week levels (STX1A KO, $p<0.0001$; STX1A+/-, p=0.0499) and were comparable to pre-injection levels (1.18±0.15; n=7). This indicates that the decline in $Ca_v1.2$ expression in male STX1A KO and STX1A+/- mice sufficiently recovered by 3-week post-TAM (Figure 20A).

Female groups showed a similar trend in which $Ca_v1.2$ fold-expression decreased 0-week post-TAM by 92% in STX1A KO mice (0.084±0.026; n=5; $p<0.0001$) and 69% in STX1A+/- mice (0.34±0.079; n=5; p=0.0008). At 3-week post-TAM, $Ca_v1.2$ fold-expression increased in

female STX1A+/- mice (0.97±0.21, n=4, p<0.0117) compared to 0-week levels. At this point, $Ca_v1.2$ expression was not different than pre-injection levels (1.05±0.14; n=7), therefore, $Ca_v1.2$ gene expression in female STX1A+/- mice sufficiently recovered by 3-week post-TAM. Female STX1A KO mice at 3-week post-TAM, not only showed an increase in $Ca_v1.2$ fold-expression (2.15±0.12, n=6, p<0.0001) compared to 0-week levels but also showed an increase compared to pre-injection levels. Therefore, at 3-week post-TAM, $Ca_v1.2$ expression recovered in female STX1A+/- mice and doubled in female STX1A KO mice (Figure 20B).

Ryanodine Receptor RyR2

The ryanodine receptor (RyR2) is located on the sarcoplasmic reticulum. It is responsible for releasing Ca^{2+} from the sarcoplasmic reticulum to initiate contraction. In both male and female STX1A KO and heterozygous mice, RyR2 fold-expression displayed a significant drop at 0-week post-TAM (Figure 20C, D). At 0-week post-TAM, RyR2 gene expression fold-change decreased by 59% (0.53±0.22, n=5, p=0.018) in male STX1A KO mice and surprisingly more (90%) in STX1A+/- mice (0.13±0.060, n=5, p=0.0002). At 3-week post-TAM, RyR2 fold-expression of male STX1A KO mice (1.40±0.12; n=6) was not significantly different than pre-injection levels (1.30±0.20; n=7) and showed a significant fold-increase from 0-week levels (p=0.0072), indicating full recovery in this group. Also, RyR2 fold-expression at 3-week post-TAM in male STX1A+/- mice did not significantly differ from 0-week levels nor pre-injection levels (Figure 20C).

In female groups, RyR2 fold-expression decreased at 0-week post-TAM with STX1A KO mice showing a 72% loss (0.30±0.093, n=5, p=0.0147) and STX1A+/- mice showing an 82% reduction (0.21±0.097, n=5, p=0.0050) in fold-change. At 3-week post-TAM, female STX1A

KO mice (1.59±0.126; n=6) and STX1A+/- mice (1.15±0.336; n=4) showed an increase of RyR2 fold-expression compared to 0-week levels (STX1A KO, $p<0.0001$; STX1A+/-, $p=0.0066$) and were similar to pre-injection levels (1.1±0.15; n=7). Therefore, after a significantly decline, RyR2 fold-expression of female STX1A KO and STX1A+/- mice recovered by 3-week post-TAM (Figure 20D).

Sarco/Endoplasmic Reticulum Ca^{2+}-ATPase (SERCA2a)

In the ventricles of the heart, the sarcoplasmic reticulum actively returns Ca^{2+} into its lumen via isoform 2a of the sarco/endoplasmic reticulum Ca^{2+}-ATPase (SERCA2a). SERCA2a expression showed significant fold-decrease in male and female groups at 0-week post-TAM (Figure 20E, F). Compared to pre-injection levels (1.07±0.10; n=7), male STX1A KO mice showed a loss of 79% (0.23±0.082, n=5, $p<0.0001$), while in male STX1A+/- mice a 72% decline (0.31±0.19, n=5, $p<0.0001$) was observed at 0-week post-TAM ($p<0.0001$). Expression remained significantly dampened in male groups at 3-week post-TAM with SERCA2a fold-expression 56% lower than pre-injection levels in both STX1A KO (0.48±0.065, n=6, $p=0.0012$) and STX1A+/- (0.48±0.074, n=4, $p=0.0044$) mice. Therefore, SERCA2a gene expression did not recover in male groups (Figure 20E).

In female groups, SERCA2a fold-change was significantly lower at 0-week post-TAM with STX1A KO mice showing a 94% decrease (0.062±0.026, n=5, $p<0.0001$) and STX1A+/- mice showing an 88% fall (0.12±0.039, n=5, $p=0.0002$) compared to pre-injection levels (1.04±0.12; n=7). By 3-week post-TAM, SERCA2a fold-expression in STX1A+/- mice (0.61±0.057; n=4) did not differ from pre-injection levels nor 0-week levels. However, SERCA2a fold-expression in female STX1A KO mice increased from 0-week ($p<0.0001$) and

pre-injection levels (p=0.0068) at 3-week post-TAM (1.70±0.25; n=6). Therefore, SERCA2a expression in STX1A+/- mice did not show significant recovery while in STX1A KO mice a significant fold-increase of SERCA2a expression was seen at 3-week post-TAM (Figure 20F).

Sodium Calcium Exchanger NCX1

The sodium calcium exchanger (NCX) can extrude Ca^{2+} from the cardiomyocyte. In the mouse heart, the NCX1 is the predominant isoform expressed. NCX1 expression was unique in that male and female mice at 0-week post-TAM did not show significantly altered fold-change compared to pre-injection levels in any of the groups (Figure 20G, H). However, at 3 weeks, NCX1 fold-expression in male STX1A KO ($p<0.0001$) and STX1A+/- ($p=0.0024$) mice showed an increase in expression compared to 0 week. Also, at 3-week post-TAM, NCX1 fold-expression of male STX1A KO mice (3.75±0.42; n=6, $p<0.0001$) was greater than pre-injection levels (1.11±0.21; n=7), indicating a fold-increase in NCX1 expression (Figure 20G). In female groups, NCX1 fold-expression at 0-week and 3-week post-TAM was not significantly different than pre-injection levels. However, female STX1A KO mice did differ at 0-week and 3-week levels as seen by an increase in NCX1 fold-change at 3-week post-TAM compared to 0-week post-TAM ($p=0.0283$) (Figure 20H). Therefore, NCX1 expression in female groups did not differ from pre-injection levels while male STX1A KO mice showed a fold-increase in NCX1 expression at 3-week post-TAM.

Lastly, the gene expression in control Cre+ mice remained relatively unchanged, confirming that the contractile changes observed are not due to TAM or MCM-activation. In summary, the drop and subsequent recovery of key calcium handling genes provides a possible

explanation for the reduced contractility phenotype seen at 0-week post-TAM in STX1A KO and STX1A+/- male and female mice.

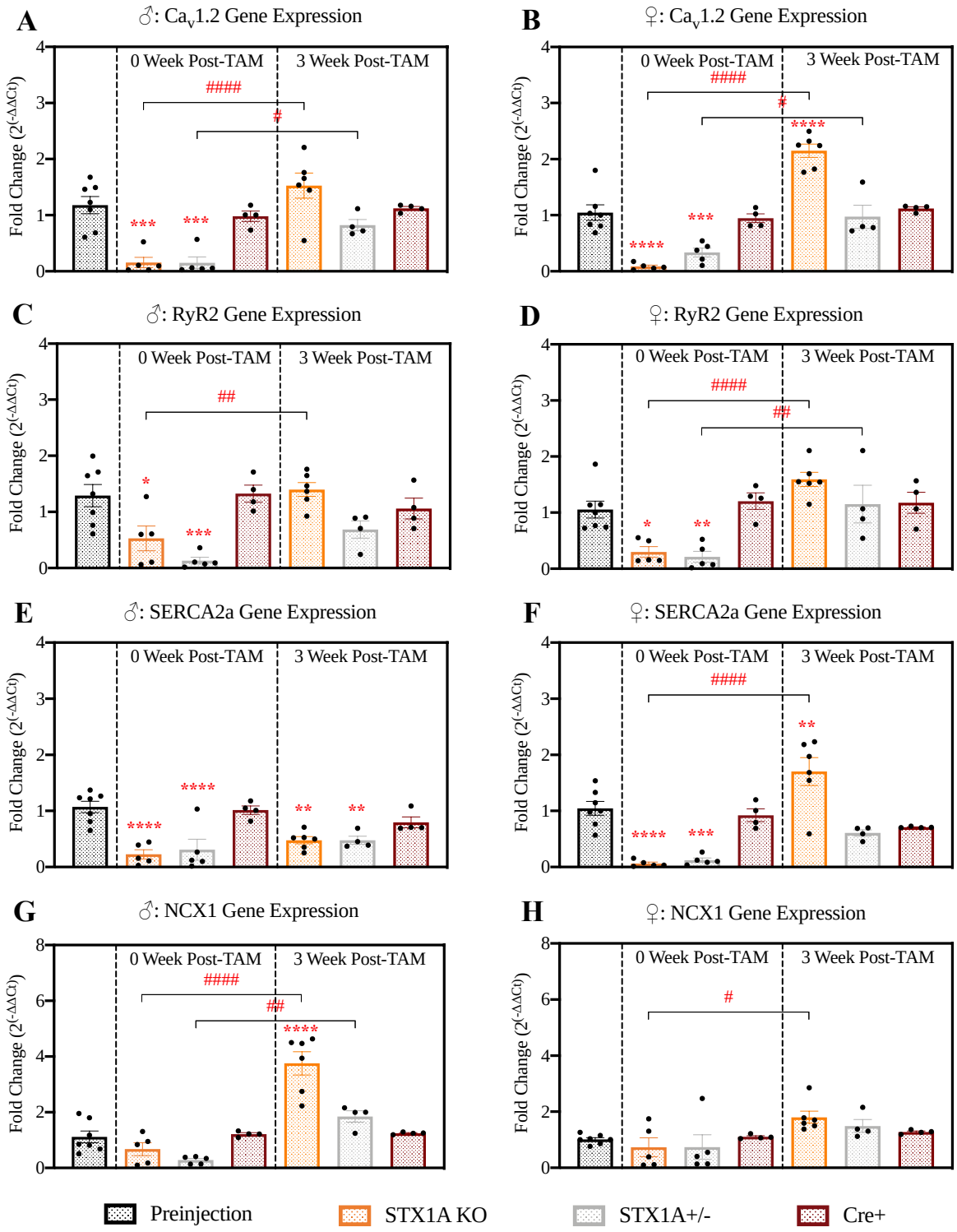


Figure 20: Calcium handling gene expression in left ventricular free wall of male (A, C, E, G) and female (B, D, F, H) groups. RT-qPCR of voltage-gated L-type calcium channels ($Ca_V1.2$), ryanodine receptor 2 (RyR2), sarco/endoplasmic reticulum Ca^{2+} ATPase 2a (SERC2a), and sodium/calcium exchanger 1 (NCX1) was done in male and female mice before TAM

injections (Pre-injection; black bars; male n=7; female n=7), directly after TAM injections (0 Week Post-TAM), and 3 weeks after TAM injections (3 Week Post-TAM). Gene expression in STX1A KO is shown by orange bars (male n=5, female n=5), STX1A+/- is shown by grey bars (male n=5, female n=5), and control Cre+ is shown by red bars (male n=4, female n=4). Reactions were run as duplicates with the fold-change computed using the $2^{(-\Delta\Delta Ct)}$ method and reported as mean±SEM. Individual values are shown as black dots. One-way ANOVA followed by Sidak's multiple comparisons test was done to determine significance, with comparisons to pre-injection states shown as red asterisks (****$p<0.0001$, ***$p<0.0002$, **$p<0.0021$, and *$p<0.0332$) and comparisons between 0 week and 3 week values shown as red pound signs (####$p<0.0001$, ##$p<0.0021$, and #$p<0.0332$).

3.9. Average C_t values for Housekeeping Genes

To confirm that changes in gene expression were not due to global decline of transcription, the average threshold cycle (Ct) of housekeeping genes utilized to calculate fold-change were examined (Figure 21). GAPDH and β-actin were selected as housekeeping genes, and the average Ct values revealed no significant change in expression levels in male and female groups. This confirmed that the changes in gene expression of the previously mentioned STXs and calcium-handling genes were not due to global changes in gene transcription brought on by the TAM-inducible Cre-Lox system.

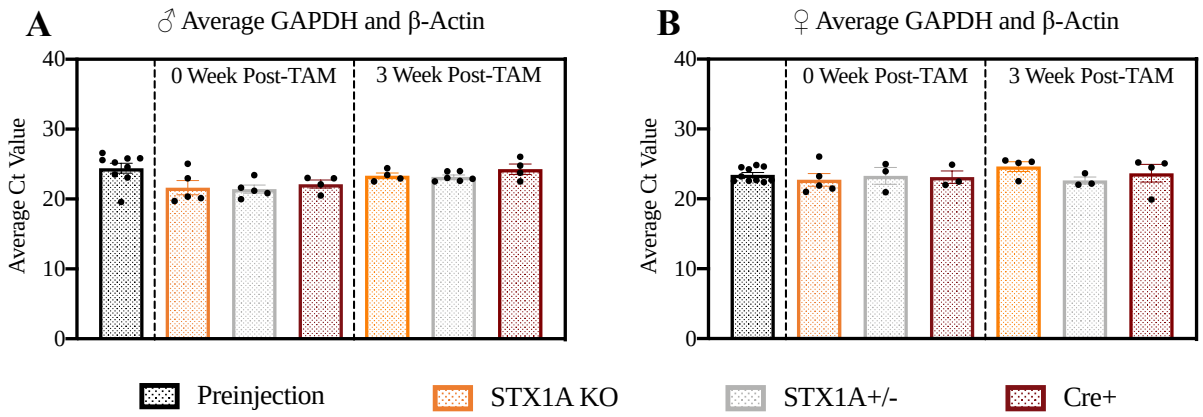


Figure 21: Average threshold cycle (Ct) values of housekeeping genes, GAPDH and β-actin, in left ventricular free wall of male and female groups. Data is displayed as mean±SEM with individual points shown as black dots. Black bars show housekeeping gene expression before TAM injections (Pre-injection; male n=9; female n=10). Gene expression was measures directly after TAM injections (0 Week Post-TAM), and 3 weeks after TAM injections (3 Week Post-TAM). Orange bars show STX1A KO groups (male n=4, female n=5), grey bars show STX1A+/- groups (male n=4, female n=4), and red bars show control Cre+ groups (male n=4, female n=4). GAPDH and β-actin were run alongside genes of interest and used to compute fold-change using the $2^{(-\Delta\Delta Ct)}$ method. All reactions were run as duplicates. One-way ANOVA followed by Sidak's multiple comparisons test revealed no statistical differences.

Chapter 4: Discussion

4.1. Summary of Results

The heart has two major roles; the first to act as a pump to circulate blood and the second to function as an endocrine organ to enact body-wide changes in response to blood pressure. However, to act as an endocrine organ the heart must possess exocytotic machinery as well. Thus, enters SNARE proteins, a super family of proteins dedicated to vesicle transport which are also present in the heart (Arien et al., 2003; Cohen et al., 2007; Trus et al., 2001; Wiser et al., 1996, 1999). SNARE proteins, specifically syntaxin-1A (STX1A), have been documented to interact and functionally inhibit voltage-gated calcium channels, which provide the initial influx of calcium (Ca^{2+}) in cardiac excitation-contraction (EC) coupling (Arien et al., 2003; Fabiato, 1983; Virdi, 2019). However, the caveat to these studies is that they were not conducted in the heart, but rather utilized *Xenopus* oocytes to artificially express and study STX1A and VGCCs in isolation. By doing so, such studies do not address the impact these interactions have on cardiac contractility, specifically EC coupling.

The Tsushima lab sought to address this question with the hypothesis that heart-specific STX1A knockout (KO) would remove the inhibitory effects of STX1A on voltage-gated Ca^{2+} channels (LTCCs), supplying a greater and faster Ca^{2+} trigger for EC coupling thus leading to a positive inotropic and chronotropic response (Virdi, 2019). It was found that STX1A KO in turn resulted in severe systolic dysfunction in adult male mice. Additionally, a delay in the time between R-wave to onset of contraction was found suggesting impaired Ca^{2+} handling during calcium-induced calcium release (CICR). Furthermore, the severely impaired cardiac phenotype was found to be transient with full recovery by week 4 after STX1A loss (Arien et al., 2003). Thus, this thesis aimed to further explore and elucidate the role of STX1A in cardiac EC

coupling with the prediction that impaired CICR is contributing to the phenotype observed and compensatory SNARE recruitment may account for the recovery seen. To build on the work done in homozygous STX1A knockout mice (STX1A KO), heterozygous STX1A knockout mice (STX1A+/-) were tested to evaluate whether a single copy of the STX1A gene was sufficient to retain normal cardiac function. Preliminary work also failed to address any inherent sex differences in adult mice, therefore, female mice were tested alongside male mice.

Echocardiography measurements showed impaired cardiac activity immediately after the 4^{th} tamoxifen injection (0 week) with subsequent recovery in the following weeks. End-systolic and end-diastolic dimension and volume, ejection fraction, and fractional shortening fully recovered at week 1. Stroke volume and cardiac output recovered at week 4 and week 3, respectively, in males. Female groups showed early recovery of cardiac output at week 1 while stroke volume recovered by 1-week in STX1A+/- mice and 3-week in STX1A KO mice. From the abovementioned trends, it was concluded that one copy of the functional STX1A gene was not enough to retain the normal phenotype and when compared to females, no significant difference based on sex was present in the mice.

A major question which was previously unanswered was what caused the loss of cardiac function to be transient. Two lines of inquiry were tested in this thesis, the first being compensatory changes to syntaxins (STXs) in response to STX1A loss and the second, alterations to key EC coupling genes. It was predicted that due to the shared sequence homology and their presence in the heart, compensatory recruitment of STX-2, 3, and/or 4 may account for the transient nature of cardiac impairment reported. Unexpectedly, gene expression of STX-2, 3, and 4 significantly declined at week 0 and displayed varying degrees of recovery at week 3. Therefore, a clear candidate for compensatory recruitment was not observed and this line of

inquiry did not explain the trends seen in echocardiographs. Interestingly, when expression of key EC coupling genes was measured, a significant decline in $Ca_v1.2$, RyR2, and SERCA2a gene expression was seen at week 0 in all groups. This corresponded to the decline seen in contractility and by week 3, $Ca_v1.2$ and RyR2 expression recovered while SERCA2a remained significantly lower in male groups. Unexpectedly, in male STX1A KO mice, a significant increase of NCX1 gene expression was observed at week 3 despite no change seen at week 0. In the case of female mice, recovery was also seen with significant increase of $Ca_v1.2$ and SERCA2a expression in female STX1A KO at 3-week. This, therefore, provided an explanation for the loss of cardiac function as the loss of contractility correlates with the transient decline in gene expression of key EC coupling genes.

4.2. Haploinsufficiency of STX1A to retain normal cardiac function in adult mouse hearts

Protein analyses confirmed that full and partial STX1A knockout was achieved in STX1A KO and STX1A+/- mice, respectively. Comparing the contractility phenotypes of STX1A KO and STX1A+/- mice revealed that a single copy of STX1A, which yielded approximately 50% of wild-type STX1A protein levels, was not sufficient to retain the normal cardiac phenotype. Systolic dysfunction, characterized by reduced ejection fraction and increased chamber size, was observed in heterozygous STX1A knockout mice as well as homozygous STX1A knockout mice. To eliminate confounding variables in the form of tamoxifen and MerCreMer activation, Cre+ mice were set as a control which received tamoxifen and possessed the MerCreMer construct. Since Cre+ mice did not display impaired contractility as seen in STX1A KO and STX1A+/- mice, it can be confidently stated that tamoxifen nor Cre toxicity are the sources of

this change. Thus, STX1A is haploinsufficient in retaining normal phenotype the adult mouse heart.

Although it is not clear why a single copy of STX1A is not sufficient to retain normal cardiac phenotype, a mechanism of haploinsufficiency can be speculated for STX1A. It has been documented that STX1A possesses the ability to dimerize via disulfide bonds of cysteine-271 and cysteine-272, however, it has also been proposed that the dimerized conformation of STX1A is the inactive form and favoured during low concentrations of STX1A (Arien et al., 2003). As seen in *Xenopus* oocytes, when concentrations of STX1A cRNA were progressively increased, the ratio of STX1A monomers to homodimers favoured monomers and a greater inhibition of Ca^{2+} currents through LTCC subunits was seen (Arien et al., 2003). The homodimer conformation of STX1A formed at low concentrations of the protein and was not the active configuration (Sieber et al., 2007). Therefore, in the case of STX1A+/- mice, which have 50% less STX1A protein, it can be speculated that the dimerized form is favoured, as such the STX1A protein which is present would be non-functional and thus analogous to a full STX1A knockout (STX1A KO). More to this, STX1A also possesses the ability to oligomerizes via its transmembrane region and form clusters containing upwards of 90 STX1A per cluster held together by weak homophilic interactions (Sieber et al., 2007). In this oligomerized state, the cytosolic N-terminal domain of STX1A can fold onto the SNARE motif and form a closed conformation in which the cytosolic domains are masked (Federmann & Hess, 1994; Jefferies & Towbin, 2010). Therefore, the dimerized or oligomerized states of STX1A could account of the indistinguishable phenotype of cardiac function in STX1A KO and STX1A+/- mice.

Since halved levels of STX1A result in qualitatively identical conditions of dilated ventricles, this conclusion can be compared to most cardiomyopathies which are also autosomal

dominant where a single effected copy of a gene can result a diseased state (Federmann & Hess, 1994; Schultheiss et al., 2019). STX1A deficient mice in this thesis display certain characteristic of dilated cardiomyopathy at week 0 such as systolic dysfunction, increased end-diastolic volume, and decreased stroke volume and cardiac output (Federmann & Hess, 1994; Schultheiss et al., 2019). Dilated cardiomyopathy is also characterized by an increase in end-diastolic pressure, presence of scar tissue, and in increase in left ventricular mass, which were not measured in this thesis (Du et al., 2007). In mouse models of dilated cardiomyopathy, an increase in left ventricular end-systolic and end-diastolic dimension coupled with decreased fractional shortening and ejection fraction were identified via echocardiography (Du et al., 2007). In this model, dilated cardiomyopathy was induced by targeting cardiac troponin T, a source of familial inheritance in which Ca^{2+} sensitivity is significantly lowered (Dellefave & McNally, 2010; Jefferies & Towbin, 2010). However, it is important to note that dilated cardiomyopathy can result from a plethora of causes routed in genetic inheritance of effected genes or develop from various systemic stressors which alter cardiac function (Jefferies & Towbin, 2010). One cause of dilated cardiomyopathy is impaired calcium homeostasis (Ashley & Niebauer, 2004). Although calcium homeostasis and calcium flux were not directly measured in this thesis, an interesting observation of prolonged ECG R-wave to onset of left ventricular contraction was seen in STX1A deficient mice. Given that ECG R-waves correspond to depolarisation of left ventricles, the prolongation of this interval suggests delay in the subsequent contraction of left ventricles following excitation of the tissue (Bers, 2002; Eisner et al., 2017; Fabiato, 1983). In STX1A KO mice, a significant delay in R-wave to onset of contraction was seen at 0- to 3-week in males and 0- to 1-week in females. Since the conversion of the electrical action potential to a physical response requires a chemical signal in the form of calcium, the

prolonged R-wave to onset of contraction suggests impaired calcium delivery which would directly effect CICR (Bers, 2002). CICR is central in supplying a rapid supply of Ca^{2+} from the SR to the intracellular space which then activates contractile proteins to achieve contraction (Fabiato, 1983). The key point of this statement is the "rapid supply" of Ca^{2+}, which signifies that it is not only the magnitude of change in intracellular Ca^{2+} concentration ($\Delta[Ca^{2+}]_i$) that is producing contraction but also how fast that change is occurring ($\Delta[Ca^{2+}]_i/\Delta t$) (Bennett et al., 1993; Bowman et al., 2019; Watson & Pessin, 2001). CICR from the SR is, therefore, dependent on the rate of Ca^{2+} delivery. The prolongation of the R-wave to onset of contraction suggests a delay in this delivery, which manifests as systolic dysfunction causing STX1A deficient mice to display characteristics similar to dilated cardiomyopathy. However, this still begs the question of why cardiac activity declines because as previously mentioned, active STX1A monomers lead to reduced Ca^{2+} currents in the presence of LTCC alpha subunits (Cav1.2) but in this thesis, loss of STX1A is leading to impaired contractility. Even more puzzling, is that the decline in cardiac activity is transient and recovery to the normal phenotype occurs between week 1 to week 4.

4.3. Decline of syntaxin genes in STX1A deficient mice

In order to address the question of transient cardiac impairment, specifically the recovery of function, genetic compensation of closely related syntaxins (STXs) in STX1A deficient mice was evaluated. It was predicted that in the absence of STX1A, other syntaxins (STXs) expressed in the heart may undergo compensatory upregulation that would account for the loss of STX1A. STX2, 3, and 4 were selected on the basis of shared sequence homology with STX1A, their localization on the plasma membrane, and their presence in the heart (Bennett et al., 1993). STX2 and STX3 were found to share 79% and 77% sequence homology with STX1A,

respectively (Kang et al., 2002). STX3 was also found to interact with Ca^{2+} channels (Kang et al., 2002; Xie et al., 2016). Although STX3 preferentially interacted with R-type channels, it also held the capability to interact and inhibit Ca^{2+} currents in L-type channels as well (Bennett et al., 1993; Bowman et al., 2019; Ferlito et al., 2010). In the case of STX4, comparatively less shared sequence homology existed (65%), however, STX4 was reported to be responsible for GLUT4 trafficking and ANP release in cardiomyocytes (El-Brolosy & Stainier, 2017). Thus, STX2, 3, and 4 were likely candidates that may undergo genetic compensation as a result of STX1A loss.

Mechanisms of genetic compensation or transcriptional adaptation can be triggered by DNA lesions and/or mutant mRNA (El-Brolosy & Stainier, 2017; Ziv et al., 2006). In the case of DNA lesions, damage to DNA could stimulate global chromatin reorganization in which compensating genes are stimulated due to easily accessible chromatin (Vance & Ponting, 2014). Mechanisms involving mutant mRNA rely on the end products from mRNA degradation. Fragmented mRNA, similar to long non-coding RNA, can recruit transcriptional factors to loci with shared homology to then stimulate those genes resulting in compensation (El-Brolosy & Stainier, 2017). In the event that RNA-binding proteins (RBPs) are shared between the targeted mRNA and the candidate compensating genes, the now available RBPs can stabilize mRNAs of compensating genes thus increasing gene expression (Bersell et al., 2013). Although, the specifics of such pathways are outside the scope of this thesis, the presence of these mechanisms reinforce that such avenues of genetic compensation have been documented.

However, in STX1A deficient mice, STX2 and STX3 gene expression significantly dropped. Varying degrees of recovery were seen, however, an increase in gene expression at week 3 was not observed for any of the genes tested compared to baseline levels. At week 3 gene expression of STX2 remained significantly lower in STX1A KO mice and STX3 expression

remained lower in male STX1A KO mice. Recovery of STX2 and STX3 at week 3 was only seen in male STX1A+/- mice. In the case of STX4, only female STX1A KO mice displayed a drop and then recovery of gene expression at week 0 and week 3, respectively.

In regard to the abovementioned mechanisms of genetic compensation, the possibility of DNA lesions/damage, for example by Cre recombinase activity, can confidently be eliminated (Liang et al., 2017; Sohal et al., 2001). Recalling that in control Cre+ mice, which were administered tamoxifen and expressed the activated MerCreMer complex, STX2, 3, and 4 expression remained stable and no significant fluctuations from un-injected mice (pre-injection) were observed. Additionally, the housekeeping genes, GAPDH and β-actin, remained stable across time points and between groups, therefore refuting the possibility that DNA damage altered gene expression. However, the second mechanism of compensation with fragments of degraded mRNA presents an interesting concept in STX1A deficient mice. Since the mechanism for heart specific STX1A knockout relies on excising exon 2 and 3 of STX1A, this results in a non-functional mRNA destined for degradation (Bers, 2002). As mentioned, mRNA fragments could stimulate loci with shared homology such as STX2, 3 and 4, therefore, it can be speculated that the degraded non-functional STX1A mRNA could play a role in the recovery of STX genes. Although direct experiments testing this were not conducted, it can be speculated if such a mode of compensation were to occur it would be prominent in STX1A KO mice where the presence of fragmented STX1A mRNA would be greater and thus in a dose-dependent manner lead to greater stimulation of gene expression. However, this was not seen since expression of STXs in STX1A KO mice, except for STX3 in female STX1A KO mice, remained significantly lower at week 3. Female STX1A KO mice also displayed significant recovery of STX4 expression. Although recovery of STX2 gene expression was not seen in male STX1A KO mice, a

significant increase from 0-week levels was indeed observed at 3-week, indicating that gene expression had begun to recover but was still lower than baseline levels. Within the groups that showed significant recovery, STX2 and STX3 recovered in male STX1A+/- mice. Thus, it can be further posited that the stressor in mice that have a heterozygous loss of STX1A is less allowing recovery to occur by week 3, while gene expression in mice with a homozygous STX1A loss are still recovering at this time. Therefore, this presents an interesting concept since STX1A knockout is sustained at week 3 and thus assumes that fragmented STX1A mRNA must also be present, albeit for a limited amount of time before full degradation. Therefore, as opposed to leading to a compensatory increase in STXs, the fragmented STX1A mRNA could instead be working to recover the drop in STX expression seen at week 0. Unfortunately, such a mechanism is merely speculation at this time and experiments directly addressing transcriptional effects of STX1A mRNA fragments have not been done. Nevertheless, returning to the original question, compensation of STXs as a mode of cardiac function recovery was not seen and does not answer why the normal cardiac phenotype returns in STX1A deficient mice.

4.4. EC coupling gene expression in STX1A deficient mice

Recalling that cardiac EC coupling is dependent on CICR, the next step was to examine expression levels of key EC coupling genes as an explanation for the phenotype observed in STX1A deficient mice. Gene expression analyses revealed a significant drop in $Ca_v1.2$ (alpha subunit of LTCCs), RyR2, and SERCA2a at 0-week followed by recovery at week 3. To reiterate, an action potential on the myocyte sarcolemma opens LTCCs producing a Ca^{2+} current that triggers the opening of RyR2s on the SR resulting in a rapid rise in $[Ca^{2+}]_i$, which activates contractile proteins (Bers, 2002). Relaxation occurs via Ca^{2+} removal by either actively pumping

Ca^{2+} into the SR via SERCA2a or exchanging it for Na^{+} at the sarcolemma via NCX1 (Eisner et al., 2017). Therefore, the drop in $Ca_v1.2$, RyR2, and SERCA2a gene expression explains the decline in cardiac activity observed via echocardiography as the genes responsible for EC coupling are severely downregulated and the subsequent recovery of these genes corresponds with the recovery of contraction.

Keeping in mind that cardiac contraction is produced by the rhythmic release and sequestering of Ca^{2+}, each cardiac cycle therefore must maintain a balance of calcium flux. Deviations from this steady state either lead to a net gain or loss of Ca^{2+} (Eisner et al., 2017; Fabiato & Fabiato, 1979). Greater influx of Ca^{2+} via LTCCs increases the available Ca^{2+} that can be loaded into the SR. By increasing SR Ca^{2+} content, Ca^{2+} transient amplitudes increase, and myocytes become more sensitive to Ca^{2+} changes whereby CICR can be triggered at lower changes to free [Ca^{2+}] (Fabiato, 1983). Increase in free $[Ca^{2+}]_i$ also results in more Ca^{2+} release events with greater tension transients until an optimal trigger concentration is achieved (Fabiato & Fabiato, 1977). However, an increase in LTCCs Ca^{2+} influx alone cannot activate contractile proteins, therefore, a positive inotropic effect is achieved through priming the SR for CICR in subsequent contractions leading to increased contractility (Shannon et al., 2003). Taking a closer look at the SR, another steady state of importance is present, this one pertaining directly to SR Ca^{2+} flux. SR free [Ca^{2+}] decreases by 50-75% during systole, hence, the Ca^{2+} efflux from RyR2s must balance Ca^{2+} influx via SERCA2a (Díaz et al., 2005). Therefore, in addition to Ca^{2+} influx via LTCCs, SR Ca^{2+} content is dependent on SERCA2a, which loads Ca^{2+} into the SR, and RyR2s, which release Ca^{2+} from the SR (Barcenas-Ruiz et al., 1987; Sipido et al., 1995). As mentioned, a steady state of Ca^{2+} flux exists and thus to counteract Ca^{2+} gain, a negative feedback loop activates modes of restricting Ca^{2+} influx while promoting efflux. This is achieved

by the NCX1 moving Ca^{2+} out of the cell due to increased $[Ca^{2+}]_i$ and the Ca^{2+} dependent inactivation of LTCCs (Brum et al., 1984; Fabiato, 1983). This will limit the entry of Ca^{2+} and the excess Ca^{2+} will be removed by promoting net movement out of the myocyte—producing lower amplitude Ca^{2+} transients and states of reduced contractility.

Having briefly explained calcium flux balance, it can now be understood how the significant decline in $Ca_v1.2$, RyR2, and SERCA2a gene expression at week 0 results in a negative inotropic effect and thus impaired contractility. Although Ca^{2+} handling and macroscopic channel currents were not directly measured in this thesis, the fold-decrease of $Ca_v1.2$ gene expression suggests a decline in LTCC currents which would directly alter contraction (Shibasaki, 1987). Macroscopic currents are expressed as the product of unitary channel conductance, the open probability of a channel, and the number of channels (Soeller & Baddeley, 2013). The single-channel conductance and open probability was not measured in this thesis, but the decrease in $Ca_v1.2$ gene expression suggests a drop in the number of channels which would in turn lead to a decline in macroscopic LTCC currents in cardiomyocytes. Therefore, the influx of Ca^{2+} which is the trigger for CICR is substantially reduced if we make the assumption that the decrease in gene expression reflects in the number of LTCC channels in STX1A deficient mice. Gene expression of RyR2 was also significantly reduced at week 0 in STX1A deficient mice. Since RyR2s form clusters on the SR in close vicinity to LTCCs, a decrease in gene expression of RyR2 can suggest a decrease in the cluster size which is normally composed of 14-100 receptors each (Soeller & Baddeley, 2013). It is well known that cluster size and organization directly affect Ca^{2+} release from RyR2 clusters. More RyR2 in a cluster cooperatively effect sensitivity to activation and termination where more RyR2s in a cluster increase the probability of that cluster being activated and prevent premature inactivation as well (Fabiato, 1983). If gene expression is assumed to

reflect number of RyR2s, then the quantity and open probability of RyR2 declines in STX1A deficient mice resulting in decreased contractility.

Recalling that the influx of Ca^{2+} via LTCCs alters SR Ca^{2+} stores, it can be speculated that SR Ca^{2+} content in STX1A deficient mice is depleted. Additionally, accumulating Ca^{2+} into the SR is time dependent and must occur before the next Ca^{2+} release event (Fabiato, 1983). Therefore, the drop in SERCA2a expression further suggests a decrease in SR Ca^{2+} stores because less Ca^{2+} would be shuttled into the SR within that time frame (Fabiato, 1983). This would explain the reduced ejection fraction and fractional shortening as this corresponds to reduced contractility. Additionally, NCX1 gene expression was also measured and at week 0 no significant change in gene expression was seen, therefore, the Ca^{2+} efflux mechanism can be assumed to remain intact and further push the Ca^{2+} steady state towards net loss. Since a fully loaded SR is more sensitive to changes in free $[Ca^{2+}]_i$ and more readily results in CICR, the lower SR Ca^{2+} content would require a greater Ca^{2+} trigger which cannot be rapidly supplied by the diminished LTCC expression (Arai et al., 1993; Studer et al., 1994). This claim is further supported by the delay in R-wave to onset of contraction which can now be explained as a delay in CICR where the limited expression of LTCCs results in a slow build-up of the Ca^{2+} trigger required to activate CICR. As such the SR, with its depleted Ca^{2+} stores, results in low amplitude Ca^{2+} transients and thus reduced contractility.

By examining expression of EC coupling genes, it can now be concluded that the impaired contractility in STX1A deficient mice is due to the downregulation of EC coupling genes at week 0 and the recovery of contraction is due to recovery of gene expression by 3-week post-TAM. At week 3, $Ca_v1.2$, RyR2, and SERCA2a gene expression recovers in female mice, with female STX1A KO mice showing a 2.1- and 1.7-fold increase in $Ca_v1.2$ and SERCA2a

expression, respectively. $Ca_v1.2$ and RyR2 recovered in male groups as well but, notably SERCA2a expression remained significantly lower and NCX1 expression significantly increased. Therefore, the recovery of contraction can be credited to the recovery of $Ca_v1.2$ and RyR2. However, this poses new questions of how STX1A loss results in downregulation of EC coupling genes with the exception of NCX1, why SERCA2a remains significantly decreased in male STX1A KO mice when an increase in seen in the corresponding female group, and what causes the recovery and in some cases the fold-increase of EC coupling gene expression.

It is interesting to note that the changes seen in the transcription levels of SERCA2a, RyR2, and NCX1 are also seen in cases of heart failure (Nishikimi et al., 2006). In a failing heart, ANP and BNP release is elevated to promote renal diuresis and natriuresis in an endocrine fashion (Klaiber et al., 2011). The cardiac natriuretic peptides can also have an autocrine and paracrine effect by activating the cGMP/PKG pathway. Guanylyl cyclase A or natriuretic peptide receptor A binds ANP and BNP to then synthesize cGMP and activate cGMP-dependent protein kinase I (PKG I) (Klaiber et al., 2011; Tokudome et al., 2005). PKG I can have anti-hypertrophic effects via inhibition of calcineurin, a phosphatase in cardiomyocytes which controls the nuclear translocation of nuclear factor of activated T cells (NFAT) (Tokudome et al., 2005). NFAT is a transcription factor that once dephosphorylated can translocate into the nucleus, associate with GATA4, and activate hypertrophy related genes (Kögler et al., 2006). Therefore, activation of PKG I via ANP/BNP can be cardioprotective as this would limit transcription of hypertrophic genes by preventing NFAT translocation. But the disadvantage to inhibiting this cell signaling pathway is that SERCA2a is also regulated by NFAT and GATA4 and thus is downregulated during elevated ANP/BNP levels (Arai et al., 1993). RyR2 also shares this inverse relationship, where RyR2 mRNA undergoes a significant decline while ventricular ANP/BNP levels increase

during heart failure (Menick et al., 2007; Studer et al., 1994). In response to alpha-adrenergic stimulation, NCX1 mRNA levels increase in the failing heart in order to compensate for the reduced SR loading during diastolic Ca^{2+} removal (D'Souza et al., 2004). In response to mechanical strain, both the release and the expression of ANP and BNP is stimulated (Bloch et al., 1986). In neonatal hearts, the atria can store ANP granules for regulated and constitutive release while the ventricles only constitutively release ANP. Quickly after birth the ANP expression from the ventricles diminishes making the atria the primary regulated ANP source in a healthy heart (Schaible & Scheuer, 1984). However, in a failing heart, ventricular synthesis of ANP increases. Since a heart-specific and not a ventricle-specific knockout of STX1A was done in this project, it can be assumed that atrial STX1A was also targeted. Recalling that STX1A contributes to regulated exocytosis, it can be speculated that the loss of atrial STX1A impairs regulated release of ANP. Therefore, only constitutive release of ANP from the atria and ANP/BNP from the ventricles would be seen. Although ANP expression was not measured, the transcriptional changes observed in STX1A deficient mice are similar to those seen in failing hearts which have elevated ventricular ANP levels. Therefore, it can be speculated that a loss of STX1A might limit the heart to constitutive ANP release which can have autocrine and paracrine effects that alter transcription via downstream intracellular signalling. However, more work is necessary to connect the transcriptional fluctuations seen in EC coupling genes to STX1A loss.

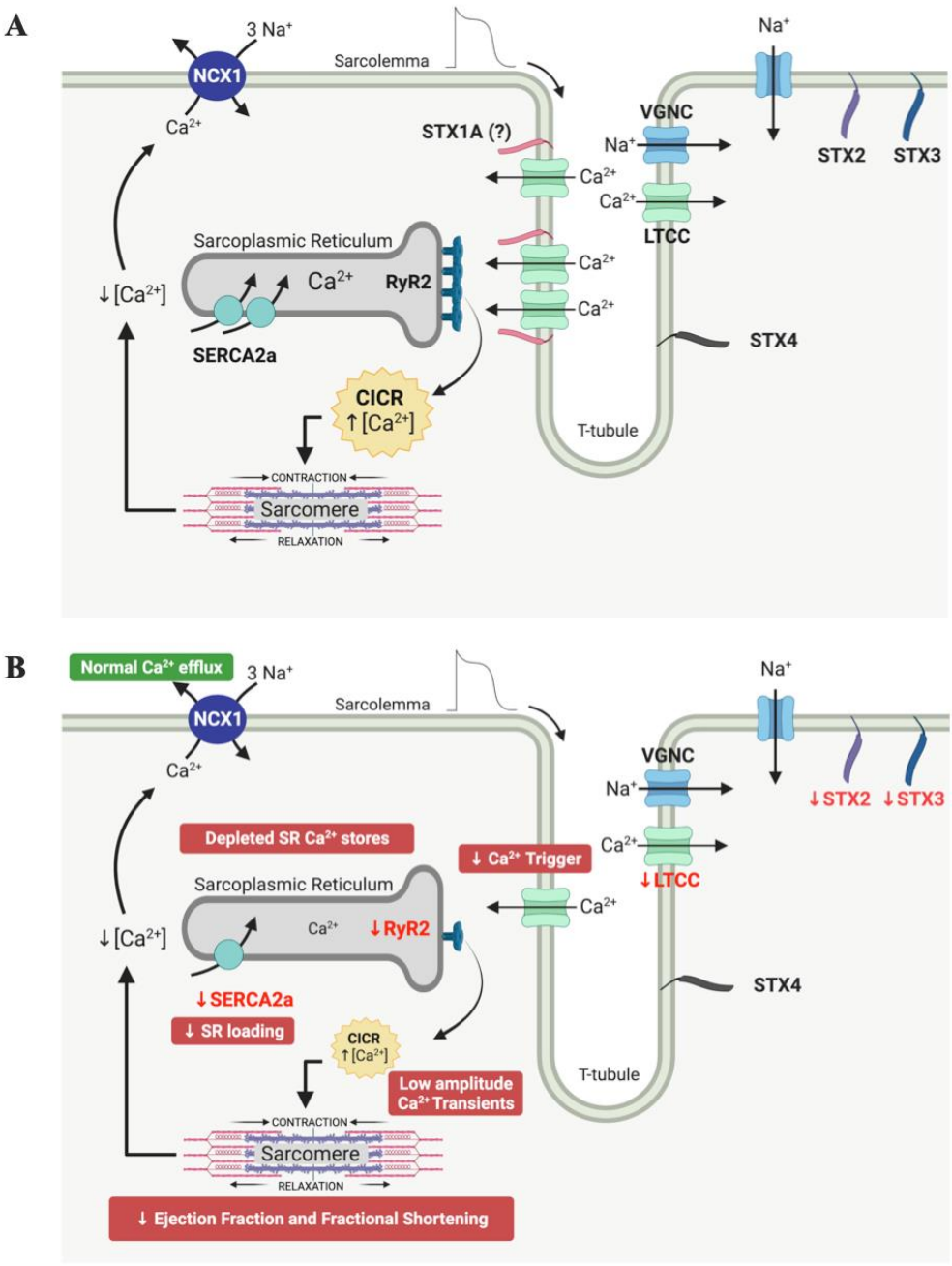


Figure 22: Cardiac excitation-contraction (EC) coupling and the proposed changes to this pathway after STX1A loss. (A) Schematic diagram of EC coupling in the healthy cardiomyocyte. (B) Transcription levels of LTCC, RyR2, and SERCA2a decrease in STX1A KO cardiomyocytes. It is proposed that decreased LTCC gene expression results in a decline in the total number of LTCC on the sarcolemma and total Ca^{2+} influx. When this is coupled with decreased RyR2 gene expression, it is hypothesized to result in reduced CICR and low amplitude Ca^{2+} transients. Depletion of SR Ca^{2+} stores are proposed due to reduced SERCA2a gene expression. No change to NCX1 gene expression suggested normal Ca^{2+} efflux. Taken together, a fall in intracellular Ca^{2+} transients is proposed to be the primary contributing factor causing the reduced contractility in STX1A KO hearts. Figure was generated using BioRender.com.

4.5. Sex differences in STX1A deficient mice

Another question addressed in this thesis was whether inherit sex differences existed in mice before STX1A loss. Studies in rat models have shown that female rats have lower ejection fraction, fractional shortening, and cardiac output (Curl et al., 2001; Farrell et al., 2010; Parks et al., 2014; Schaible & Scheuer, 1984). Contrary to this, the transgenic mice in this thesis did not show differences of ejection fraction and fractional shortening prior to tamoxifen treatment. However, stroke volume and cardiac output were found to be greater in male STX1A+/- mice compared to corresponding female mice of the same genotype. A similar difference was not seen in STX1A KO nor Cre+ groups at baseline values. In studies where mice were the model, cardiac differences *in vivo* were not seen in ejection fraction and fractional shortening. The studies which report sex differences of cardiac activity utilize isolated cardiomyocytes that do not replicate conditions *in vivo* and many studies have used rats as their model (Mahmoodzadeh et al., 2013).

In this thesis, molecular comparisons between male and female mice were not done, however, in response to STX1A loss similar decline in cardiac function was observed in male and female mice without a stark sexual dimorphism. A noticeable difference was seen in posterior wall thickness, where female mice showed a significant thickening of the left ventricular posterior wall for both STX1A KO and STX1A+/- mice while only STX1A+/- male mice showed posterior wall thickening at week 1. Although myocardial hypertrophy was not directly measured, the thickening of the posterior wall in female mice corresponds with occurrence of concentric hypertrophy in females compared to eccentric hypertrophy in males (Mahmoodzadeh et al., 2013). It is proposed that females cope better to cardiovascular stressors and are able to sustain left ventricular function better compared to males. This is thought to occur due to 17β-estradiol being cardioprotective again physiological and pathological stressors and

contribute to the activation of connexin 43, alpha-myosin heavy chain, matrix metalloproteinases, and atrial natriuretic peptide (Gao et al., 2005; Panidis et al., 1984). However, the increase in posterior wall thickness was transient and returned to normal by week 3, therefore, permanent morphological changes did not occur in STX1A deficient mice. Regression of hypertrophy can occur when left ventricular structural and functional changes are moderate and can be estimated by observing a moderate increase in left ventricular mass (25-50%) (Mahmoodzadeh et al., 2013; Panidis et al., 1984). Measuring left ventricular mass using echocardiography is a non-invasive method of gauging the hypertrophic response because an increase in mass is common to both concentric and eccentric hypertrophy (Merlo et al., 2018; Panidis et al., 1984). Left ventricular mass was not measured in this thesis, but it can be posited that the increase in posterior wall thickness corresponds to a moderate increase in left ventricular mass. Additionally, in dilated cardiomyopathy, timely treatment with vasodilators that improve cardiac function have shown regression of myocardial hypertrophy (Gao et al., 2005). Regression of hypertrophy has also been identified in mouse models where the stressor, such as a pressure overload, is removed with rapid and complete recovery seen when the stressor is removed earlier (Kukurba & Montgomery, 2015). Therefore, the timely removal or treatment of the stressor can result in regression of hypertrophy.

It can be speculated that the reduced contractility at week 0 promotes myocardial hypertrophy in STX1A deficient mice at week 1, which would also contribute to the recovery of cardiac function also seen at week 1. Given that compared to males, female hearts display concentric hypertrophy, this would be seen as an increase in posterior wall thickness in female mice, which is consistent with the results. The regression of posterior wall thickness at week 3 coincides with the removal of the impaired contractility stressor which is thought to occur due to

the recovery of EC coupling genes at week 3. In order to further evaluate whether the increase in posterior wall thickness at week 1 is a hypertrophic response and whether sexual dimorphism in myocardial hypertrophy exists in STX1A deficient mice, the expression of hypertrophic markers and left ventricular mass must be examined.

4.6. Conclusion and Future Directions

From the data presented in this thesis it can be concluded that the loss of STX1A, whether it be a full heart-specific knockout or a heterozygous knockout, cardiac activity experiences similar transient systolic dysfunction followed by recovery to the normal phenotype starting at week 1. This trend was shared between male and female mice with no significant difference found between the sexes either. Compensatory changes to closely related STXs was not found but surprisingly these STXs showed a decline in gene expression after STX1A loss. However, the key finding in this thesis, and one that provides the beginnings of an explanation for the trends seen, was the expression levels of EC coupling genes after STX1A loss. Corresponding to the loss of cardiac activity, key EC coupling genes, which dictate normal cardiac contraction, were found to drastically decrease in expression and recover by week 3, analogous to the phenotypic recovery seen in echocardiographs. Since STX1A levels remained diminished when recovery is seen, it can be speculated that the loss of STX1A is not directly leading to the drop in EC coupling genes and thus the phenotype observed, but rather a self-limiting pathway is triggered by the loss of STX1A. Hence, from the limited information that is known of STX1A in the adult mouse heart, it is proposed that a feedback mechanism is triggered upon STX1A loss which leads to a drop in EC coupling genes and closely related STXs, manifesting as impaired contractility and, due to the self-limiting nature of this pathway, recovery is seen despite STX1A levels remaining lowered. What this mechanism is and what is producing the self-limiting

characteristic that reverts the phenotype to normal is unknown and requires further, extensive work.

To build on the current data, the following can be done. Since qPCR data indicated a severe decline in select STXs and EC coupling genes, the next step would be to determine whether the decline in gene expression is reflected in protein levels. Hence, western blots on STX2, 3, and 4 as well as $Ca_v1.2$, RyR2, SERCA2a, and NCX1 should be done. To further reveal the molecular expression changes brought on from STX1A KO, an unbiased and broad look at mRNA expression should be done. Since the general trend for the genes tested in this thesis was a fold-decrease followed by varying degrees of recovery, RNA sequencing on STX1A deficient mice should be done to investigate whether this trend is shared by more genes and following up by identifying the effected molecular pathways (Arien et al., 2003). Additionally, haploinsufficiency of STX1A in the heart was proposed due to dimerization and oligomerization of STX1A monomers, which transitions the protein into an inactive configuration (Arien et al., 2003). To address whether the dimerized form is abundant in STX1A+/- mice, an experiment similar to that done by (Arien et al., 2003) in which the monomer-to-homodimer ratios were determined should be done. By preparing protein samples in the absence of SDS and dithiothreitol, the thiol bonds of Cys-271 and Cys-272 would be preserved, allowing STX1A dimers to be visualized on western blots (Gorski et al., 2018). Such experiments would provide further evidence for the claims made in this thesis, which at the current stage are speculation.

Given that impaired calcium handling was suggested as a possible explanation for the phenotype observed in STX1A deficient mice, this provides an avenue for future experiments. For example, Ca^{2+} transient measurements and SR Ca^{2+} content evaluations would provide additional information directly pertaining to the claims of impaired calcium handling and

depleted SR Ca^{2+} stores. By analyzing Ca^{2+} transient waveforms, information such as the rate of Ca^{2+} release, magnitude and duration of high $[Ca^{2+}]_i$ state, and rate of Ca^{2+} removal can be determined (Efimov et al., 2004). All these parameters encompass calcium kinetics and directly evaluate CICR in cardiomyocytes. Additionally, caffeine-induced unloading of the SR can be done to empirically determine whether SR Ca^{2+} stores are depleted upon STX1A loss as speculated in this thesis. Furthermore, a delay in R-wave to onset of contraction was observed that suggested potential EC uncoupling in STX1A deficient mice. To address this, multiparametric optical imaging can be done which simultaneously measures transmembrane potential and intracellular Ca^{2+} transients of intact cardiac tissue (Zhao et al., 2015). This would, therefore, supply greater evidence for the spatiotemporal relationship of voltage propagation in cardiac muscle and the changes in $[Ca^{2+}]_i$ while maintaining the integrity of the tissue to an extent. The possibility of a hypertrophic response, which eventually regresses by week 3 was suggested in STX1A deficient mice. However, hypertrophy was not directly addressed in this thesis. Therefore, to explore the claims made based on posterior wall thickness, hypertrophy in STX1A deficient mice must be addressed. Hallmarks of hypertrophy include increased heart weight and cardiomyocyte size, increased type I collagen and alpha-smooth muscle actin that indicate fibrosis in the heart, as well as elevated expression of beta-myosin heavy chain, ANP/BNP, and skeletal muscle alpha actin, which are markers of cardiac hypertrophy (Humphrey & McCulloch, 2003; Thiriet, 2008).

Therefore, the added data from these experiments will address new questions which have arisen and provide a better understanding of the role of STX1A has in the adult mouse heart.

References

Aalto, M. K., Ronne, H., & Keränen, S. (1993). Yeast syntaxins Sso1p and Sso2p belong to a family of related membrane proteins that function in vesicular transport. *The EMBO Journal*, *12*(11), 4095–4104. https://doi.org/10.1002/j.1460-2075.1993.tb06093.x

Arai, M., Alpert, N. R., MacLennan, D. H., Barton, P., & Periasamy, M. (1993). Alterations in sarcoplasmic reticulum gene expression in human heart failure. A possible mechanism for alterations in systolic and diastolic properties of the failing myocardium. *Circulation Research*, *72*(2), 463–469. https://doi.org/10.1161/01.RES.72.2.463

Arien, H., Wiser, O., Arkin, I. T., Leonov, H., & Atlas, D. (2003). Syntaxin 1A Modulates the Voltage-gated L-type Calcium Channel (Cav1.2) in a Cooperative Manner. *Journal of Biological Chemistry*, *278*(31), 29231–29239. https://doi.org/10.1074/jbc.M301401200

Ashley, E., & Niebauer, J. (2004). Chapter 3 Conquering the ECG. In *Cardiology Explained*.

Barcenas-Ruiz, L., Beuckelmann, D. J., & Wier, W. G. (1987). Sodium-calcium exchange in heart: membrane currents and changes in [Ca2+] i. *Science*, *238*(4834), 1720–1722.

Bennett, M. K., Garcia-Arrarás, J., Elferink, L. A., Peterson, K., Fleming, A. M., Hazuka, C. D., & Scheller, R. H. (1993). The syntaxin family of vesicular transport receptors. *Cell*, *74*(5), 863–873. https://doi.org/10.1016/0092-8674(93)90466-4

Bers, D. M. (2002). Cardiac excitation–contraction coupling. *Nature*, *415*(6868), 198–205. https://doi.org/10.1038/415198a

Bersell, K., Choudhury, S., Mollova, M., Polizzotti, B. D., Ganapathy, B., Walsh, S., Wadugu, B., Arab, S., & Kühn, B. (2013). Moderate and high amounts of tamoxifen in α-MHC-MerCreMer mice induce a DNA damage response, leading to heart failure and death. *Disease Models & Mechanisms*. https://doi.org/10.1242/dmm.010447

Bloch, K. D., Seidman, J. G., Naftilan, J. D., Fallon, J. T., & Seidman, C. E. (1986). Neonatal atria and ventricles secrete atrial natriuretic factor via tissue-specific secretory pathways. *Cell*, *47*(5), 695–702. https://doi.org/10.1016/0092-8674(86)90512-X

Bowman, P. R. T., Smith, G. L., & Gould, G. W. (2019). Cardiac SNARE Expression in Health and Disease. *Frontiers in Endocrinology*, *10*. https://doi.org/10.3389/fendo.2019.00881

Brillantes, A.-M. B., Ondrias, K., Scott, A., Kobrinsky, E., Ondriašová, E., Moschella, M. C., Jayaraman, T., Landers, M., Ehrlich, B. E., & Marks, A. R. (1994). Stabilization of calcium release channel (ryanodine receptor) function by FK506-binding protein. *Cell*, *77*(4), 513–523. https://doi.org/10.1016/0092-8674(94)90214-3

Brum, G., Osterrieder, W., & Trautwein, W. (1984). ?-Adrenergic increase in the calcium conductance of cardiac myocytes studied with the patch clamp. *Pfl*[illegible]*gers Archiv European Journal of Physiology*, *401*(2), 111–118. https://doi.org/10.1007/BF00583870

Chen, Y. A., & Scheller, R. H. (2001). SNARE-mediated membrane fusion. *Nature Reviews Molecular Cell Biology*, *2*(2), 98–106. https://doi.org/10.1038/35052017

Chu, S. H., Sutherland, K., Beck, J., Kowalski, J., Goldspink, P., & Schwertz, D. (2005). Sex differences in expression of calcium-handling proteins and beta-adrenergic receptors in rat heart ventricle. *Life Sciences*, *76*(23), 2735–2749. https://doi.org/10.1016/j.lfs.2004.12.013

Cohen, R., Marom, M., & Atlas, D. (2007). Depolarization-Evoked Secretion Requires Two Vicinal Transmembrane Cysteines of Syntaxin 1A. *PLoS ONE*, *2*(12), e1273. https://doi.org/10.1371/journal.pone.0001273

Curl, C. L., Wendt, I. R., & Kotsanas, G. (2001). Effects of gender on intracellular [Ca2+] in rat cardiac myocytes. *Pflügers Archiv*, *441*(5), 709–716. https://doi.org/10.1007/s004240000473

D'Souza, S. P., Davis, M., & Baxter, G. F. (2004). Autocrine and paracrine actions of natriuretic peptides in the heart. *Pharmacology & Therapeutics*, *101*(2), 113–129. https://doi.org/10.1016/j.pharmthera.2003.11.001

de Bold, A. J., Borenstein, H. B., Veress, A. T., & Sonnenberg, H. (1981). A rapid and potent natriuretic response to intravenous injection of atrial myocardial extract in rats. *Life Sciences*, *28*(1), 89–94. https://doi.org/10.1016/0024-3205(81)90370-2

de Bold, A. J., Raymond, J. J., & Bencosme, S. A. (1978). Atrial specific granules of the rat heart: light microscopic staining and histochemical reactions. *Journal of Histochemistry & Cytochemistry*, *26*(12), 1094–1102. https://doi.org/10.1177/26.12.83339

Dellefave, L., & McNally, E. M. (2010). The genetics of dilated cardiomyopathy. *Current Opinion in Cardiology*, *25*(3), 198–204. https://doi.org/10.1097/HCO.0b013e328337ba52

Díaz, M. E., Graham, H. K., O'Neill, S. C., Trafford, A. W., & Eisner, D. A. (2005). The control of sarcoplasmic reticulum Ca content in cardiac muscle. *Cell Calcium*, *38*(3–4), 391–396. https://doi.org/10.1016/j.ceca.2005.06.017

Du, C.-K., Morimoto, S., Nishii, K., Minakami, R., Ohta, M., Tadano, N., Lu, Q.-W., Wang, Y.-Y., Zhan, D.-Y., Mochizuki, M., Kita, S., Miwa, Y., Takahashi-Yanaga, F., Iwamoto, T., Ohtsuki, I., & Sasaguri, T. (2007). Knock-In Mouse Model of Dilated Cardiomyopathy Caused by Troponin Mutation. *Circulation Research*, *101*(2), 185–194. https://doi.org/10.1161/CIRCRESAHA.106.146670

Efimov, I. R., Nikolski, V. P., & Salama, G. (2004). Optical Imaging of the Heart. *Circulation Research*, *95*(1), 21–33. https://doi.org/10.1161/01.RES.0000130529.18016.35

Eisner, D. A., Caldwell, J. L., Kistamás, K., & Trafford, A. W. (2017). Calcium and Excitation-Contraction Coupling in the Heart. *Circulation Research*, *121*(2), 181–195. https://doi.org/10.1161/CIRCRESAHA.117.310230

El-Brolosy, M. A., & Stainier, D. Y. R. (2017). Genetic compensation: A phenomenon in search of mechanisms. *PLOS Genetics*, *13*(7), e1006780. https://doi.org/10.1371/journal.pgen.1006780

Fabiato, A. (1983). Calcium-induced release of calcium from the cardiac sarcoplasmic reticulum. *American Journal of Physiology-Cell Physiology*, *245*(1), C1–C14. https://doi.org/10.1152/ajpcell.1983.245.1.C1

Fabiato, A., & Fabiato, F. (1977). Calcium release from the sarcoplasmic reticulum. *Circulation Research*, *40*(2), 119–129. https://doi.org/10.1161/01.RES.40.2.119

Fabiato, A., & Fabiato, F. (1979). Use of chlorotetracycline fluorescence to demonstrate Ca2+-induced release of Ca2+ from the sarcoplasmic reticulum of skinned cardiac cells. *Nature*, *281*(5727), 146–148. https://doi.org/10.1038/281146a0

Farrell, S. R., Ross, J. L., & Howlett, S. E. (2010). Sex differences in mechanisms of cardiac excitation-contraction coupling in rat ventricular myocytes. *American Journal of Physiology-Heart and Circulatory Physiology*, *299*(1), H36–H45. https://doi.org/10.1152/ajpheart.00299.2010

Federmann, M., & Hess, O. M. (1994). Differentiation between Systolic and Diastolic Dysfunction. *European Heart Journal*, *15*(suppl D), 2–6. https://doi.org/10.1093/eurheartj/15.suppl_D.2

Ferlito, M., Fulton, W. B., Zauher, M. A., Marbán, E., Steenbergen, C., & Lowenstein, C. J. (2010). VAMP-1, VAMP-2, and syntaxin-4 regulate ANP release from cardiac myocytes. *Journal of Molecular and Cellular Cardiology*, *49*(5), 791–800. https://doi.org/10.1016/j.yjmcc.2010.08.020

Fujiwara, T. (2006). Analysis of Knock-Out Mice to Determine the Role of HPC-1/Syntaxin 1A in Expressing Synaptic Plasticity. *Journal of Neuroscience*, *26*(21), 5767–5776. https://doi.org/10.1523/JNEUROSCI.0289-06.2006

Gao, X.-M., Kiriazis, H., Moore, X.-L., Feng, X.-H., Sheppard, K., Dart, A., & Du, X.-J. (2005). Regression of pressure overload-induced left ventricular hypertrophy in mice. *American Journal of Physiology-Heart and Circulatory Physiology*, *288*(6), H2702–H2707. https://doi.org/10.1152/ajpheart.00836.2004

Gerst, J. E. (1999). SNAREs and SNARE regulators in membrane fusion and exocytosis. *Cellular and Molecular Life Sciences*, *55*(5), 707–734. https://doi.org/10.1007/s000180050328

Gordon, A. M., Regnier, M., & Homsher, E. (2001). Skeletal and Cardiac Muscle Contractile Activation: Tropomyosin "Rocks and Rolls." *Physiology*, *16*(2), 49–55. https://doi.org/10.1152/physiologyonline.2001.16.2.49

Gorski, P. A., Kho, C., & Oh, J. G. (2018). Measuring Cardiomyocyte Contractility and Calcium Handling In Vitro. In *Methods in Molecular Biology* (pp. 93–104). https://doi.org/10.1007/978-1-4939-8597-5_7

Grandy, S. A., & Howlett, S. E. (2006). Cardiac excitation-contraction coupling is altered in myocytes from aged male mice but not in cells from aged female mice. *American Journal of Physiology-Heart and Circulatory Physiology*, *291*(5), H2362–H2370. https://doi.org/10.1152/ajpheart.00070.2006

Hougen, K., Aronsen, J. M., Stokke, M. K., Enger, U., Nygård, S., Andersson, K. B., Christensen, G., Sejersted, O. M., & Sjaastad, I. (2010). Cre-loxP DNA recombination is possible with only minimal unspecific transcriptional changes and without cardiomyopathy in Tg(αMHC-MerCreMer) mice. *American Journal of Physiology-Heart and Circulatory Physiology*, *299*(5), H1671–H1678. https://doi.org/10.1152/ajpheart.01155.2009

Humphrey, J. D., & McCulloch, A. D. (2003). The Cardiovascular System — Anatomy, Physiology and Cell Biology. In *Biomechanics of Soft Tissue in Cardiovascular Systems* (pp. 1–14). Springer Vienna. https://doi.org/10.1007/978-3-7091-2736-0_1

Jefferies, J. L., & Towbin, J. A. (2010). Dilated cardiomyopathy. *The Lancet*, *375*(9716), 752–762. https://doi.org/10.1016/S0140-6736(09)62023-7

Kang, Y., Huang, X., Pasyk, E. A., Ji, J., Holz, G. G., Wheeler, M. B., Tsushima, R. G., & Gaisano, H. Y. (2002). Syntaxin-3 and syntaxin-1A inhibit L-type calcium channel activity, insulin biosynthesis and exocytosis in beta-cell lines. *Diabetologia*, *45*(2), 231–241. https://doi.org/10.1007/s00125-001-0718-0

Klaiber, M., Dankworth, B., Kruse, M., Hartmann, M., Nikolaev, V. O., Yang, R.-B., Völker, K., Gaßner, B., Oberwinkler, H., Feil, R., Freichel, M., Groschner, K., Skryabin, B. V., Frantz, S., Birnbaumer, L., Pongs, O., & Kuhn, M. (2011). A cardiac pathway of cyclic GMP-independent signaling of guanylyl cyclase A, the receptor for atrial natriuretic peptide. *Proceedings of the National Academy of Sciences*, *108*(45), 18500–18505. https://doi.org/10.1073/pnas.1103300108

Klec, C., Ziomek, G., Pichler, M., Malli, R., & Graier, W. F. (2019). Calcium Signaling in ß-cell Physiology and Pathology: A Revisit. *International Journal of Molecular Sciences*, *20*(24), 6110. https://doi.org/10.3390/ijms20246110

Kögler, H., Schott, P., Toischer, K., Milting, H., Van, P. N., Kohlhaas, M., Grebe, C., Kassner, A., Domeier, E., Teucher, N., Seidler, T., Knöll, R., Maier, L. S., El-Banayosy, A., Körfer, R., & Hasenfuss, G. (2006). Relevance of Brain Natriuretic Peptide in Preload-Dependent Regulation of Cardiac Sarcoplasmic Reticulum Ca 2+ ATPase Expression. *Circulation*, *113*(23), 2724–2732. https://doi.org/10.1161/CIRCULATIONAHA.105.608828

Koitabashi, N., Bedja, D., Zaiman, A. L., Pinto, Y. M., Zhang, M., Gabrielson, K. L., Takimoto, E., & Kass, D. A. (2009). Avoidance of Transient Cardiomyopathy in Cardiomyocyte-Targeted Tamoxifen-Induced MerCreMer Gene Deletion Models. *Circulation Research*, *105*(1), 12–15. https://doi.org/10.1161/CIRCRESAHA.109.198416

Kukurba, K. R., & Montgomery, S. B. (2015). RNA Sequencing and Analysis. *Cold Spring Harbor Protocols*, *2015*(11), pdb.top084970. https://doi.org/10.1101/pdb.top084970

Laver, D. R., & Honen, B. N. (2008). Luminal Mg2+, A Key Factor Controlling RYR2-mediated Ca2+ Release: Cytoplasmic and Luminal Regulation Modeled in a Tetrameric Channel. *Journal of General Physiology*, *132*(4), 429–446. https://doi.org/10.1085/jgp.200810001

Leblanc, N., Chartier, D., Gosselin, H., & Rouleau, J.-L. (1998). Age and gender differences in excitation-contraction coupling of the rat ventricle. *The Journal of Physiology*, *511*(2), 533–548. https://doi.org/10.1111/j.1469-7793.1998.533bh.x

Liang, T., Qin, T., Xie, L., Dolai, S., Zhu, D., Prentice, K. J., Wheeler, M., Kang, Y., Osborne, L., & Gaisano, H. Y. (2017). New Roles of Syntaxin-1A in Insulin Granule Exocytosis and Replenishment. *Journal of Biological Chemistry*, *292*(6), 2203–2216. https://doi.org/10.1074/jbc.M116.769885

Mahmoodzadeh, S., Fliegner, D., & Dworatzek, E. (2013). Sex Differences in Animal Models for Cardiovascular Diseases and the Role of Estrogen. In *Handbook of Experimental Pharmacology* (pp. 23–48). https://doi.org/10.1007/978-3-642-30726-3_2

Marx, S. O., Gaburjakova, J., Gaburjakova, M., Henrikson, C., Ondrias, K., & Marks, A. R. (2001). Coupled Gating Between Cardiac Calcium Release Channels (Ryanodine Receptors). *Circulation Research*, *88*(11), 1151–1158. https://doi.org/10.1161/hh1101.091268

McGrath, M. F., Kuroski de Bold, M. L., & de Bold, A. J. (2005). The endocrine function of the

heart. *Trends in Endocrinology & Metabolism*, *16*(10), 469–477. https://doi.org/10.1016/j.tem.2005.10.007

Menick, D. R., Renaud, L., Buchholz, A., Muller, J. G., Zhou, H., Kappler, C. S., Kubalak, S. W., Conway, S. J., & Xu, L. (2007). Regulation of Ncx1 Gene Expression in the Normal and Hypertrophic Heart. *Annals of the New York Academy of Sciences*, *1099*(1), 195–203. https://doi.org/10.1196/annals.1387.058

Merlo, M., Cannatà, A., Gobbo, M., Stolfo, D., Elliott, P. M., & Sinagra, G. (2018). Evolving concepts in dilated cardiomyopathy. *European Journal of Heart Failure*, *20*(2), 228–239. https://doi.org/10.1002/ejhf.1103

Nerbonne, J. M., & Kass, R. S. (2005). Molecular Physiology of Cardiac Repolarization. *Physiological Reviews*, *85*(4), 1205–1253. https://doi.org/10.1152/physrev.00002.2005

Nishikimi, T., Maeda, N., & Matsuoka, H. (2006). The role of natriuretic peptides in cardioprotection. *Cardiovascular Research*, *69*(2), 318–328. https://doi.org/10.1016/j.cardiores.2005.10.001

Ohara-Imaizumi, M., Fujiwara, T., Nakamichi, Y., Okamura, T., Akimoto, Y., Kawai, J., Matsushima, S., Kawakami, H., Watanabe, T., Akagawa, K., & Nagamatsu, S. (2007). Imaging analysis reveals mechanistic differences between first- and second-phase insulin exocytosis. *Journal of Cell Biology*, *177*(4), 695–705. https://doi.org/10.1083/jcb.200608132

Panidis, I. P., Kotler, M. N., Ren, J.-F., Mintz, G. S., Ross, J., & Kalman, P. (1984). Development and regression of left ventricular hypertrophy. *Journal of the American College of Cardiology*, *3*(5), 1309–1320. https://doi.org/10.1016/S0735-1097(84)80192-8

Parks, R. J., Ray, G., Bienvenu, L. A., Rose, R. A., & Howlett, S. E. (2014). Sex differences in SR Ca2+ release in murine ventricular myocytes are regulated by the cAMP/PKA pathway. *Journal of Molecular and Cellular Cardiology*, *75*, 162–173. https://doi.org/10.1016/j.yjmcc.2014.07.006

Parmacek, M. S., & Solaro, R. J. (2004). Biology of the troponin complex in cardiac myocytes. *Progress in Cardiovascular Diseases*, *47*(3), 159–176. https://doi.org/10.1016/j.pcad.2004.07.003

Peters, C. G., Miller, D. F., & Giovannucci, D. R. (2006). Identification, localization and interaction of SNARE proteins in atrial cardiac myocytes. *Journal of Molecular and Cellular Cardiology*, *40*(3), 361–374. https://doi.org/10.1016/j.yjmcc.2005.12.007

Pugach, E. K., Richmond, P. A., Azofeifa, J. G., Dowell, R. D., & Leinwand, L. A. (2015). Prolonged Cre expression driven by the α-myosin heavy chain promoter can be cardiotoxic. *Journal of Molecular and Cellular Cardiology*, *86*, 54–61. https://doi.org/10.1016/j.yjmcc.2015.06.019

Rubattu, S., Stanzione, R., Di Angelantonio, E., Zanda, B., Evangelista, A., Tarasi, D., Gigante, B., Pirisi, A., Brunetti, E., & Volpe, M. (2004). Atrial Natriuretic Peptide Gene Polymorphisms and Risk of Ischemic Stroke in Humans. *Stroke*, *35*(4), 814–818. https://doi.org/10.1161/01.STR.0000119381.52589.AB

Saifee, O., Wei, L., & Nonet, M. L. (1998). The Caenorhabditis elegans unc-64 Locus Encodes a

Syntaxin That Interacts Genetically with Synaptobrevin. *Molecular Biology of the Cell*, *9*(6), 1235–1252. https://doi.org/10.1091/mbc.9.6.1235

Schaible, T. F., & Scheuer, J. (1984). Comparison of heart function in male and female rats. *Basic Research in Cardiology*, *79*(4), 402–412. https://doi.org/10.1007/BF01908140

Schultheiss, H.-P., Fairweather, D., Caforio, A. L. P., Escher, F., Hershberger, R. E., Lipshultz, S. E., Liu, P. P., Matsumori, A., Mazzanti, A., McMurray, J., & Priori, S. G. (2019). Dilated cardiomyopathy. *Nature Reviews Disease Primers*, *5*(1), 32. https://doi.org/10.1038/s41572-019-0084-1

Schulze, K. L., Broadie, K., Perin, M. S., & Bellen, H. J. (1995). Genetic and electrophysiological studies of drosophila syntaxin-1A demonstrate its role in nonneuronal secretion and neurotransmission. *Cell*, *80*(2), 311–320. https://doi.org/10.1016/0092-8674(95)90414-X

Seidah, N. G., Lazure, C., Chrétien, M., Thibault, G., Garcia, R., Cantin, M., Genest, J., Nutt, R. F., Brady, S. F., & Lyle, T. A. (1984). Amino acid sequence of homologous rat atrial peptides: natriuretic activity of native and synthetic forms. *Proceedings of the National Academy of Sciences*, *81*(9), 2640–2644. https://doi.org/10.1073/pnas.81.9.2640

Shannon, T. R., Guo, T., & Bers, D. M. (2003). Ca2+ scraps local depletions of free [Ca2+] in cardiac sarcoplasmic reticulum during contractions leave substantial Ca2+ reserve. *Circulation Research*, *93*(1), 40–45. https://doi.org/10.1161/01.RES.0000079967.11815.19

Shibasaki, T. (1987). Conductance and kinetics of delayed rectifier potassium channels in nodal cells of the rabbit heart. *The Journal of Physiology*, *387*(1), 227–250. https://doi.org/10.1113/jphysiol.1987.sp016571

Sieber, J. J., Willig, K. I., Kutzner, C., Gerding-Reimers, C., Harke, B., Donnert, G., Rammner, B., Eggeling, C., Hell, S. W., Grubmüller, H., & Lang, T. (2007). Anatomy and Dynamics of a Supramolecular Membrane Protein Cluster. *Science*, *317*(5841), 1072–1076. https://doi.org/10.1126/science.1141727

Sipido, K. R., Callewaert, G., & Carmeliet, E. (1995). Inhibition and rapid recovery of Ca2+ current during Ca2+ release from sarcoplasmic reticulum in guinea pig ventricular myocytes. *Circulation Research*, *76*(1), 102–109.

Soeller, C., & Baddeley, D. (2013). Super-resolution imaging of EC coupling protein distribution in the heart. *Journal of Molecular and Cellular Cardiology*, *58*, 32–40. https://doi.org/10.1016/j.yjmcc.2012.11.004

Sohal, D. S., Nghiem, M., Crackower, M. A., Witt, S. A., Kimball, T. R., Tymitz, K. M., Penninger, J. M., & Molkentin, J. D. (2001). Temporally Regulated and Tissue-Specific Gene Manipulations in the Adult and Embryonic Heart Using a Tamoxifen-Inducible Cre Protein. *Circulation Research*, *89*(1), 20–25. https://doi.org/10.1161/hh1301.092687

Söllner, T. H. (2003). Regulated exocytosis and SNARE function. *Molecular Membrane Biology*, *20*(3), 209–220. https://doi.org/10.1080/0968768031000104953

Stephenson, T. J., & Broughton Pipkin, F. (1990). Atrial natriuretic factor: the heart as an endocrine organ. *Archives of Disease in Childhood*, *65*(12), 1293–1294. https://doi.org/10.1136/adc.65.12.1293

Studer, R., Reinecke, H., Bilger, J., Eschenhagen, T., Böhm, M., Hasenfuss, G., Just, H., Holtz, J., & Drexler, H. (1994). Gene expression of the cardiac Na(+)-Ca2+ exchanger in end-stage human heart failure. *Circulation Research*, *75*(3), 443–453. https://doi.org/10.1161/01.RES.75.3.443

Stypmann, J., Engelen, M. A., Epping, C., van Rijen, H. V. M., Milberg, P., Bruch, C., Breithardt, G., Tiemann, K., & Eckardt, L. (2006). Age and gender related reference values for transthoracic Doppler-echocardiography in the anesthetized CD1 mouse. *The International Journal of Cardiovascular Imaging*, *22*(3–4), 353–362. https://doi.org/10.1007/s10554-005-9052-9

Thiriet, M. (2008). Anatomy of the Cardiovascular System. In *Biology and Mechanics of Blood Flows* (pp. 9–33). Springer New York. https://doi.org/10.1007/978-0-387-74849-8_1

Tokudome, T., Horio, T., Kishimoto, I., Soeki, T., Mori, K., Kawano, Y., Kohno, M., Garbers, D. L., Nakao, K., & Kangawa, K. (2005). Calcineurin–Nuclear Factor of Activated T Cells Pathway–Dependent Cardiac Remodeling in Mice Deficient in Guanylyl Cyclase A, a Receptor for Atrial and Brain Natriuretic Peptides. *Circulation*, *111*(23), 3095–3104. https://doi.org/10.1161/CIRCULATIONAHA.104.510594

Trus, M., Wiser, O., Goodnough, M. ., & Atlas, D. (2001). The transmembrane domain of syntaxin 1A negatively regulates voltage-sensitive Ca2+ channels. *Neuroscience*, *104*(2), 599–607. https://doi.org/10.1016/S0306-4522(01)00083-5

Ungermann, C., & Langosch, D. (2005). Functions of SNAREs in intracellular membrane fusion and lipid bilayer mixing. *Journal of Cell Science*, *118*(17), 3819–3828. https://doi.org/10.1242/jcs.02561

Vance, K. W., & Ponting, C. P. (2014). Transcriptional regulatory functions of nuclear long noncoding RNAs. *Trends in Genetics*, *30*(8), 348–355. https://doi.org/10.1016/j.tig.2014.06.001

Virdi, M. (2019). *Characterizing the Role of Syntaxin 1A in the Heart* (Issue October). York University.

Wasserstrom, J. A., Kapur, S., Jones, S., Faruque, T., Sharma, R., Kelly, J. E., Pappas, A., Ho, W., Kadish, A. H., & Aistrup, G. L. (2008). Characteristics of intracellular Ca 2+ cycling in intact rat heart: a comparison of sex differences. *American Journal of Physiology-Heart and Circulatory Physiology*, *295*(5), H1895–H1904. https://doi.org/10.1152/ajpheart.00469.2008

Watson, R. T., & Pessin, J. E. (2001). Transmembrane domain length determines intracellular membrane compartment localization of syntaxins 3, 4, and 5. *American Journal of Physiology-Cell Physiology*, *281*(1), C215–C223. https://doi.org/10.1152/ajpcell.2001.281.1.C215

Weber, T., Zemelman, B. V., McNew, J. A., Westermann, B., Gmachl, M., Parlati, F., Söllner, T. H., & Rothman, J. E. (1998). SNAREpins: Minimal Machinery for Membrane Fusion. *Cell*, *92*(6), 759–772. https://doi.org/10.1016/S0092-8674(00)81404-X

Wessels, A., & Sedmera, D. (2003). Developmental anatomy of the heart: a tale of mice and man. *Physiological Genomics*, *15*(3), 165–176. https://doi.org/10.1152/physiolgenomics.00033.2003

Wilkins, M. R., Redondo, J., & Brown, L. A. (1997). The natriuretic-peptide family. *The Lancet*, *349*(9061), 1307–1310. https://doi.org/10.1016/S0140-6736(96)07424-7

Wiser, O., Bennett, M. K., & Atlas, D. (1996). Functional interaction of syntaxin and SNAP-25 with voltage-sensitive L- and N-type Ca2+ channels. *The EMBO Journal*, *15*(16), 4100–4110. https://doi.org/10.1002/j.1460-2075.1996.tb00785.x

Wiser, O., Cohen, R., & Atlas, D. (2002). Ionic dependence of Ca 2+ channel modulation by syntaxin 1A. *Proceedings of the National Academy of Sciences*, *99*(6), 3968–3973. https://doi.org/10.1073/pnas.052017299

Wiser, O., Trus, M., Hernández, A., Renström, E., Barg, S., Rorsman, P., & Atlas, D. (1999). The voltage sensitive Lc-type Ca2+ channel is functionally coupled to the exocytotic machinery. *Proceedings of the National Academy of Sciences of the United States of America*, *96*(1), 248–253. https://doi.org/10.1073/pnas.96.1.248

Xie, L., Dolai, S., Kang, Y., Liang, T., Xie, H., Qin, T., Yang, L., Chen, L., & Gaisano, H. Y. (2016). Syntaxin-3 Binds and Regulates Both R- and L-Type Calcium Channels in Insulin-Secreting INS-1 832/13 Cells. *PLOS ONE*, *11*(2), e0147862. https://doi.org/10.1371/journal.pone.0147862

Yamada, Y., Namba, K., & Fujii, T. (2020). Cardiac muscle thin filament structures reveal calcium regulatory mechanism. *Nature Communications*, *11*(1), 153. https://doi.org/10.1038/s41467-019-14008-1

Zhang, J. Z., Waddell, H. M. M., & Jones, P. P. (2015). Regulation of RYR2 by sarcoplasmic reticulum Ca 2+. *Clinical and Experimental Pharmacology and Physiology*, *42*(6), 720–726. https://doi.org/10.1111/1440-1681.12364

Zhao, W., Zhao, T., Chen, Y., Zhao, F., Gu, Q., Williams, R. W., Bhattacharya, S. K., Lu, L., & Sun, Y. (2015). A Murine Hypertrophic Cardiomyopathy Model: The DBA/2J Strain. *PLOS ONE*, *10*(8), e0133132. https://doi.org/10.1371/journal.pone.0133132

Ziv, Y., Bielopolski, D., Galanty, Y., Lukas, C., Taya, Y., Schultz, D. C., Lukas, J., Bekker-Jensen, S., Bartek, J., & Shiloh, Y. (2006). Chromatin relaxation in response to DNA double-strand breaks is modulated by a novel ATM- and KAP-1 dependent pathway. *Nature Cell Biology*, *8*(8), 870–876. https://doi.org/10.1038/ncb1446

Appendix A

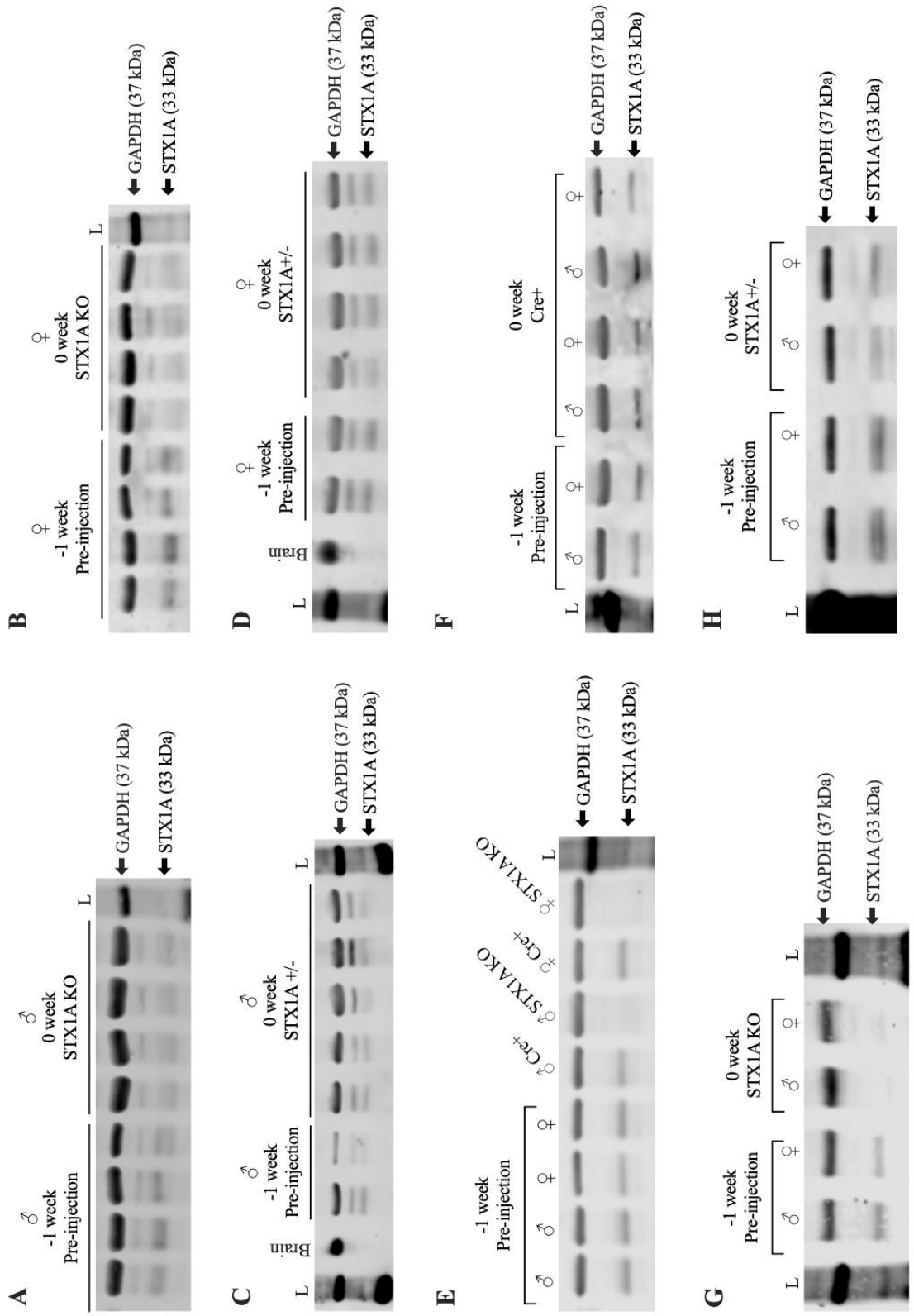


Figure 1: Western blots used for STX1A densitometry before tamoxifen injections (-1 week) and directly after the last tamoxifen injection (0 week). A total of 30 µg of protein was loaded with STX1A appearing as a band at 33 kDa and GAPDH, which was used as a loading control, appearing as a band at 37 kDa.